DIAGNOSTIC STUDY OF A WARM

BLOCKING ANTICYCLONE

by

Lodovica Illari

Atmospheric Physics Group
Department of Physics
Imperial College of Science and
Technology
London

A thesis submitted for the Degree of Doctor of Philosophy
in the University of London

1982

A B S T R A C T

During the Summer of 1976, western and central Europe were abnormally hot and dry, due to a warm blocking high which persisted during the months of June, July and August.

Dynamical features of this blocking high are studied using station and 2.5° gridded N.M.C. data. To determine the importance of transient eddies in the maintenance of the warm anticyclone, the dynamical variables are separated into monthly mean and eddy components, and monthly time-averaged budgets of vorticity, heat and potential vorticity are evaluated at standard pressure levels.

The block is a region of high temperatures and low potential, as well as relative, vorticity. Eddy forcing is found to be crucial in the maintenance of the block. The transient eddies induce anticyclonic mean flow near the tropopause. The resulting mean vertical motion (evaluated as residual in the vorticity equation with zero vertical velocity at the tropopause) is downwards in the blocking region and corresponds well with the monthly average rainfall deficit. The residual in the time-averaged thermodynamic equation shows diabatic cooling in the blocking region which is less than the adiabatic warming due to sinking motion, resulting in a warm anticyclone. The anticyclonic vorticity brought down to the surface is dissipated by frictional torque.

Eddy-activity is found to be concentrated in the northern branch of the split jet. The eddy fluxes have a large non-divergent part which vector-rotates round the storm tracks. A rotational flux which balances the advection of eddy-variance can be identified which is associated with the spatial growth and decay of eddies.

CONTENTS

ABSTRACT 1

CHAPTER 1 : DROUGHT '76 - CASE STUDY OF A BLOCKING ANTICYCLONE

1.1 Definition of "blocking anticyclone" 5

1.2 Summer '76: synoptic description of a blocking anticyclone 8

CHAPTER 2 : THE BLOCKING AND ITS DYNAMICAL ASPECTS

2.1 Blocking mechanisms 16

2.1.1 Theoretical investigations of blocking mechanisms 16

2.1.2 Observations and blocking mechanisms 19

2.2 Mean motion and the action of the eddies 21

2.2.1 Introduction 21

2.2.2 Momentum equation for large scale motion 23

2.2.3 Vorticity equation for large scale motion 25

2.2.4 Thermodynamic equation for large scale motion 27

2.3 Transient eddies during Summer '76 29

2.3.1 Wind statistics from station data 29

2.3.2 Reynolds stress distribution 31

CHAPTER 3 : VORTICITY AND HEAT BUDGETS

3.1 Gridded data 40

3.1.1 Introduction 40

3.1.2 NMC analysis 40

3.2 The spherical polar formulation 43

3.2.1 Introduction 43

3.2.2 Vorticity and thermodynamic equations 44

3.3 Mean flow 46

3.4 Maintenance of the mean vorticity 48

3.4.1 Introduction 48

3.4.2 Mean flow advection 48

3.4.3 Eddy-vorticity forcing 50

3.4.4 Total vorticity forcing 53

3.5 Vertical velocity 55

3.5.1 Introduction 55

3.5.2 Vertical velocity into the boundary layer 57

3.6 Maintenance of the mean temperature 59

3.6.1 Mean temperature field 59

3.6.2 Static stability 59

3.6.3 Mean and eddy advection of heat 61

3.6.4 Diabatic and adiabatic heating 65

3.7 Discussion 68

3.7.1 Area-averages of vorticity and heat budgets 68

3.7.2 Summary 69

CHAPTER 4 : THE BLOCK IN TERMS OF POTENTIAL VORTICITY

4.1 The potential vorticity conservation 70

4.1.1 Ertel and quasi-geostrophic potential vorticity 70

4.2 Quasi-geostrophic potential vorticity budget 73

4.2.1 Introduction 73

4.2.2 The block and its mean potential vorticity 75

4.2.3 Mean flow advection of potential vorticity 78

4.2.4 Eddy-q-flux divergence 78

4.2.5 Residual in the potential vorticity equation 83

Discussion (on Chapters 3 and 4) 84

CHAPTER 5 : EDDY-FLUX

5.1	Introduction	68
5.2	Eddy activity: storm tracks and eddy-kinetic energy	90
5.3	Eddy flux	92
5.3.1	Eddy heat flux	92
5.3.2	Eddy potential energy equation	95
5.3.3	Rotational heat flux balancing advection of eddy potential energy	98
5.3.4	Eddy potential vorticity flux	103
5.4	Summary	108

CONCLUSIONS AND SUGGESTIONS FOR FUTURE WORK 110

REFERENCES 112

ACKNOWLEDGEMENTS 117

CHAPTER 1

DROUGHT '76 - CASE STUDY OF A BLOCKING ANTICYCLONE

1.1 Definition of "blocking anticyclone"

"Hard and fast definitions of blocking are undesirable - one's interest should be in all persistent large-scale flow anomalies" (Charney, "Atmospheric Blocking Meeting" - LONDON - September '79). Perhaps our hesitance to define a "blocking anticyclone" is a sign of a lack of understanding of the phenomenon itself. Our working definition, therefore, will be a descriptive and not a mechanistic one.

Fig.1.1 (from Rex's "Aerological study of a blocking action", 1950) shows the sequence of events occurring at 500 mb level during the development of a "block". It shows quite clearly the passage from a nearly zonal flow to a configuration where the westerlies are blocked by a ridge around which baroclinic disturbances travel. Based on these observations Rex adopted the following definition of a block in his study: "A blocking case must exhibit the following characteristics:

a) the basic westerly current must split into two branches;

b) each branch current must transport an appreciable mass;

c) the double jet system must extend over at least 45° of longitude;

d) a sharp transition from zonal type flow upstream to meridional type downstream must be observed across the current split; and

e) the pattern must persist with recognisable continuity for at least ten days".

Although these features can vary from one block to another, clearly in synoptic terms "blocking" is an interruption of the midlatitude

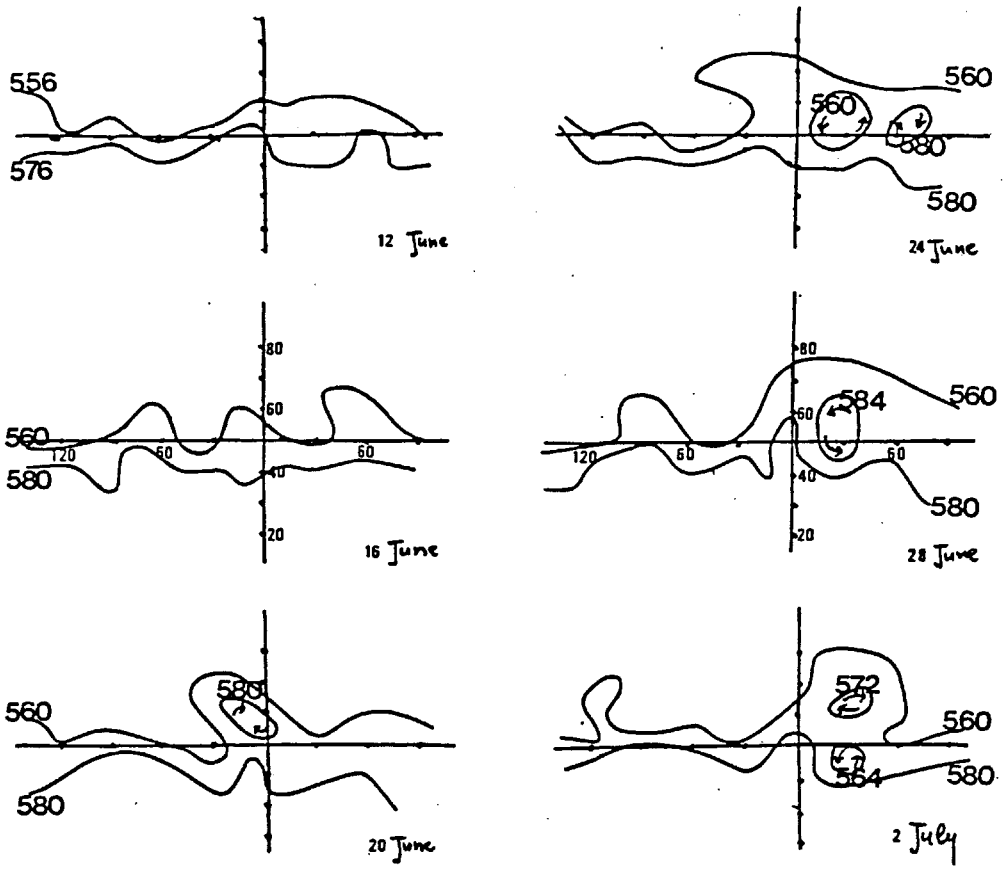


Fig.1.1: A series of plates showing the development of a block at the 500 mb level at 0300 GMT during July 1949. Contour heights in dam. (From Rex, 1950.)

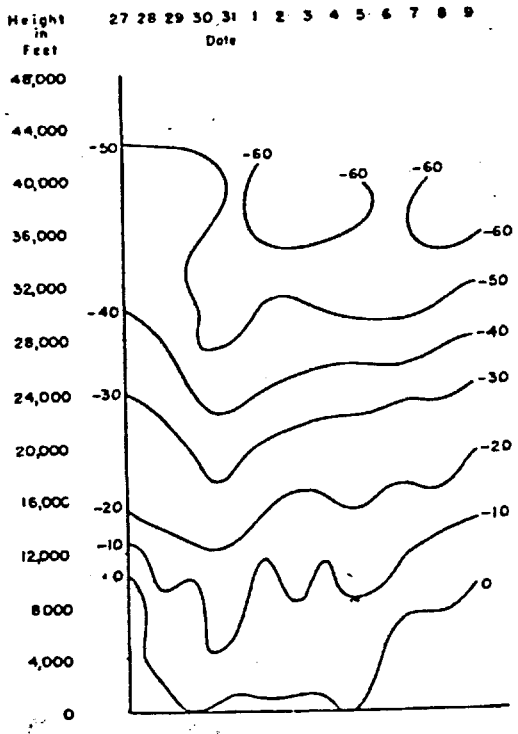
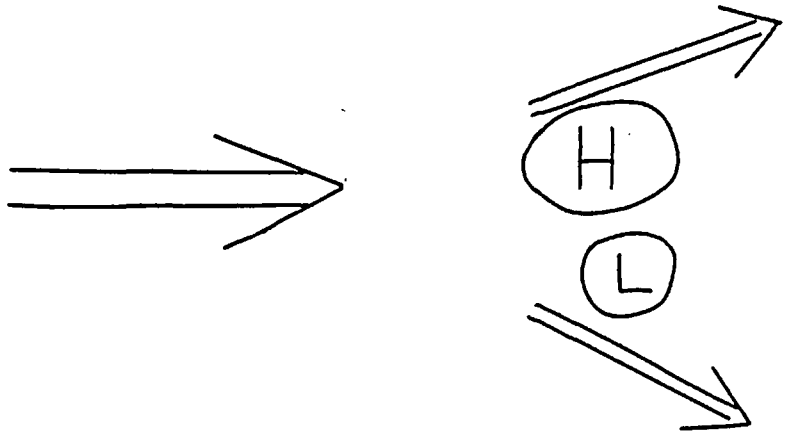


Fig.1.2: Time cross section of the temperature at Longview, Alaska, during the formative stage of a blocking high, 27 March-9 April, 1948. "Note that when the anticyclone is stabilizing (30 March), the troposphere gradually warms, especially in the lower part, but the stratosphere remains cold..." (from Elliott and Smith, 1949).

westerly flow by a slow moving ridge, or anticyclone, extending up to 500 mb or higher. In most cases the 500 mb westerly jet is split over a range of longitude, one branch passing poleward of the block and the other equatorward, giving a high, low dipole structure, as shown in the following schematic picture:



All blocking highs have a typical vertical structure. Blocks tend to be warm in the troposphere and cold in the stratosphere and the phase lines are vertical (see Fig.1.2). This is in marked contrast with the structure of other stationary anticyclones, such as the Siberian anticyclone with lower level tropospheric cooling, upper level warming and a 180^{o} phase shift in the vertical.

The two preferred locations for blocking are near the east coasts of Europe and the States,at the end of the Atlantic and Pacific storm tracks (see Rex (1950), Sanders (1953), Montalto, Conte and Urbani (1973) and Austin (1980)). Their duration can vary from case to case. Rex's survey showed a peak at fourteen days for Atlantic blocks, but this has not been confirmed by other authors. Austin's analysis in the Atlantic, for example, shows rather weak maxima at eight and twelve

days. Both surveys show that blocks which persist for more than ∿30 days are rare.

The incidence of blocking varies considerably from year to year but it is not certain whether any long trends or periodicity are involved. It is evident, however, that late Autumn and early Spring are the periods of the year with large incidences of blocking cases.

A review of possible blocking mechanisms is postponed to the following chapter. Here we simply restrain ourselves to a descriptive approach of the phenomenon, choosing as a case study the European drought of 1976, when an intense blocking anticyclone persisted for the uncommonly long period of three months (June, July and August '76).

1.2 Summer '76: synoptic description of a blocking anticyclone

The development of large-amplitude, persistent anticyclones in midlatitudes ("blocking anticyclones") can play an important role in determining regional climate. Because of their long duration and their large effects on local temperature and on the movement of synoptic systems, blocking ridges cause significant deviations from seasonal normals of temperature and precipitation. The climatological impact of such anomalies have been studied, for example, by Bergren and Bolin (1949), Rex (1950), Sumner (1959) and Namias (1947, 1964).

During the summer of 1976 the British Isles, with all Western and Central Europe, were affected by the presence of an intense blocking anticyclone which resulted in low rainfall over a substantial area. The phenomenon is now remembered as the "Drought '76", in recognition of its extensive impact.

In the early 1970's there was a succession of mild European

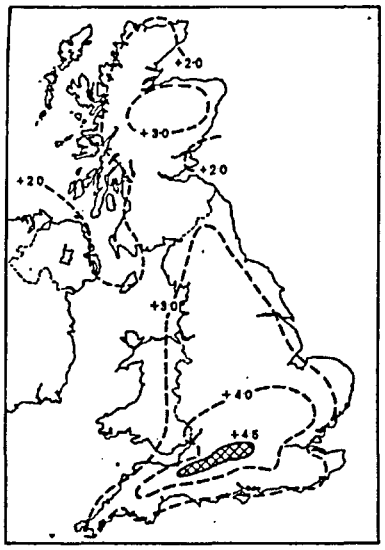


Fig.1.3: Departure from average (1941-70) of mean daily maximum temperature for summer (June to August) 1976 over the United Kingdom (from Murray, 1977).

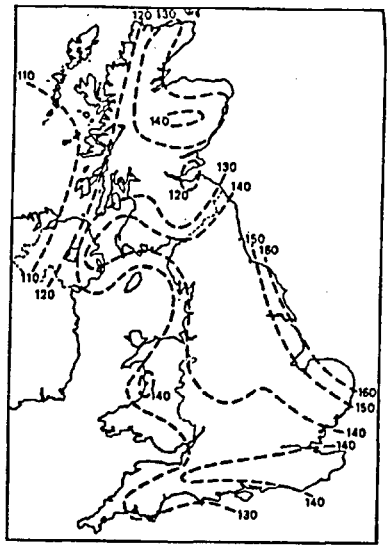


Fig.1.4: Sunshine duration as percentage of average (1941) for Summer (June to August) 1976 over the United Kingdom (from Murray, 1977).

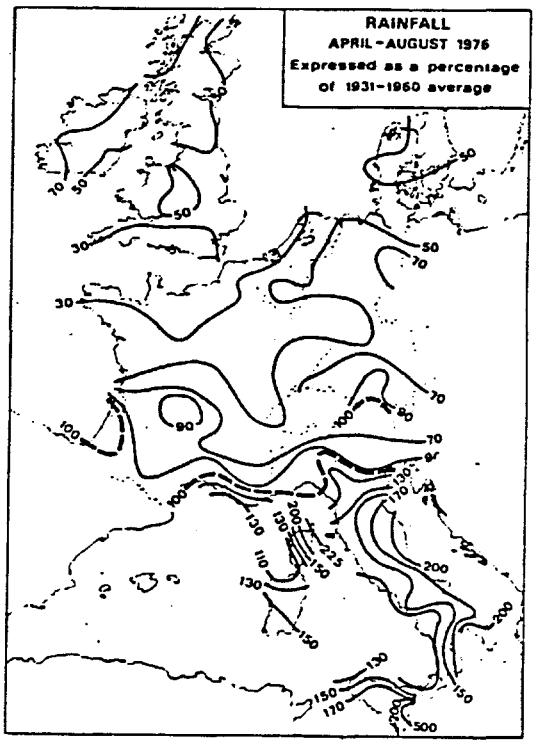


Fig.1.5: (from "Atlas of Drought in Britain 1975-76").

winters (and, incidentally, cold Pacific winters) associated with the northward displacement of the East Atlantic jet stream. In fact, the sixteen months from May 1975 to August 1976 was the driest sixteen-month period since records began in 1727. So the summer of 1976 can be seen as part of a continuous evolution of the hemispheric circulation over a period of several years (Ratcliffe, 1977). The below average precipitation during Summer '75 and Winter '75-'76 made the impact of very low precipitation over England in the summer of 1976 even greater.

The westerly flow remained blocked around England and Northern Europe for almost the whole of June, July and August 1976 and the resulting anticyclonic circulation gave very hot and dry weather. Anomalies of mean daily maximum temperature and sunshine duration for the three-month period June to August 1976 are presented in Fig. 1.3 and 1.4 respectively (Murray, 1977). Between 20 June to 6 July a "heat wave" affected first western England and then all Britain, giving the longest and hottest spell of weather since at least the 18th century (and probably much longer) (Shaw, 1977).

The anticyclonic circulation meant that most areas received well below average rainfall - Fig.1.5 shows the rainfall distribution over Europe during the period April '76 - August '76. The worst affected area was southern England and northern France where, in some places, August was the eleventh successive month with less than average rainfall. The drought reached its maximum intensity in June, when almost all the E.E.C. countries had less than 50% of their average rainfall. July was particularly dry over U.K., Denmark and Continental areas bordering the English Channel and North Sea. The Mediterranean experienced some heavy showers. August was generally

dry; only Italy and southern France had above average rainfall.

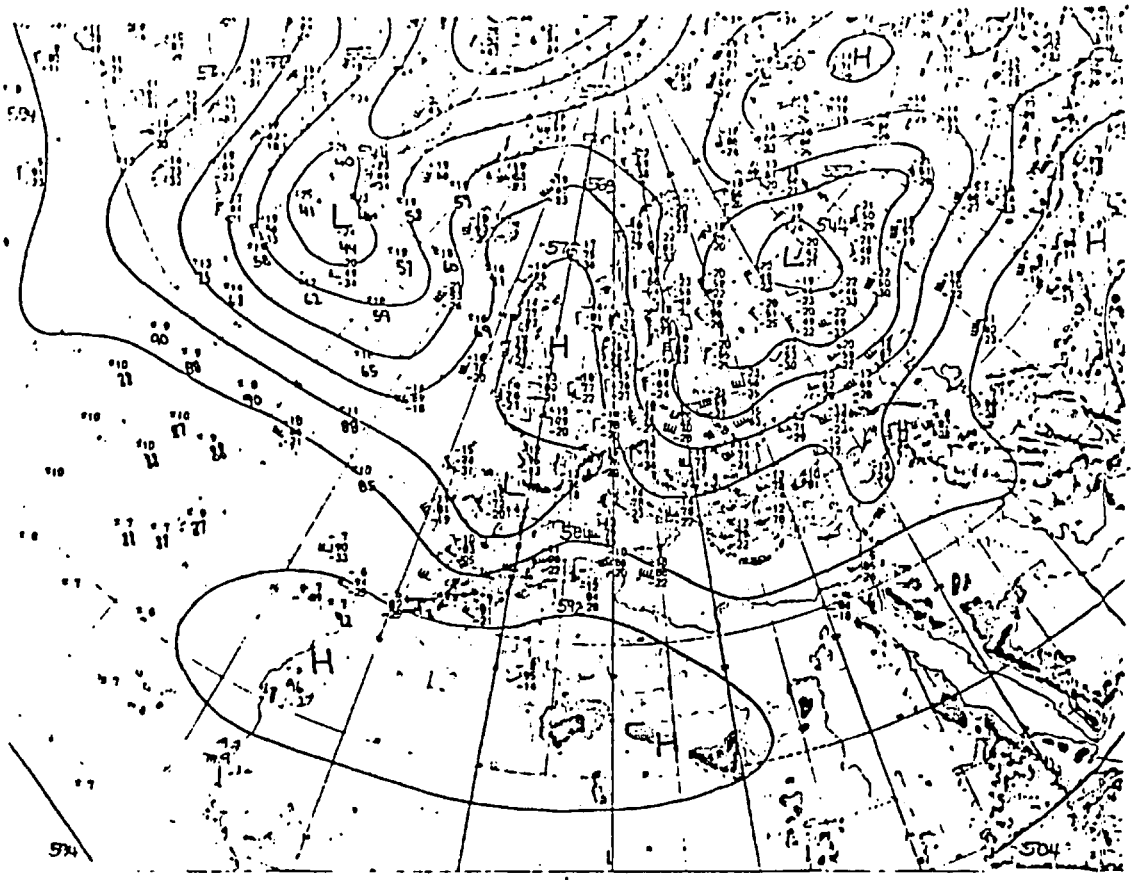
The rainfall pattern is well correlated with the splitting of the jet stream. The westerly winds were split with one branch displaced north and the other south (at about 60°N and 30°N respectively) steering the weather systems to the north or south, leaving the area in between with no substantial precipitation.

Analysis of the daily synoptic charts for July '76, when the block was at its peak, shows high pressure cells growing over western Europe in the first days of the month. They then move slowly eastward giving a block and associated split jet over western and central Europe. This blocking configuration (see Fig.1.6(a) - day 6) persists for about a week. Towards the middle of the month the highs grow preferentially over western and central Europe, move eastward and block the flow particularly over eastern Europe. This configuration (see Fig.1.6(b) - day 15) is maintained for ten days, with the high pressure cells continuously being replaced. As this system decays over western Asia, new highs grow over Europe and a split appears again over central Europe (see Fig.1.7(a) - day 25), lasting until nearly the end of the month. In the meantime, yet more high pressure systems approached Europe from the Atlantic with a split jet already evident westward of the British Isles (see Fig.1.7(b) - day 30).

These observations show that the blocking moved around during the month with a ridge staying over western-central Europe during the first half of the month and then moving eastward during the second half, to reappear west of Europe at the end of the month.

Although in daily synoptic charts we can observe the blocked flow and the split jet, it is not a static phenomenon. Synoptic-scale transient systems are evident: slowly moving high pressure cells grow,

a) 6 July '76



b) 15 July '76

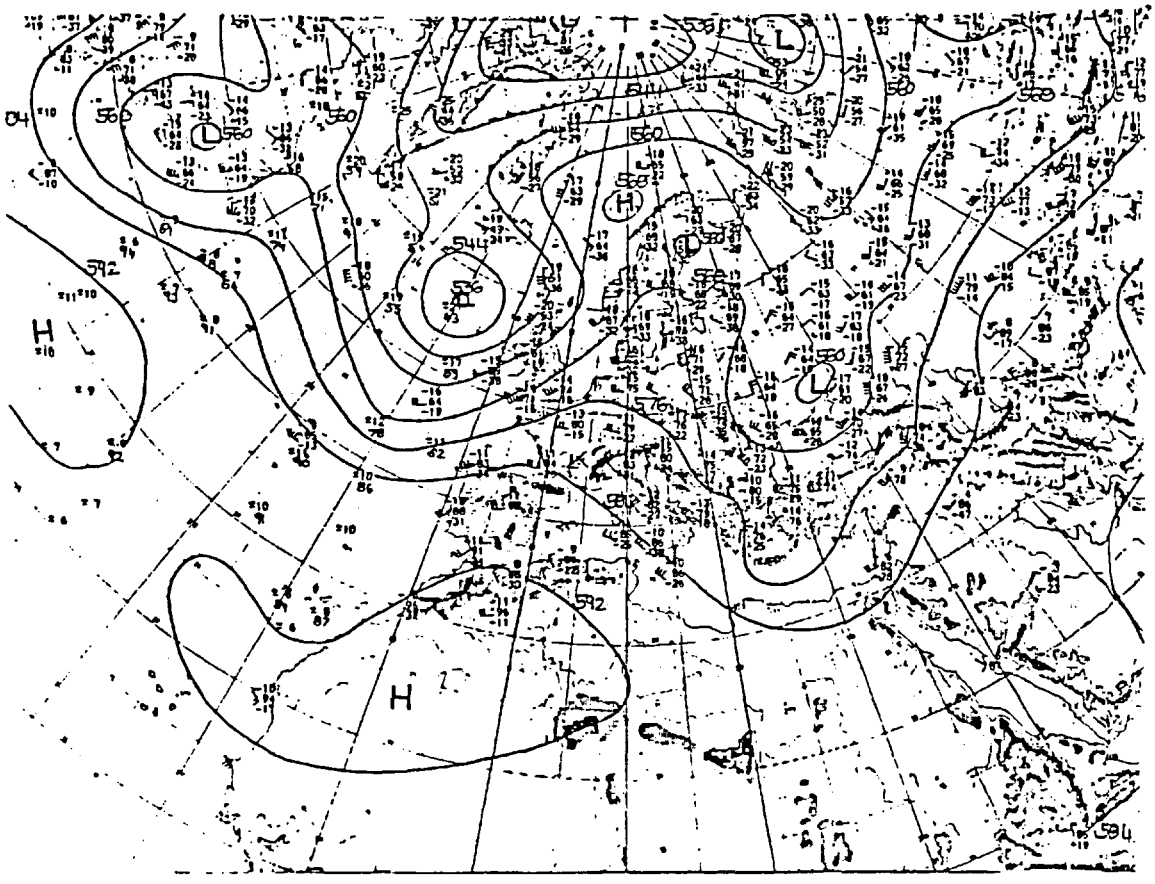
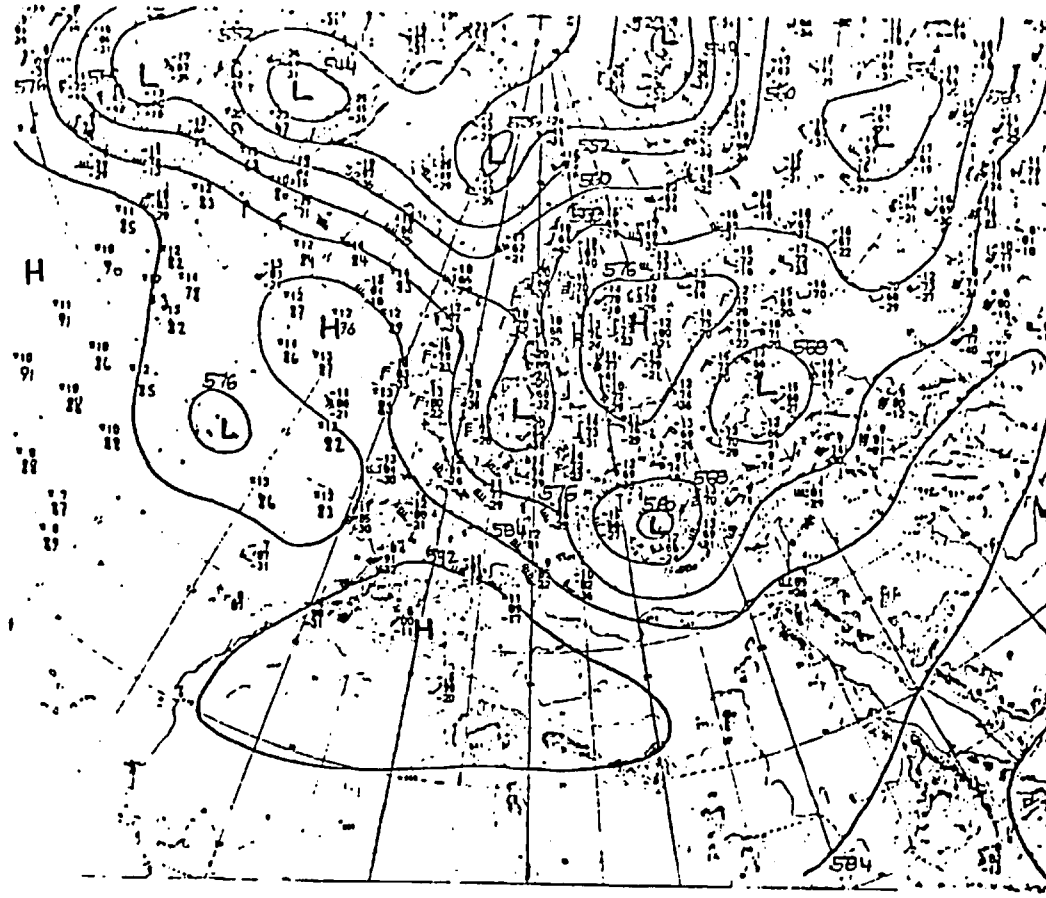


Fig.1.6: A series of 500 mb charts for July '76, showing various phases in the development of the blocking system. Contour heights at 8 dam spacing.

a) 25 July '76



b) 30 July '76

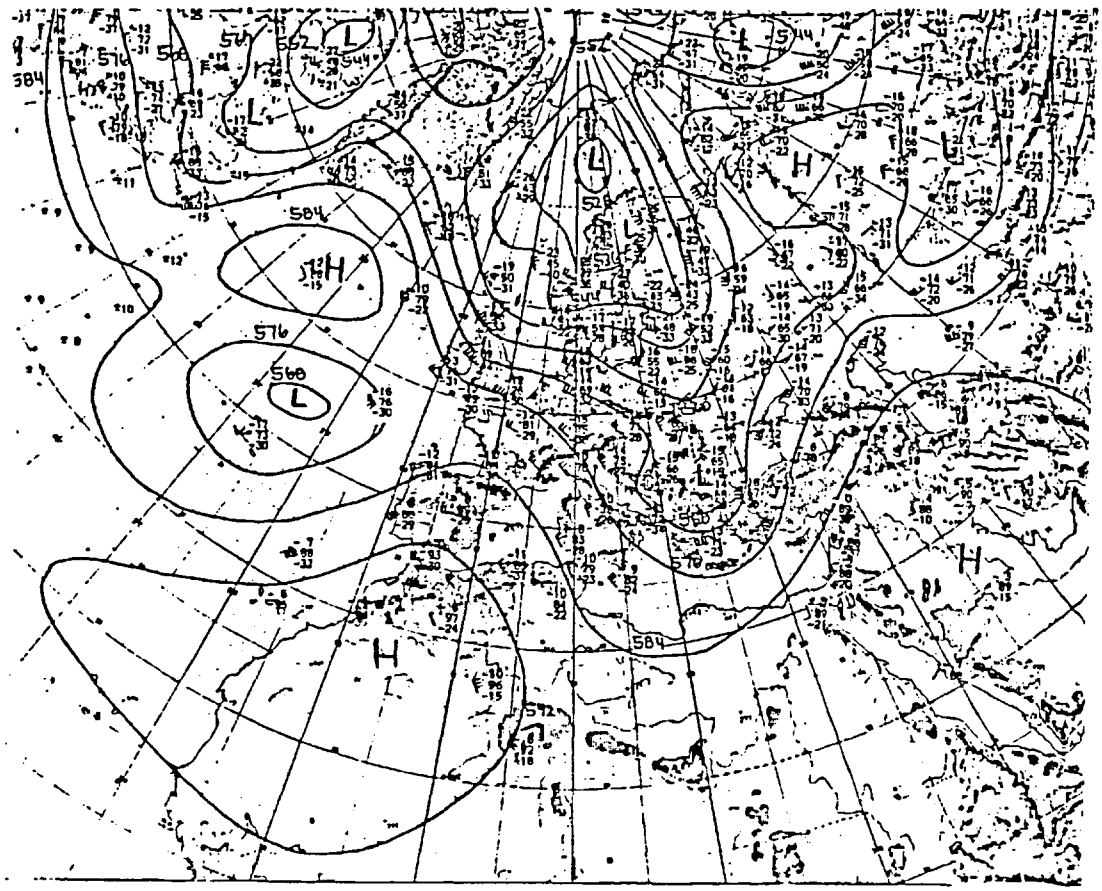


Fig.1.7: 'as in Fig.1.6.

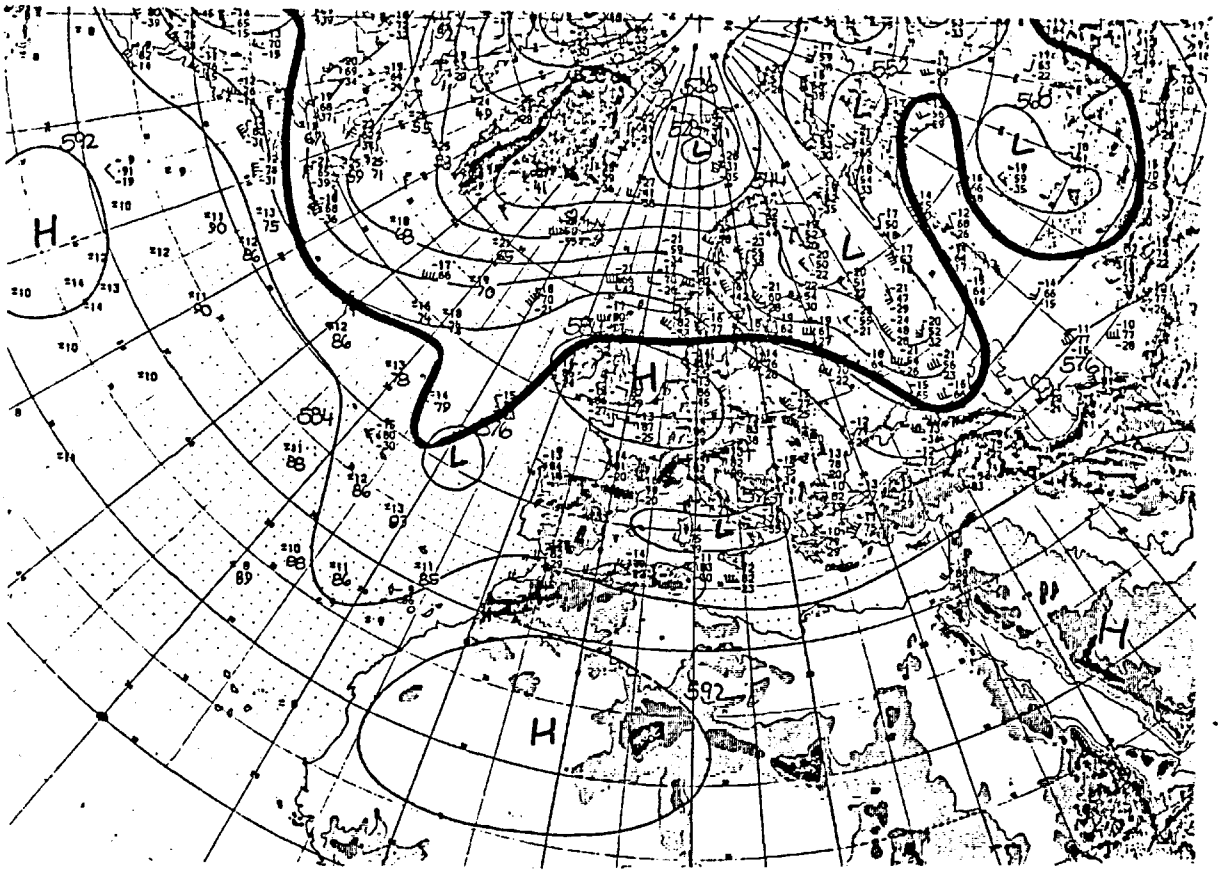


Fig.1.8 : a) 500 mb chart for 1 July. Contour heights at 8 dam spacing. Thick black line: isotherm -15°C. Notice the ridge over the British Isles, warm compared with the trough over western Russia.

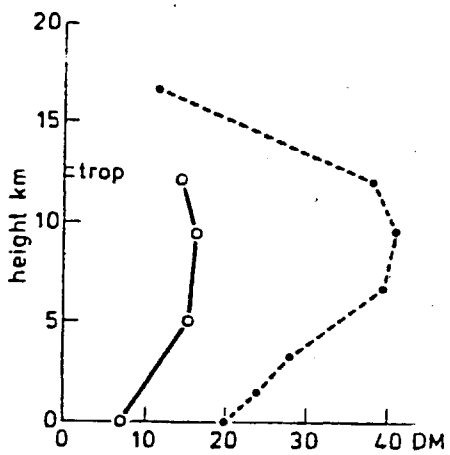


Fig.1.8 : b) Change in isobaric height between the ridge over southern England and the trough over western Russia. Continuous line: mean for July '76. Dashed line: values for 1 July, '76. (From Green, 1977.)

block the flow, decay, and then new systems replace them.

The depressions, which are diverted by the blocking ridge, tend to pass predominantly northward of the high pressure cells. In the month, approximately seven depressions crossed the Greenwich meridian north of the British Isles, while only two or three intense depressions passed southward, giving the observed high rainfall over southern France and the Mediterranean.

Daily charts also show that the blocking ridge is warm compared with the accompanying trough over western Russia (Fig.1.8(a)). This means that the contrast in isobaric height of these two features must increase going upwards. Fig.1.8(b) amplifies the point, showing that the contrast increases up to the tropopause at a rate which implies that the high is some 6^{o} warmer than the low. Above the tropopause there is an abrupt change, with the high becoming cooler than the low.

CHAPTER 2

THE BLOCKING AND ITS DYNAMICAL ASPECTS

2.1 Blocking mechanisms

The problem of understanding and explaining the mechanism of blocking has always been considered crucial in meteorology and many investigations and observational studies of the structure and climatology of blocks have been carried out. A brief summary of these studies is presented in the following paragraphs.

2.1.1 Theoretical investigations of blocking mechanisms

There is not yet a generally accepted theoretical explanation for the blocking phenomenon but the mechanisms which have been proposed can be separated into two different groups: a) those which are based on barotropic interaction between the scales of motion and (b) those which use thermal forcing.

a) Barotropic mechanisms

Many of the current theories for blocking consider the distribution of zonal mean wind for which a free wave becomes stationary. Stationary forcing may, then, result in a large amplitude resonant response by this mode. Some of these free waves have structure resembling that of blocks.

Yeh (1949), and more recently Tung and Lindzen (1979), suggested

that atmospheric blocking could be explained in terms of linear resonance of planetary-scale waves with surface forcing (orography or land-sea contrast).

Egger (1978) developed a model in which barotropic non-linear interaction between forced and slowly moving free waves gave blocking.

Charney and De Vore (1979), investigating non-linear interaction of waves with the zonal mean flow, have shown that a multiplicity of stationary equilibrium states is possible for given momentum and thermal sources. In particular, their momentum forcing, intended to represent orography, produces two stable states of which one, called a "high index" state has strong zonal flow and weak long wave response. The other, the "low index" state, has weak zonal flow and strong long wave response. The former resembles a weakly perturbed circumpolar current, whereas the latter resembles a strongly perturbed blocking configuration. Their work suggests that non-linearity is an essential ingredient of blocking and that blocking may be a quasi-equilibrium state in resonance with topography and/or thermal forcing.

Charney, Shukla and Mo (1981) incorporate observed topography in their barotropic non-linear model and multiple stationary equilibria are again obtained. Of 34 blocking events selected from daily 500 mb observation of 15 consecutive winters, 19 of these appear to be explainable qualitatively as one or another of the calculated equilibria. Their highly truncated spectral model, however, did not provide a definite answer to the localised character of the blocking ridge or to the mechanism of transition to and from the blocking configurations.

Barotropic instability in relation to the breakdown of the "westerlies" has been studied by Illari, Malguzzi and Speranza (1981).

The transition of middle-latitude atmospheric circulation from "zonal" to "meridional" type due to the growth of a local disturbance is very frequent over Europe, where it can often lead to a block. The conditions that determine a local disturbance to amplify *in situ* (absolute instability) or to grow only when it moves downstream (convective instability) are studied for a barotropic basic flow, consisting of a uniform zonal wind with superimposed latitudinally uniform Rossby wave. They show that for "large" amplitude of the Rossby wave and "weak" zonal flow, the perturbation grows essentially *in situ* with a time scale of days, while for "small" amplitude of the Rossby wave and "strong" westerly flow, the perturbation moves downstream as it grows on a space scale of 10^4 km. Comparison with real data in the European region shows that the growth of local disturbances and consequent breakdown of the zonal flow depends critically on the properties of the approaching wave packet.

Because of their local nature, it has been tried to determine whether blocks resemble any of the special solitary wave solutions of the dynamical equations ("modons"). These solutions are local in nature and maintain their structure by balancing linear dispersive effects with non-linear effects. There is no forcing or dissipation. McWilliams (1980) has shown some similarity between blocking and modon solution of the equivalent barotropic equation.

b) Thermal mechanisms

From the knowledge that blocking ridge activity usually occurs over the ocean in the autumn and winter, Namias (1950, 1959, 1964) postulated that enhanced heat flux from the ocean may modify the baroclinic instability processes and that this was an important factor in the development of the blocks. Indeed, White and Clark (1975) found

that anomalous distribution of heat transfer was strongly correlated with blocking ridge development.

In a two-layer theoretical study by Haltiner (1967), baroclinic instability was modified by sensible heat transfer. He found that for typical winter values of the background flow, the normally stable stationary long wave became unstable when sensible heat transfer was allowed. The wavelength and the growth rate for the unstable stationary wave are very similar to those of blocking ridges. Haltiner's theory also accounts for the seasonal and year-to-year variability in blocking activity in terms of corresponding fluctuations in sensible heat transfer and strengths of mean westerly winds. However, Geisler (1977) pointed out that Haltiner's findings cannot be extended to continuously stratified models. Nevertheless, the studies of Namias (1964), White and Clark (1975) and the observation that blocking occurs at certain preferred geographical positions, suggest that the phenomenon cannot be understood without taking into consideration zonal variations in the surface conditions. This view is supported by the studies of Kikuki (1969, 1971), who investigated the importance of orography and land-sea thermal contrast in a numerical model of blocking, and found that orography was important in determining the growth of well developed ridges at certain preferred longitudes.

2.1.2 Observations and blocking mechanisms

The structure and the climatological impact of blocking have been analysed since the early study of Bergren et al.(1949), Rex (1950, 1951), Brezowsky et al.(1951) and Sumner (1959). Namias (1947, 1964, 1978) has shown a constant interest in the climatological effects of abnormal

general circulation patterns. He suggested that the physical causes of blocks, or other climatic fluctuations, lie in complex feedback phenomena between the atmosphere and the underlying surface. The purposes of his papers are: ".... to describe, to inter-relate and to speculate on factors associated with climatic fluctuation and its physical causes, with the help not only of data taken in the atmosphere, but also at the surface of sea and land (precipitation, both rain and snow)...." (Namias, 1978).

To understand more completely these complex feedback mechanisms and to test different hypotheses, further analysis of observed blocking cases seem to be necessary.

Edmon (1980) has shown that anomalies of contour height charts for several winters have vertical phase lines (i.e. equivalent barotropic) and are cold low or warm high modifications to the normal January mean climate. It is also known (as described in Chapter 1) that "blocking phenomena" are characterized by warm anticyclones which extend throughout the depth of the troposphere. This suggests that thermal forcing is an unlikely mechanism in view of the consequent 180^{o} vertical phase shift. The only possible way in which thermally forced motion could be consistent with observations is if heating anomolies existed in the lower stratosphere. Lower stratospheric cooling could cause adiabatic descent and then lead to a warm anticyclone. Green (1977), in a brief study of the July '76 circulation, when a block was over Europe, showed that the stratospheric cooling rates would have to be prohibitively large to account for the observed intensity of the blocking. Instead, Green suggested that the block could be mechanically driven by the action of eddies on the scale of weather systems: he supposed that depressions move to the north and south in the split jet and produce at upper levels anomalous vorticity

forcing, which maintains blocking in that region. Descent of air transfers vorticity from upper to lower levels and ensures that the anticyclone becomes warm. Surface friction eventually removes anticyclonic vorticity at low levels, maintaining a steady circulation. Therefore the blocking anticyclone and the warming of the troposphere are dynamically driven by the action of synoptic scale eddies. Because the weather systems are generated in the baroclinic zones, the split jet and their associated baroclinic zones are not only symptoms of blocking, as it is normally assumed in synoptic analysis, but become an essential feature of the maintenance of the system.

An observational study to investigate whether moving weather disturbances are important for the maintenance of quasi-stationary phenomena, like blocking, was made by Savijarvi (1977). He compared vorticity and temperature balances for a blocking case, and a non-blocking case. The effect of large scale Reynolds stresses was found to be important, but systematic differences between the two cases were not evident. However his results were not conclusive, possibly because his choice of averaging period over-emphasized the role of mean processes.

Further case studies of intense blocks need to be carried out in order to test hypotheses and so gain an understanding of their initiation, maintenance and decay.

2.2 Mean motion and the action of the eddies

2.2.1 Introduction

To verify models of climate and of the general circulation of the atmosphere, it is important to know, not only the statistics of basic

climatological variables,but also the way in which physical balances are fulfilled with respect to vorticity, heat, energy, etc.

In the diagnostic studies of the atmosphere designed for this purpose, the emphasis has been mainly put on the zonally-averaged state (e.g. Oort and Rasmusson, 1971). An important question to ask, however, is how the balance requirements are fulfilled locally. Aspects of this problem have been considered in some recent studies (Holopainen, 1978, 1981; Lau, 1979).

It is the effect of the large scale eddies on the time-mean local flow in a blocking episode, which is the principal object of this study.

Suppose there is an arbitrary variable χ, governed by the advective equation $\frac{D\chi}{Dt} = 0$. The variable χ is split into a time-averaged and mean part:

$$\chi = \overline{\chi} + \chi'$$

where $\overline{\chi}$ is the mean component over some fixed period

χ' is the deviation from the mean, or the transient component.

Although by definition $\overline{\chi'} = 0$, $\overline{\chi}$ can be altered by the eddy-field if correlations of $\underset{\sim}{v}'$ with χ' give rise to non-zero divergence of the eddy-flux of χ, $\overline{\underset{\sim}{v}'\chi'}$. Eddy transfer is introduced by substituting into the advective term and time-averaging.

The equation for $\overline{\chi}$ becomes:

$$\frac{\overline{D}\overline{\chi}}{Dt} = -\overline{\underset{\sim}{v}' \cdot \nabla \chi'} = -\nabla \cdot \left(\overline{\underset{\sim}{v}'\chi'}\right)$$

if $\underset{\sim}{v}$ is not divergent.

The interaction between transient eddies and the time-mean flow clearly depends on the averaging period. Many studies have been based on yearly averages and some on seasonal averages (Blackmon (1977) and Lau (1979)). We consider a month to be a suitable average for our purposes because it is long enough to include several transient systems and not so long as to average out the anomalous circulation.

2.2.2 Momentum equation for large-scale motion

The horizontal momentum equation (neglecting friction) in pressure coordinates is:

$$\frac{\partial \underset{\sim}{v}}{\partial t} = -\left(\underset{\sim}{v}\cdot\nabla_H\right)\underset{\sim}{v} - \omega\frac{\partial \underset{\sim}{v}}{\partial p} - f\,\underset{\sim}{k}\wedge\underset{\sim}{v} - \nabla_H\phi \qquad \text{—(2.1)}$$

where $\underset{\sim}{v} = (u,v)$ is the horizontal velocity with components u and v in the zonal and meridional directions

$\omega = \frac{Dp}{Dt}$ is the pressure velocity

f : the Coriolis parameter

ϕ : geopotential

∇_H : horizontal gradient operator $\left[\left(\frac{\partial}{\partial x}\right)_p, \left(\frac{\partial}{\partial y}\right)_p\right]$

In order to separate mean and eddy processes, we split the variables into mean and eddy components, substitute them into Eqn.(2.1) and average to give:

$$\frac{\partial}{\partial t}\underset{\sim}{\bar{v}} = -\left(\underset{\sim}{\bar{v}}\cdot\nabla_H\right)\underset{\sim}{\bar{v}} - \bar{\omega}\frac{\partial}{\partial p}\underset{\sim}{\bar{v}} - \nabla_H\bar{\phi} - f\,\underset{\sim}{k}\wedge\underset{\sim}{\bar{v}} + \underset{\sim}{R}_H - \frac{\partial}{\partial p}\left(\overline{\omega'\underset{\sim}{v}'}\right) \qquad \text{—(2.2)}$$

	(A)	(B)	(C)	(D)	(E)	(F)
m s^{-2}						
10^{-6}	10^{-4}	*	10^{-3}	10^{-3}	10^{-4}	*

The terms labelled by * cannot be evaluated using our data: station data of T, U and V and N.M.C. analysis of h, u, v, and T.

where typical magnitudes are for mid-tropospheric monthly mean conditions (Savijarvi, 1977). The local change in the mean horizontal wind is small compared with other terms, which thus have to balance one another. The terms are:

(A) and (B) : horizontal and vertical mean advection of the mean flow

(C) : the mean pressure gradient acceleration

(D) : Coriolis acceleration

(E) and (F) : large-scale turbulence (eddy-forcing).

Holopainen (1978) showed that mean and eddy vertical advection of momentum (terms labelled by *) were small, so that to good approximation we can simplify Eqn.(2.2) by:

$$\frac{\partial}{\partial t}\underset{\sim}{\bar{V}} = -\left(\underset{\sim}{\bar{V}}\cdot\nabla_H\right)\underset{\sim}{\bar{V}} - \nabla_H\bar{\varphi} - f\underset{\sim}{k}\wedge\underset{\sim}{\bar{V}} + \underset{\sim}{R}_H \qquad \text{—(2.3)}$$

where $\underset{\sim}{R}_H$ is the horizontal forcing term by the eddies due to the correlation of horizontal velocity components (Reynolds stresses):

$$R_x = -\frac{\partial}{\partial x}\overline{u'^2} - \frac{\partial}{\partial y}\overline{u'v'}$$

$$R_y = -\frac{\partial}{\partial x}\overline{u'v'} - \frac{\partial}{\partial y}\overline{v'^2}$$

It is convenient to write $\underset{\sim}{R}_H$ in the form:

$$\underset{\sim}{R}_H = -\overline{\underset{\sim}{V}'\nabla_H\underset{\sim}{V}'} = -\nabla_H\frac{\overline{(u'^2+v'^2)}}{2} - \underset{\sim}{k}\wedge\overline{\left(\underset{\sim}{V}'\zeta'\right)}$$

where $\overline{\underset{\sim}{v}'\zeta'}$ is the eddy-relative vorticity flux. If we add the term $\overline{\frac{1}{2}(u'^2+v'^2)}$ to the pressure term (it does not affect the generation of mean vorticity), Eqn.(2.3) can be rewritten:

$$\frac{\partial}{\partial t}\underset{\sim}{\bar{V}} = -\left(\underset{\sim}{\bar{V}}\cdot\nabla_H\right)\underset{\sim}{\bar{V}} - \nabla_H\left[\bar{\varphi} + \frac{1}{2}\overline{(u'^2+v'^2)}\right] - f\underset{\sim}{k}\wedge\underset{\sim}{\bar{V}} - \underset{\sim}{k}\wedge\overline{\left(\underset{\sim}{V}'\zeta'\right)} \qquad \text{—(2.4a)}$$

where $\overline{u'\zeta'} = -\frac{1}{2}\frac{\partial}{\partial y}\left(\overline{u'^2 - v'^2}\right) + \frac{\partial}{\partial x}\left(\overline{u'v'}\right)$ —(2.4b)

and

$$\overline{v'\zeta'} = -\frac{1}{2}\frac{\partial}{\partial x}\left(\overline{u'^2 - v'^2}\right) - \frac{\partial}{\partial y}\left(\overline{u'v'}\right)$$

are the zonal and meridional fluxes of relative vorticity and

$\overline{u'v'}$ represents the transfer of zonal momentum by meridional wind and also the transfer of meridional momentum by zonal winds

and

$\overline{u'^2 - v'^2}$ represents the transfer of SW-NE component of momentum by NW-SE component of the wind:

$$\frac{1}{2}\left(\overline{u'^2 - v'^2}\right) = \frac{1}{\sqrt{2}}\overline{(u' + v')}\,\frac{1}{\sqrt{2}}(u' - v')$$

2.2.3 Vorticity equation for large scale motion

The vorticity equation for the time-mean motion obtained from Eqn.(2.2) is:

$$\frac{\partial}{\partial t}\bar{\zeta} = -\left(\bar{\underset{\sim}{V}}\cdot\nabla_H\right)\left(\bar{\zeta} + f\right) + \underset{\sim}{k}\cdot\nabla_H\wedge\underset{\sim}{R}_H + f\frac{\partial\bar{\omega}}{\partial p} + \left[\bar{\zeta}\frac{\partial\bar{\omega}}{\partial p} - \bar{\omega}\frac{\partial\bar{\zeta}}{\partial p} - \underset{\sim}{k}\cdot\nabla_H\bar{\omega}\wedge\frac{\partial\bar{\underset{\sim}{V}}}{\partial p} + \underset{\sim}{k}\cdot\nabla_H\wedge\left(\frac{\partial}{\partial p}\left(\overline{\omega'\underset{\sim}{V}'}\right)\right)\right] \quad —(2.5)$$

where $\zeta = \underset{\sim}{k}\cdot\nabla\wedge\underset{\sim}{V}$ is the vertical component of the relative vorticity.

Observations indicate that, for the large scale circulation above the boundary layer, the terms in parenthesis are (at least in middle and high latitudes) small[1] (see Lau (1979), Holopainen (1978)), allowing us to simplify Eqn.(2.5) to:

---

1. Lau 1979 evaluated the $\overline{\omega'\chi'}$ term using the ω from an operational forecast model and showed that the $\underset{\sim}{k}\cdot\nabla_H\wedge\frac{\partial}{\partial p}\left(\overline{\omega'\underset{\sim}{V}'}\right)$ term is an order of magnitude smaller than the $\underset{\sim}{k}\cdot\nabla_H\wedge\underset{\sim}{R}_H$ term.

$$\frac{\partial \bar{\zeta}}{\partial t} = -\left(\bar{\underset{\sim}{v}} \cdot \nabla_H\right)\left(\bar{\zeta} + f\right) + \underset{\sim}{k} \cdot \nabla_H \wedge \bar{\underset{\sim}{R}}_H + f\frac{\partial \bar{\omega}}{\partial p} \qquad \text{—(2.6)}$$

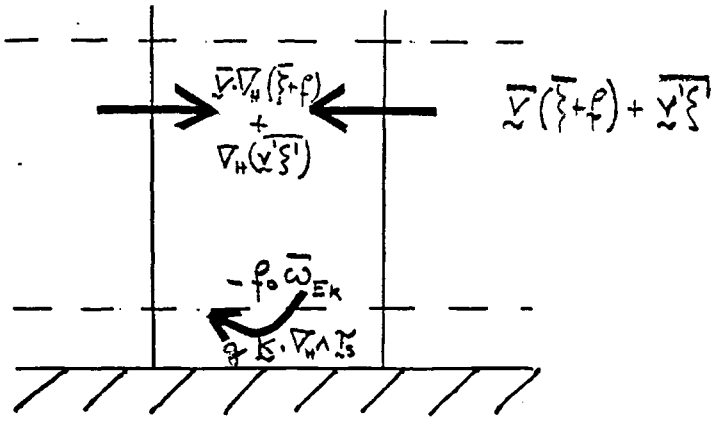
(A) (B) (C)

The terms (A) and (B) depend on horizontal velocities and represent the redistribution of vorticity in the horizontal: they have their largest amplitude in the upper troposphere, where the velocites are large.

The vortex stretching term (C) represents the redistribution of vorticity in the vertical, causing a vertical exchange of vorticity between different layers of the atmosphere. So the mean steady state vorticity balance in extratropical latitudes is:

$$0 = -\left(\bar{\underset{\sim}{v}} \cdot \nabla_H\right)\left(\bar{\zeta} + f\right) + \underset{\sim}{k} \cdot \nabla_H \wedge \bar{\underset{\sim}{R}}_H + f\frac{\partial \bar{\omega}}{\partial p} \qquad \text{—(2.6a)}$$

The balance of the various terms are shown schematically in the diagram below:



"Vorticity balance of an air column"

In the diagram the vertical velocity at the top of the surface boundary layer has been related to the surface stress.

The most important question for the purpose of this study is the relative contribution of mean and eddy transfer of vorticity in the maintenance of the mean vorticity pattern. In particular, we are interested in the role of the term:

$$\underset{\sim}{k}\cdot\nabla_H\wedge\underset{\sim}{R}_H=\frac{\partial^2}{\partial x\partial y}\left(\overline{u'^2}-\overline{v'^2}\right)+\left(\frac{\partial^2}{\partial y^2}-\frac{\partial^2}{\partial x^2}\right)\overline{(u'v')}=-\nabla_H\cdot\left(\overline{\underset{\sim}{v}'\zeta'}\right) \qquad —(2.7)$$

representing the convergence of the eddy vorticity flux associated with the transient system, which depends on the spatial distribution of the wind statistics $(\overline{u'v'},\ \overline{u'^2-v'^2})$

2.2.4 Thermodynamic equation for large-scale motion

The thermodynamic equation in pressure coordinates is:

$$\frac{\partial}{\partial t}T+\underset{\sim}{v}\cdot\nabla_H T-S_p\omega=H \qquad —(2.8)$$

where $S_p\equiv\frac{RT}{pc_p}-\frac{\partial T}{\partial p}=-\frac{T}{\theta}\frac{\partial\theta}{\partial p}$ is the static stability

R = gas constant

c_p = specific heat at constant pressure

$H=\dot{q}/c_p=$ is the diabatic heating ($\dot{q}$ is the rate of heating per unit mass due to radiation and latent heat release)

If we split, as before, the dynamical variables into time mean and eddy components and then time-average, the thermodynamic equation takes the following form:

$$\frac{\partial}{\partial t}\overline{T}+\overline{\underset{\sim}{v}}\cdot\nabla_H\overline{T}+\nabla_H\cdot\left(\overline{\underset{\sim}{v}'T'}\right)-S_p\overline{\omega}+\left[\frac{\partial}{\partial p}\left(\overline{\omega'T'}\right)-\frac{R}{pc_p}\left(\overline{\omega'T'}\right)\right]=$$

$$=\overline{H} \qquad —(2.9)$$

The terms in brackets represent the vertical eddy transport by eddies.

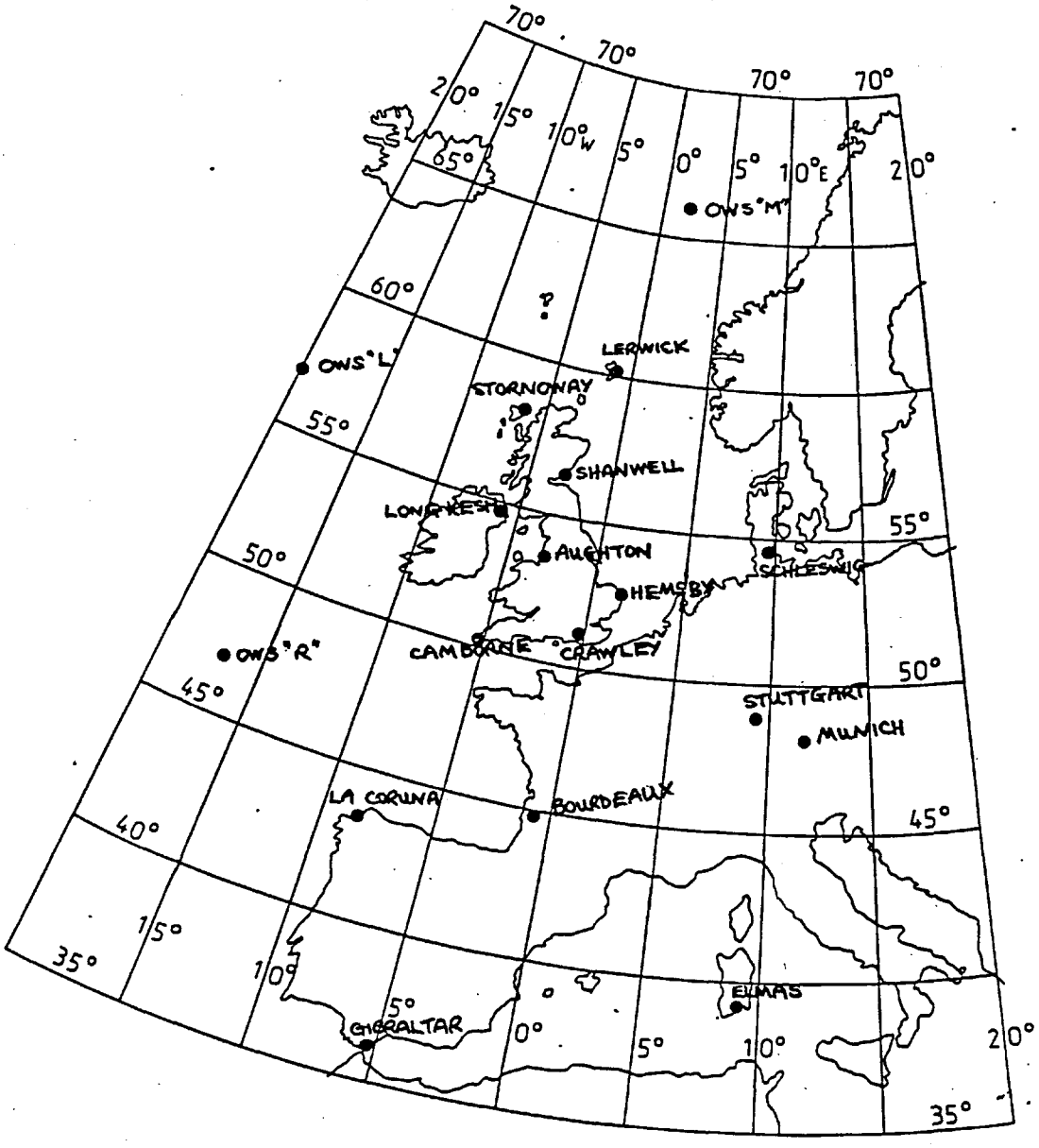


Fig.2.1 : European stations used to build wind statistic in the blocking area.

Statistics compiled by Lau (1979) have shown that the largest absolute values of these terms (which occur over the major oceanic tracks) are negligible in comparison with the net heating rates. Therefore, neglecting these terms, Eqn.(2.9) becomes:

$$\underbrace{\frac{\partial \overline{T}}{\partial t}}_{(A)} + \underbrace{\overline{\underset{\sim}{v}} \cdot \nabla_H \overline{T}}_{(A)} + \underbrace{\nabla_H \cdot \left(\overline{\underset{\sim}{v}'T'}\right)}_{(B)} - \underbrace{S_p \overline{\omega}}_{(C)} = \overline{H} \qquad \text{—(2.10)}$$

where:

(A) represents the advection of heat by the horizontal component of the mean flow

(B) represents the divergence of horizontal heat transport by the transient eddies

and

(C) the effects of time-mean vertical motions in advecting heat and in producing temperature changes due to adiabatic expansion and compression.

2.3 Transient eddies during Summer '76

In this section the diagnostics presented by Green (1977) on the July '76 circulation, using station data, have been extended.

2.3.1 Wind statistics from station data

Wind speed and wind direction, taken once a day (00. GMT) from the Aerological Data of the British Daily Weather Report for the British stationsand Atlantic ships, and from the European Meteorologica Bulletin (of the German Weather Service) for other European stations, are used to calculate wind statistics for Summer '76 over western and central Europe (Fig.2.1).

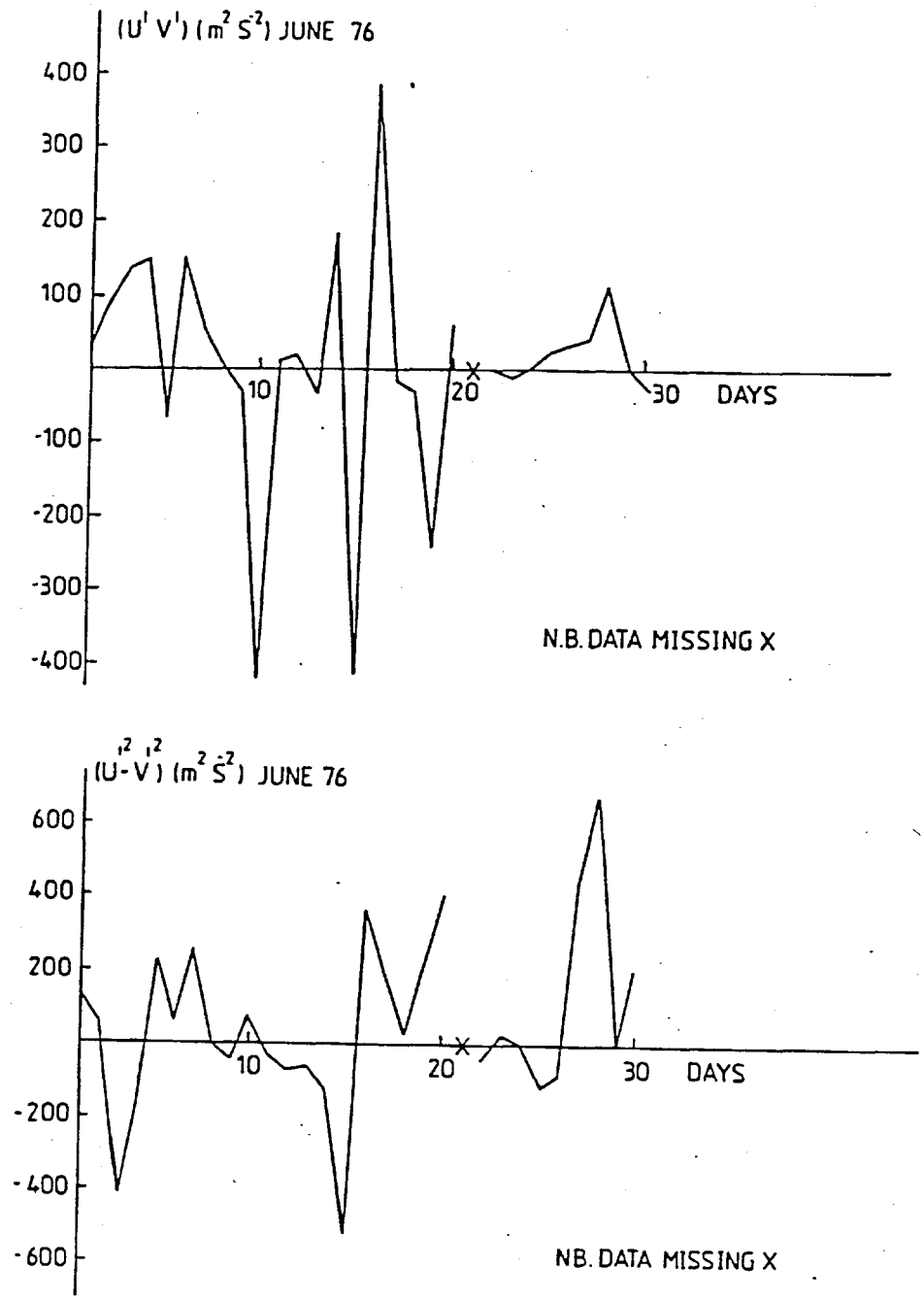


Fig.2.2 Temporal variation of momentum transfer at 500 mb during Summer '76 at Lerwick.

Eddy momentum transfer $(\overline{u'v'}, \overline{u'u'}, \overline{v'v'})$ is evaluated from monthly average wind $(\bar{u}, \bar{v})$ and monthly average products $(\overline{uv}, \overline{uu}, \overline{vv})$ in accordance with the following general expression:

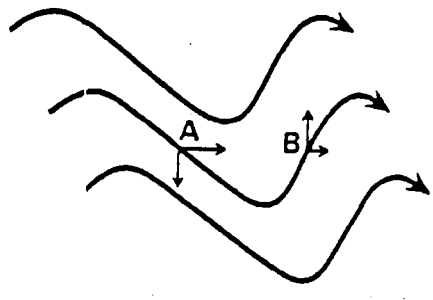
$\overline{ab} = \bar{a}\cdot\bar{b} + \overline{a'b'}$, where — is the monthly mean and ' the deviation from the monthly mean.

2.3.2 Reynolds stresses distribution

a) Temporal distribution

Analysis of the day-by-day contribution to the momentum transfer shows that this was intermittent and associated with the passage of intense depressions.

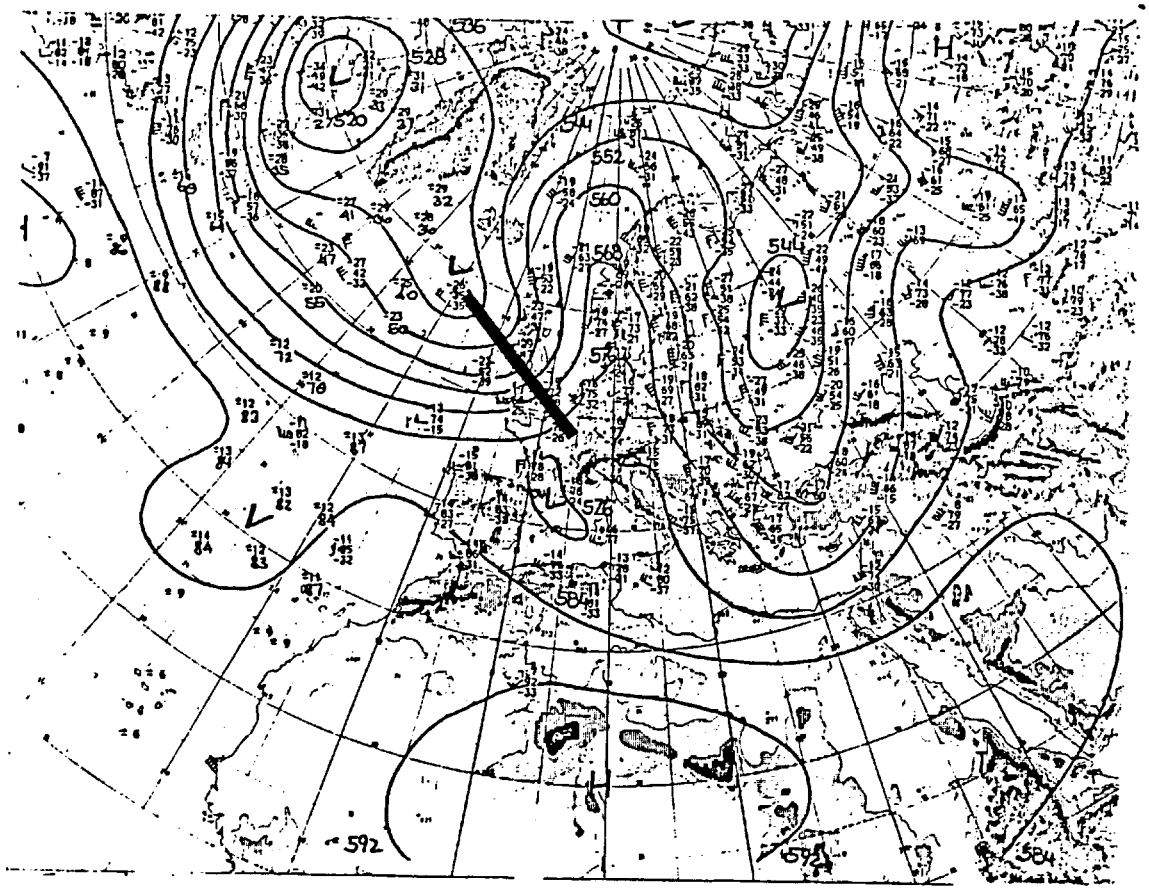
Fig. 2.2 shows graphs of momentum transfer as a function of time at Lerwick, north of the British Isles. Consider, for example, the graph of $u'v'$ for June at Lerwick at 500 mb. It shows that the day-by-day transfer can be positive or negative: the tilt with latitude of the trough-line of the depressions passing over the station, changes from day to day. A westward tilt with latitude of the trough-line means that the air moving equatorwards has a greater zonal component of velocity than air moving towards the pole, implying southwards transfers of momentum (see following diagram).



Orientation of a trough that carries westerly momentum southwards. Parcels of air at A and B have the same magnitude but opposite sign of northward velocity, but A has more westerly component of velocity than B.

from Green (1977)

a) 10 June '76 : u'v' < 0



b) 14 June '76 : u'v' > 0

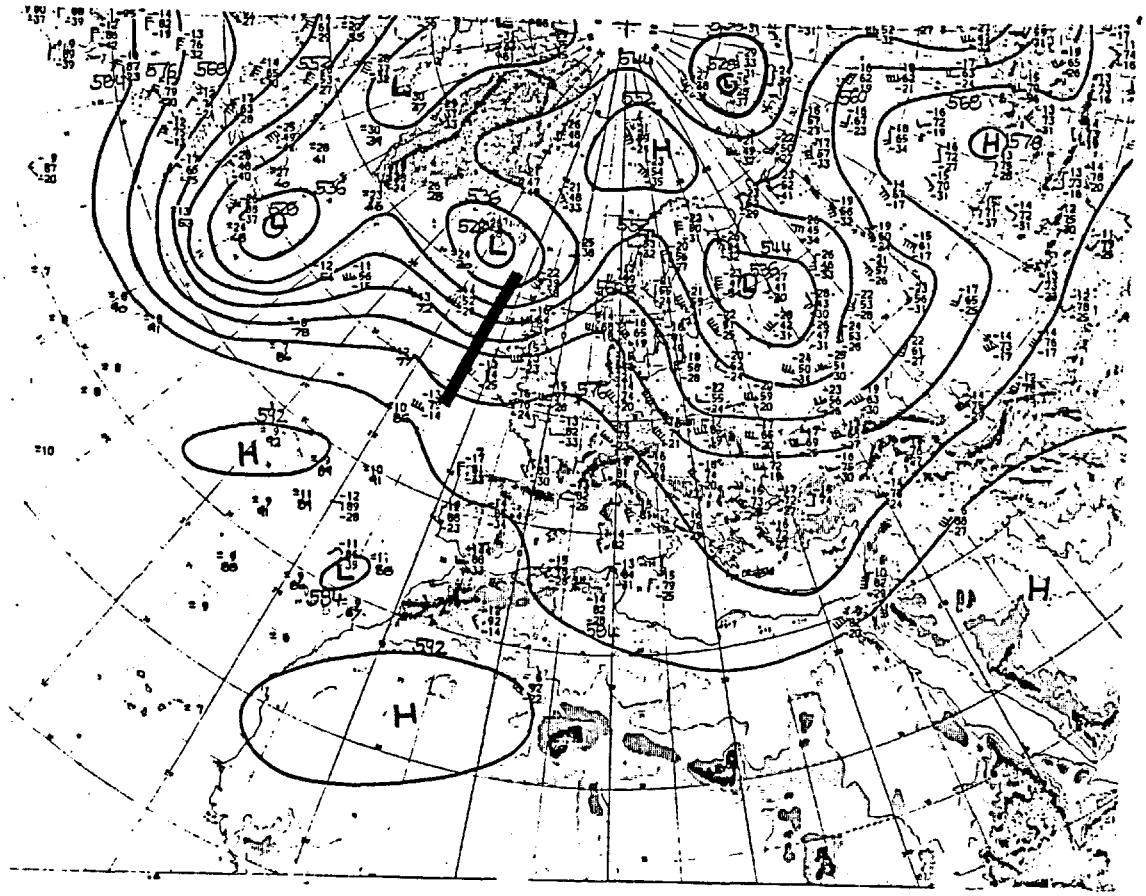


Fig.2.3: Momentum transfer and tilt of the trough line (thick black line) at 500 mb.

For example, on day 10, the transfer is southwards ($\overline{u'v'} < 0$) and the synoptic chart at 500 mb shows a trough over the British Isles with a westwards tilt (Fig. 2.3(a)). *Vice versa* on day 14, the transfer is northwards ($\overline{u'v'} > 0$) and the synoptic chart shows an eastwards tilt of the trough (Fig. 2.3(b)).

It is also interesting that not all the depressions result in a maximum momentum transfer. Perhaps this is not surprising, taking into consideration the relatively short scale of the summer weather systems and the complex variations of the transfer properties across them.

b) Vertical distribution

The plots of $\overline{u'v'}$ and $\overline{u'^2-v'^2}$ as a function of height at different stations, show that the transfer of momentum by the eddies is somewhat larger in the upper troposphere compared with the lower. For example, Fig.2.4 shows the distribution of $\overline{u'v'}$ and $\overline{u'^2-v'^2}$ as a function of height for June '76 at Lerwick. This is largest between 300 and 200 mb as is normally observed. The transfer is larger during the drought period than the zonal average (Oort and Rasmusson, 1971) and the annual average at the same station (Buch, 1950); thereby the suggestion that anomalously high momentum transfer is a feature of the blocking episode, gains a measure of support.

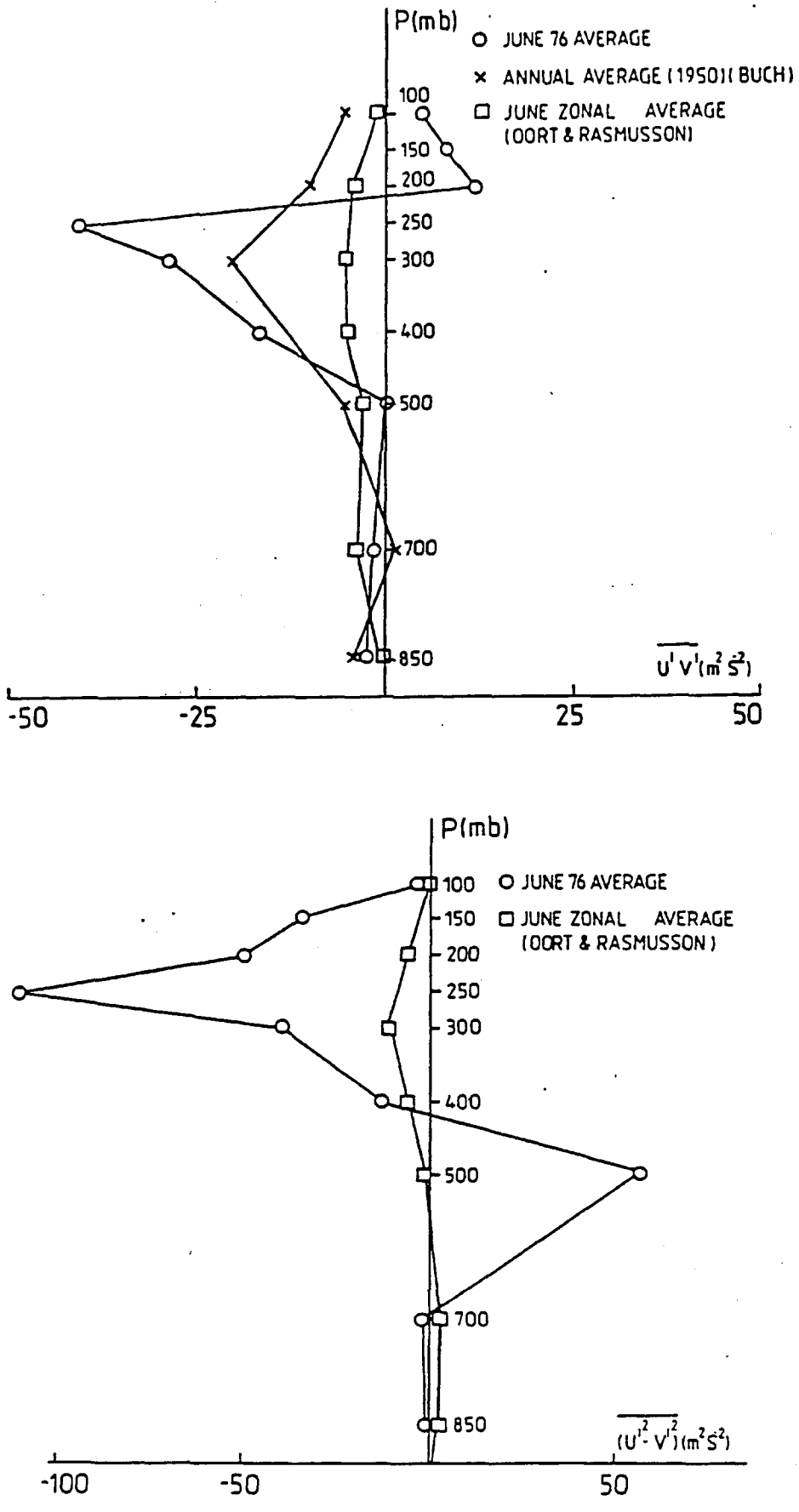


Fig.2.4: Vertical distribution of momentum transfer at Lerwick ($\sim 60^{\circ}$N) for June '76, compared with the annual average at the same station, and the zonal average at the same latitude.

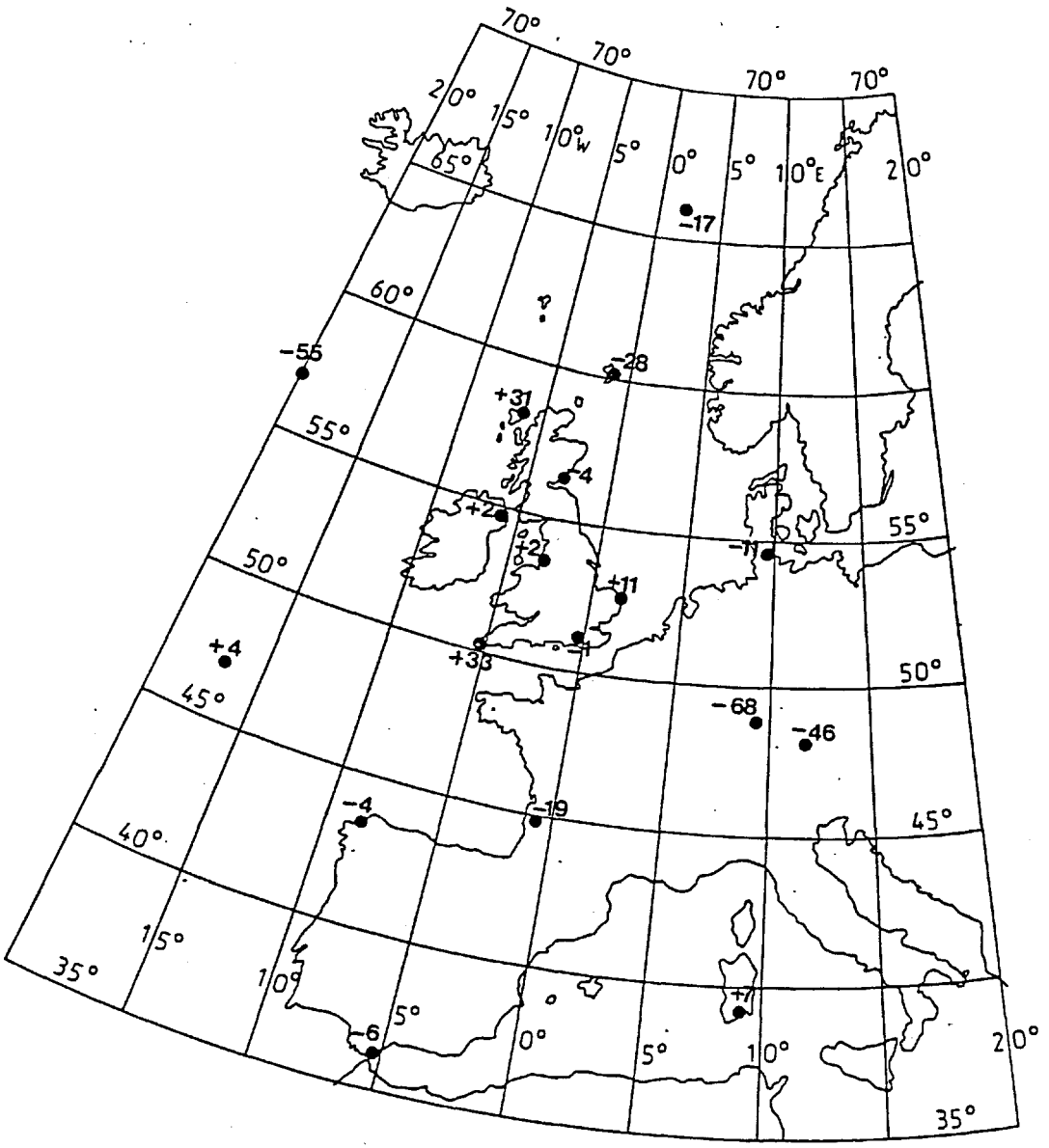
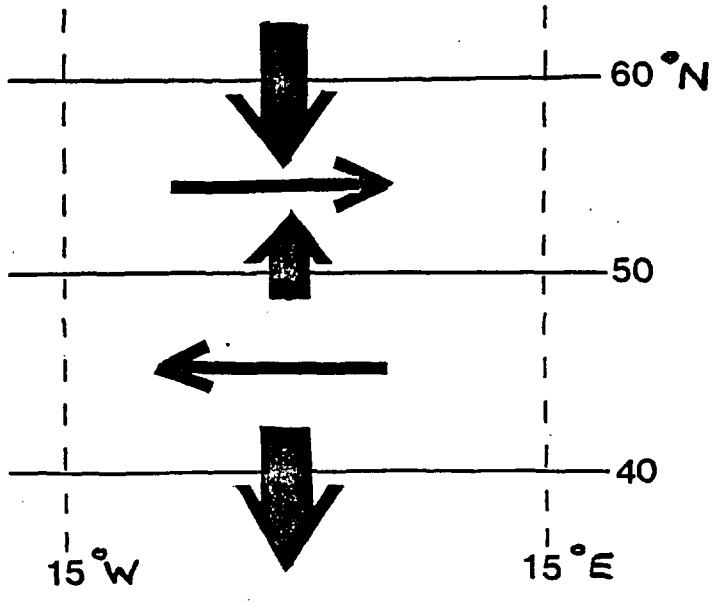


Fig.2.5: Horizontal distribution of momentum transfer $\overline{u'v'}$ (m^2s^{-2}) at 300 mb for June '76.

c) Horizontal distribution

Since the momentum transfer is peaked at upper levels, the 300 mb level has been chosen to show the horizontal distribution. Fig.2.5 shows the spatial distribution of $\overline{u'v'}$ at this level. There is southward transfer of westerly momentum north of the British Isles, northward transfer over the British Isles, N.W. Europe, and southwards transfer south of the British Isles, over Italy and eastern and central Europe. We show this schematically below:



As pointed out in Green (1977), the magnitude of the southward transfer of westerly momentum is typical of this region during the summer. What is unusual is the small northwards flux over the British Isles around 50°N. Normally it is southwards here. The meridional gradients of this momentum transfer result in an accelerating tendency between 60° and 50° N and a decelerating one between 50° and

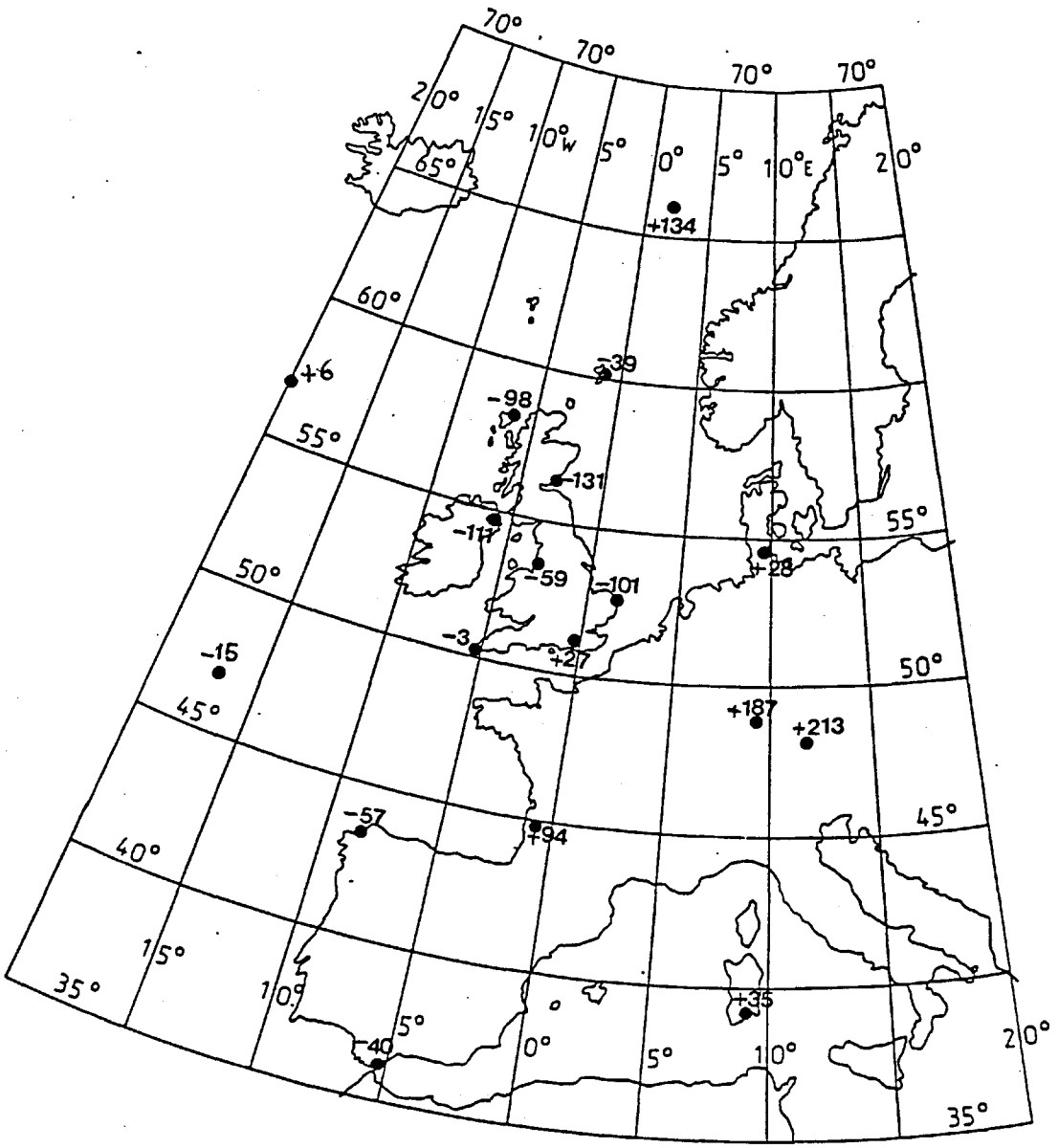


Fig.2.6: Horizontal distribution of momentum transfer $\overline{u'^2-v'^2}$ (m^2s^{-2}) at 300 mb for June '76.

40°N, i.e. such as to generate anticyclonic circulation. This led Green to suppose that anomalous momentum transfer may be an important process in the dynamics of the anticyclone.

However, meridional gradients of $\overline{u'v'}$ do not take into account the total forcing of the mean by the eddies, as we can see from Eqn.(2.4). The mean zonal wind is forced not only by the meridional gradients of $\overline{u'v'}$ but also by longitudinal gradients of $\overline{u'^2-v'^2}$. A map of $\overline{u'^2-v'^2}$ for June at 300 mb is presented in Fig.2.6. This quantity is predominantly negative over the British Isles and positive over Europe. To the west of the British Isles the longitudinal gradient is strongly positive and so this term tends to decelerate the zonal flow in opposition to the meridional gradient of $\overline{u'v'}$.

In the zonal average, only the $\overline{u'v'}$ term can force the zonal mean flow, but here zonal gradients of $\overline{u'^2-v'^2}$ are of comparable importance and their contribution must be taken into account.

Eqn.(2.4) shows that we must look at the vector flux of eddy relative vorticity to determine the net effect of eddies in the momentum equation. Lau (1978), Lau and Wallace (1979) have shown that this eddy flux often has a large rotational component, particularly at upper levels. With this in mind we split the eddy flux into its rotational and divergent components:

$$\overline{\underset{\sim}{V}'\zeta'} = \underset{\sim}{R}_{ot} + \underset{\sim}{D}_{iv} \qquad \underset{\sim}{R}_{ot} = -\underset{\sim}{k} \wedge \nabla\Psi$$

where Ψ is the potential for $\underset{\sim}{R}_{ot}$

and rewrite the momentum equation (2.4) as follows:

$$\frac{\partial}{\partial t}\underset{\sim}{\bar{V}} = -\left(\underset{\sim}{\bar{V}}\cdot\nabla_H\right)\underset{\sim}{\bar{V}} - \nabla_H\left[\bar{\Phi} + \frac{1}{2}\left(\overline{u'^2+v'^2}\right) + \Psi\right] - \underset{\sim}{k} \wedge \left(\overline{\underset{\sim}{V}'\zeta'}\right)_{Div} \qquad -(2.11)$$

So if we look at the total vorticity flux, $\overline{\underset{\sim}{v}'\xi'}$ (Eq.2.4) and try to measure the eddy contribution through the horizontal gradients of $\overline{u'v'}$ and $\overline{u'^2-v'^2}$ we may include a large rotational component, which cannot generate vorticity.

It seems sensible, therefore, to discuss the dynamics of our anti-cyclone directly in terms of vorticity and vorticity flux divergence. Since this requires the evaluation of second derivatives of Reynolds stresses (an impossible task using our sparse station data) in the next chapter we will use NMC gridded data.

CHAPTER 3

VORTICITY AND HEAT BUDGETS

3.1 Gridded data

3.1.1 Introduction

In this Chapter diagnostics of the Summer 1976 blocking anticyclone are presented, using the twice daily gridded data of the National Meteorological Center (NMC). Attention is focussed on the month of July, when the block was at its peak, and on a region covering Western and Central Europe.

3.1.2 NMC analysis

The compilation of high space and time resolution statistics of the general circulation is central to the understanding of the dynamics of climate. This often involves the transformation of observed values, taken on an irregular array of stations, to a regular mesh. Difficulties arise over data-sparse regions such as the oceans and other remote regions. These gaps exist even in the middle latitudes of the Northern Hemisphere. Fig.3.1(a) (from Lau and Oort, 1981) shows the distribution of reporting radiosonde stations during a typical month in the early 1970's. A method of filling in such gaps is required. One such method, called global analysis, is to use short-range forecast models to help interpolate the observations on to a regular mesh and fill up the data-sparse regions. The NMC analysis is of this type and provides a particularly convenient data base from which to build large-scale circulation

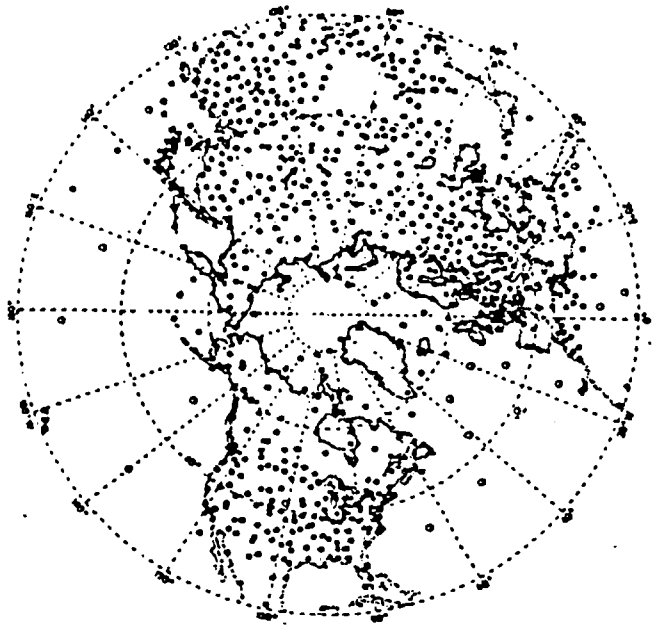
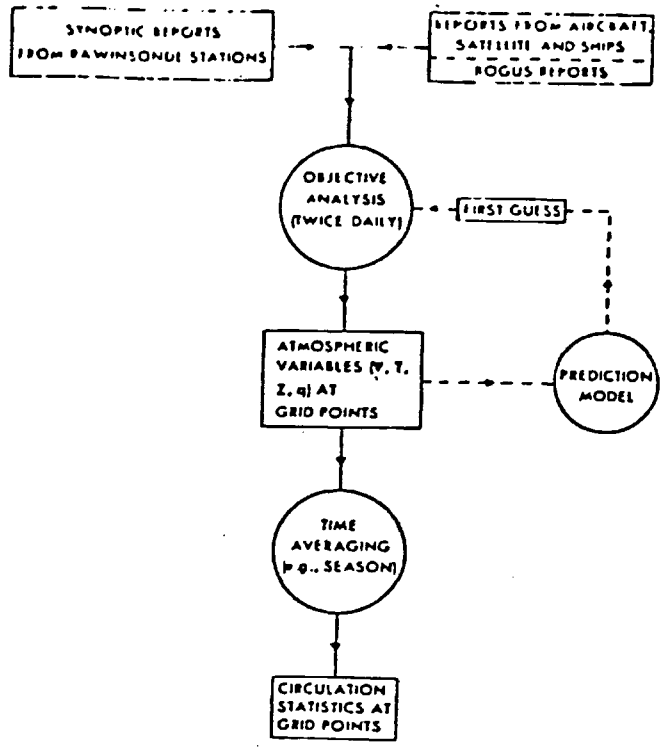


Fig.3.1: a) Distribution of reporting rawinsonde stations during the month of January 1971 (from Lau and Oort, 1981).



(NMC)

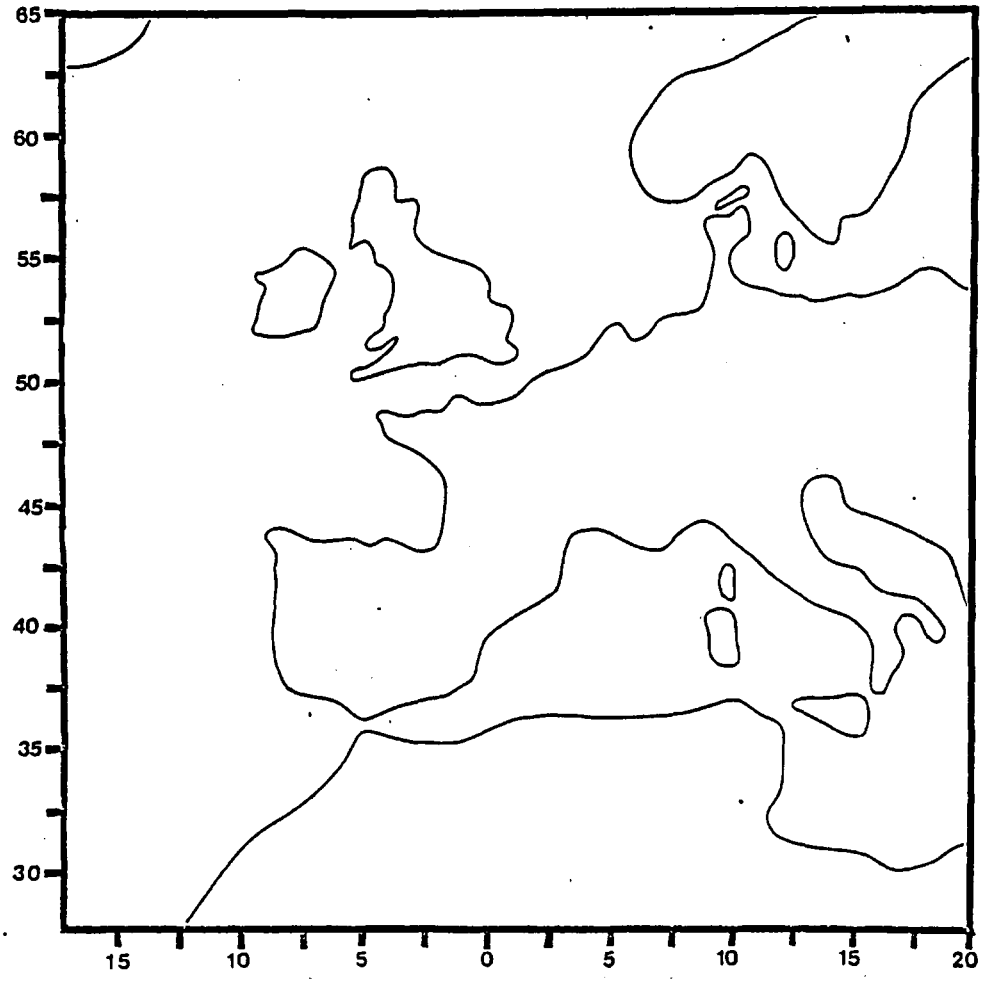
Fig.3.1: b) Flow diagram to illustrate the processing scheme for compiling general circulation statistics by N.M.C.

statistics. They incorporate observations from radiosonde, satellite and aircraft, the data are gridded and ordered, and so relatively straightforward to manipulate. However, uncertainties do exist in using NMC analysis for building statistics because the analysis was designed for operational weather forecasts, rather than for climate research.

The initial guess field used by NMC for the global analysis is taken from a (12 h) forecast, produced by the global prediction model. Any observation which varies greatly from the forecast is liable to be modified, or even rejected, on the grounds that it would otherwise create spurious gravity waves in the prediction model (Fig.3.1(b)). Therefore the prediction model acts to filter the observations, removing noise, but also perhaps some real information. However, comparison between statistics computed from conventional data and NMC analysis (Rosen and Salstein, 1980) showed that gridded data suffers less from gaps in the data, because they also incorporate satellite and aircraft measurements. There are some problems in the tropics due to the elimination of mean meridional circulation (wind is forced to be essentially non-divergent in the analysis process) but north of 30^{o} Rosen and Salstein conclude that gridded data may be superior to the station data in several respects. The most important advantage is that the analysis is consistent and far easier to manipulate and work with than station data.

The NMC data set, used in this diagnostic study, consists of the twice-daily (00 and 12 h GMT) analysis of geopotential height, wind, temperature and humidity on a 2.5^{o} horizontal grid covering the globe at 12 levels in the vertical (1000, 850, 700, 500, 400, 300, 250, 200, 150, 100, 70, and 50 mb). Monthly mean and eddy statistics have been

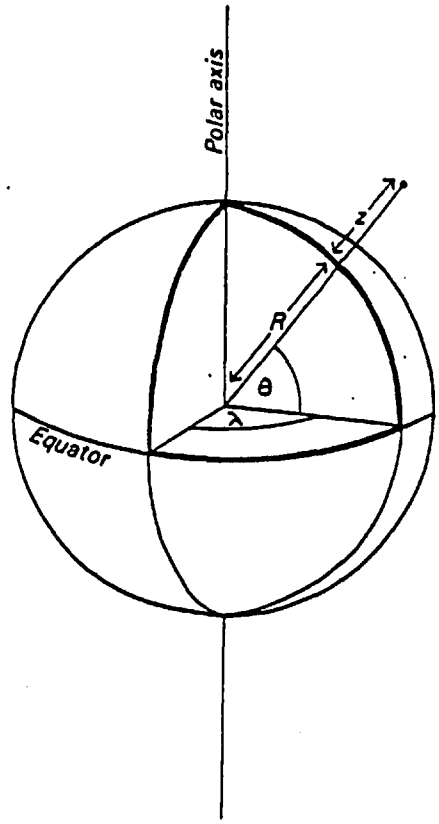
evaluated at the different levels on à 20 x 20 grid, from 22.5°N to 70°N and from 22.5°W to 25°E, covering western, northern and central Europe and centred on the blocking anticyclone (see diagram below):



3.2 The spherical polar formulation

3.2.1 Introduction

A spherical polar system, in which the basic coordinates λ, ϑ and z - respectively longitude, latitude and height above the earth, is used to express the vorticity and thermodynamic equations, as illustrated in the following diagram:



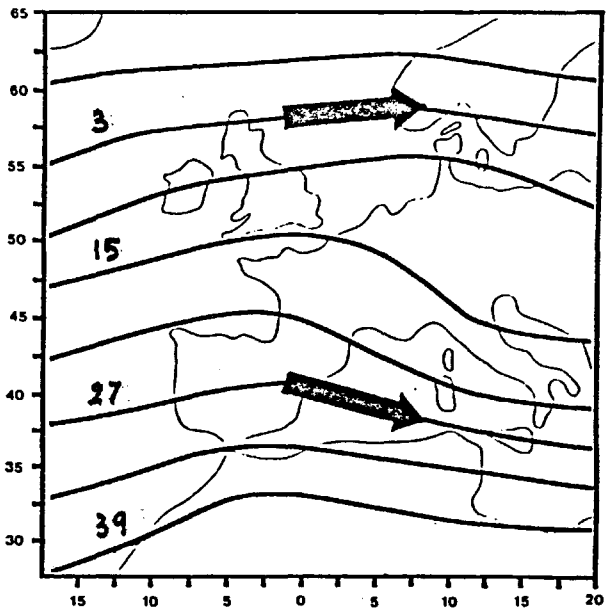
Note that in this system the horizontal divergence operator is:

$$\nabla_H \cdot \underset{\sim}{A} = \frac{1}{R\cos\vartheta}\left[\frac{\partial}{\partial\lambda}(A_\lambda) + \frac{\partial}{\partial\vartheta}(A_\vartheta \cos\vartheta)\right]$$

3.2.2 Vorticity and thermodynamic equations

The steady state vorticity equation (Eqn.(2.6)) in spherical coordinates is:

$$\underbrace{\frac{\bar{u}}{R\cos\vartheta}\frac{\partial}{\partial\lambda}\bar{\xi} + \frac{\bar{v}}{R}\frac{\partial}{\partial\vartheta}(\bar{\xi}+f)}_{\text{mean flow advection of absolute vorticity}} + \underbrace{\frac{1}{R\cos\vartheta}\left(\frac{\partial}{\partial\lambda}\overline{u'\xi'} + \frac{\partial}{\partial\vartheta}\left(\overline{v'\xi'}\cos\vartheta\right)\right)}_{\text{eddy-vorticity flux divergence}} = \underbrace{f_0\frac{\partial\bar{\omega}}{\partial p}}_{\text{vortex stretching}} \qquad \text{—(3.1)}$$



$\delta\bar{R} = \bar{R} - \bar{R}_A$

$\bar{R}_A = 927$ dam

Fig.3.2 : a) July '76 mean height of the 300 mb surface. Thin black line: contour height $\delta\bar{R}$ (dam), as deviation from hemispheric averaged values $\bar{R}_A$ Black arrows: position of the split jet.

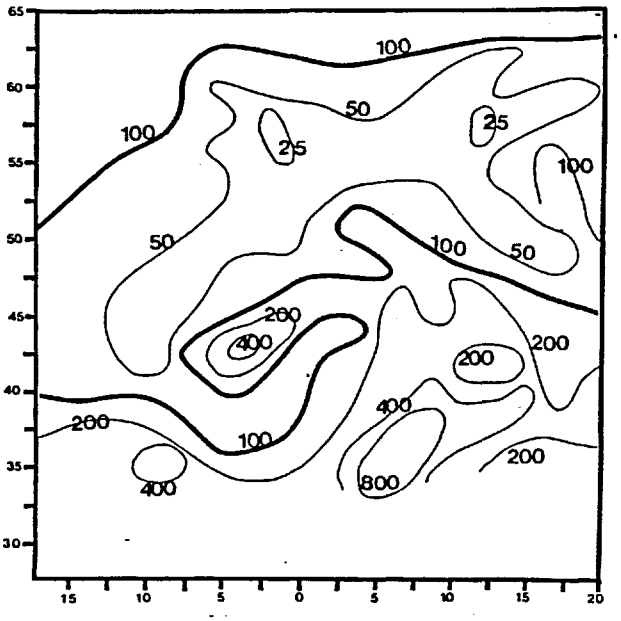


Fig.3.2 : b) July '76 rainfall expressed as a percentage of 1931-60 average.

where:

$$\zeta = (\text{curl}\ \underset{\sim}{v})_z = \frac{1}{R\cos\vartheta}\left(\frac{\partial v}{\partial\lambda} - \frac{\partial}{\partial\vartheta}(u\cos\vartheta)\right)$$

In the same system, the steady-state thermodynamic equation (Eqn. (2.10)) is:

$$\underbrace{\frac{\bar{u}}{R\cos\vartheta}\frac{\partial\bar{\pi}}{\partial\lambda} + \frac{\bar{v}}{R}\frac{\partial\bar{\pi}}{\partial\vartheta}}_{\text{mean flow advection of temperature}} + \underbrace{\frac{1}{R\cos\vartheta}\left(\frac{\partial}{\partial\lambda}\overline{u'\pi'} + \frac{\partial}{\partial\vartheta}\left(\overline{v'\pi'}\cos\vartheta\right)\right)}_{\text{eddy-heat flux divergence}} - \quad (3.2)$$

$$\underbrace{-\ S_p\bar{\omega}}_{\substack{\text{adiabatic heating due} \\ \text{to vertical motion}}} = \underbrace{\bar{H}}_{\text{diabatic heating}}$$

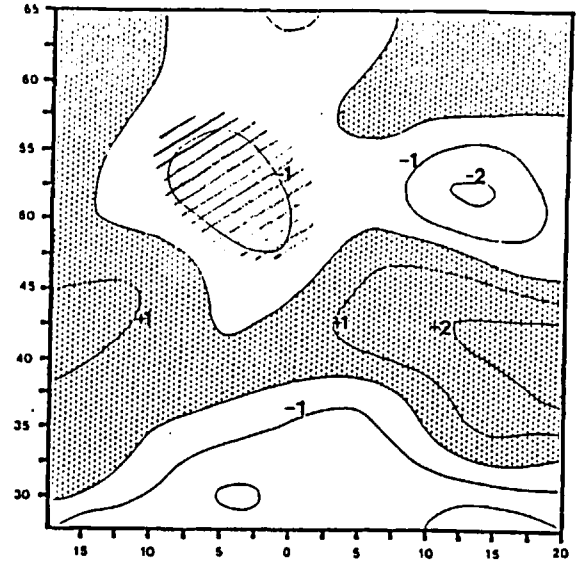
Terms in Eqns. (3.1) and (3.2) are evaluated using space centred difference approximations.

3.3 Mean flow

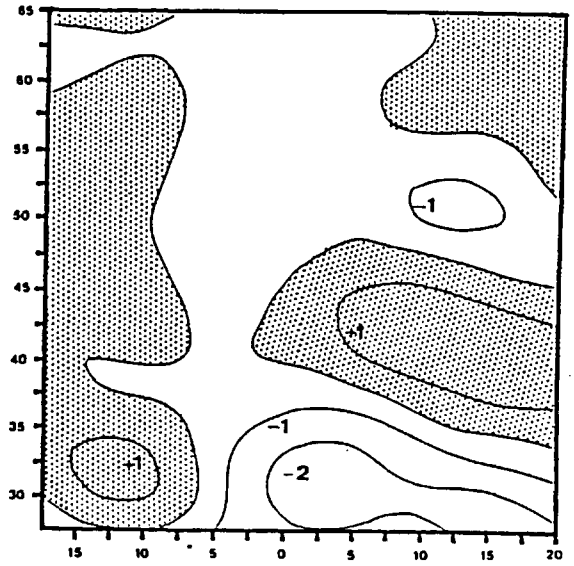
The mean height of the 300 mb surface for July '76 is shown in Fig. 3.2(a). A ridge is blocking the zonal flow, which is split into two branches, one passing poleward and the other equatorward of the ridge: a typical "blocking" configuration, in accordance with our description of Chapter 1.

The mean relative vorticity, Fig. 3.3, shows an extensive anticyclonic region covering a large part of Europe. It has two maxima of about $2 \times 10^{-5}\ s^{-1}$ (or 1/5 the local value of f): one to the west, the other to the east of the British Isles. Their position is consistent with the observation that the anticyclone moved systematically during the month (see Chapter 1). The highs were concentrated predominantly towards the west during the first half of the month and towards the east during the second half, giving the observed double maxima in the

a) 300 mb



b) 500 mb



c) 700 mb

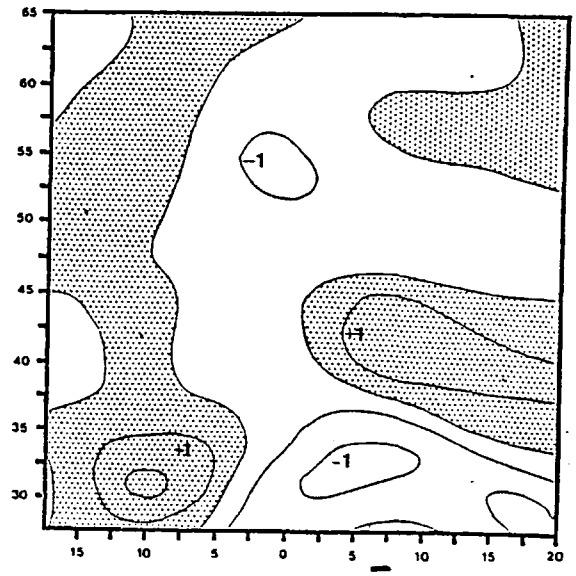


Fig.3.3 : Mean relative vorticity $\bar{\zeta}$ ($10^{-5}s^{-1}$). CI = 1 $10^{-5}s^{-1}$.
Dotted region: cyclonic vorticity.
White region: anticyclonic vorticity.
For area integral over hatched area in Fig.3.3(a) see section 3.7.1.

monthly mean. Many of our monthly mean statistics show this bi-modal structure due to the shift of the blocking centre during the averaging period.

The ridge and associated anticyclone extend through the whole depth of the atmosphere. It is particularly vertically coherent above 500 mb (the phase lines are vertical), where it is most intense. The maximum anticyclonic vorticity occurs at 300 mb. The distribution of the monthly mean rainfall deficit (Fig.3.2(b)) is well correlated with the mean vorticity pattern: the rainfall tends to be low towards the centre of the anticyclone, suggesting that weather systems were steered to the north or to the south, by the split jet, resulting in the low precipitation in between.

3.4 Maintenance of the mean vorticity

3.4.1 Introduction

We are interested in the processes which transported vorticity into the blocking region to maintain the monthly mean anticyclonic vorticity pattern against frictional dissipation at the ground. Here the contribution of vorticity advection by mean flow and eddies is evaluated.

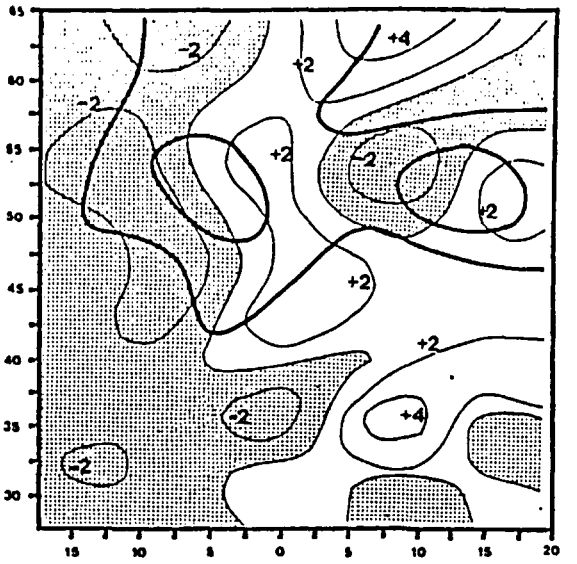
3.4.2 Mean flow advection: $\bar{\underset{\sim}{v}} \cdot \nabla_H \bar{\xi}$

The term ($\bar{\underset{\sim}{v}} \cdot \nabla_H \bar{\xi}$) has been evaluated at each standard pressure level. Fig.3.4 shows the distribution of ($\bar{\underset{\sim}{v}} \cdot \nabla_H \bar{\xi}$) at 300, 500 and 700 mb. The major features of the 300 mb relative vorticity pattern (the thick black line) are superimposed so that the field can be viewed relative to the block.

The mean flow advection reaches a maximum at 300 mb where the

a) 300 mb

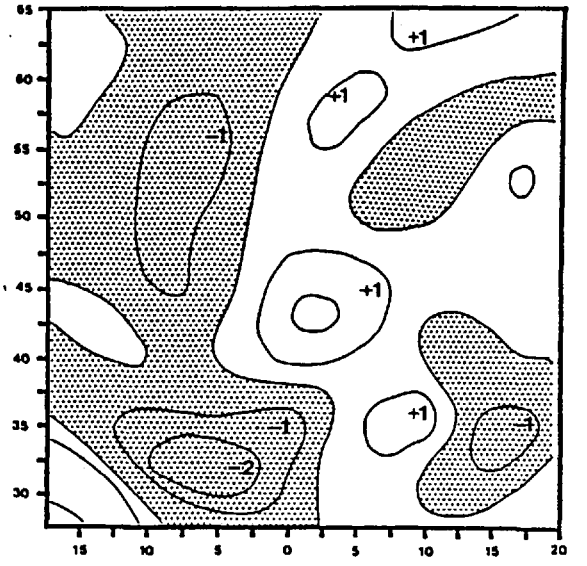
CI=2 $10^{-10}s^{-2}$



$\bar{v} \cdot \nabla_H \bar{\zeta}$

b) 500 mb

CI=1 $10^{-10}s^{-2}$



c) 700 mb

CI=1 10^{-10} s^{-2}

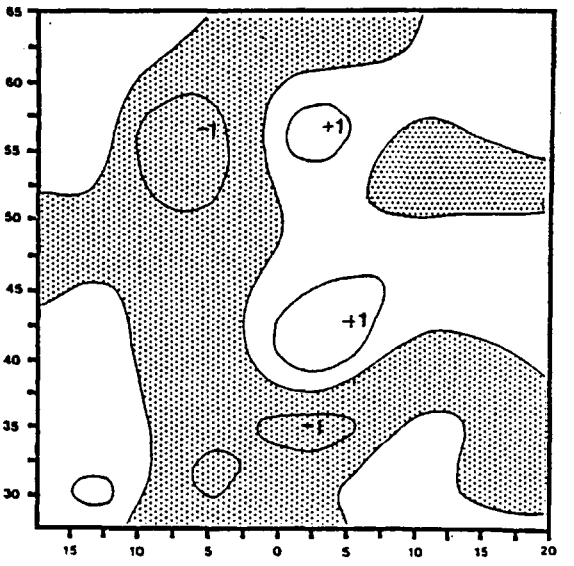
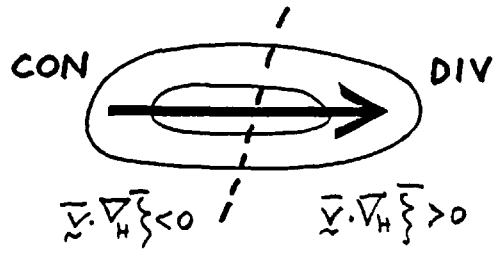


Fig.3.4: Horizontal advection of relative vorticity by the mean flow: $\bar{v} \cdot \nabla_H \bar{\zeta}$ (10^{-10} s^{-2}). Thick black line: $\bar{\zeta}$ at 300 mb.

mean flow is strongest and the anticyclone most intense. The pattern is easily understood as a result of the mean zonal flow "blowing through" the relative vorticity pattern, giving a convergence to the west and a divergence to the east of each anticyclonic maxima (as represented schematically in the following diagram):



The magnitude of ($\bar{\underset{\sim}{V}}\cdot\nabla_H\bar{\zeta}$) at 300 mb of 2×10^{-10} s^{-2} is a result of a wind of 20 m s^{-1} moving through vorticity of 10^{-5} s^{-1} with a scale of 10^3 km.

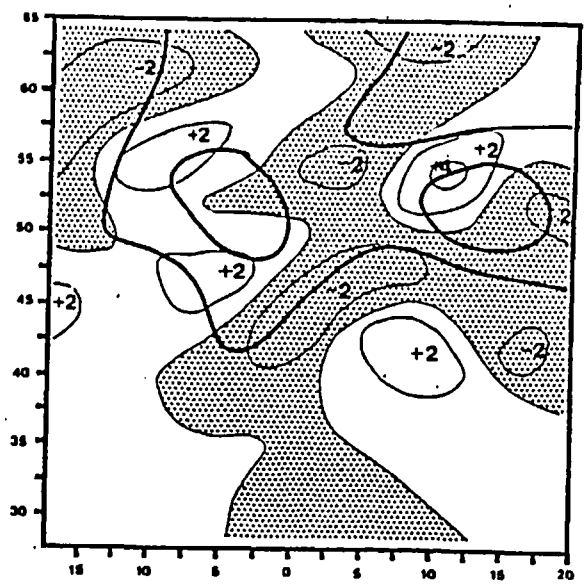
It is evident that the average effect of mean flow advection over a region limited by a line of zero relative vorticity will be zero (the convergence upstream is cancelled by the divergence downstream), showing that this term by itself cannot maintain the anticyclone. The mean advection is trying to advect the anticyclone downstream.

3.4.3 Eddy vorticity forcing: $\nabla_H\cdot(\overline{\underset{\sim}{V}'\zeta'})$

The eddy-relative vorticity forcing is also large at upper levels reaching a maximum at 300 mb (see Fig.3.5). It is of the same magnitude as the mean flow advection. There is eddy flux divergence to the west and convergence to the east of the anticyclonic maxima. The most significant feature is the tendency for the eddy-flux divergence to balance the mean flow advection. If there is an eddy vorticity flux divergence out of a region, the mean flow tends to compensate by advecting mean vorticity into the region and *vice-versa*.

a) 300 mb

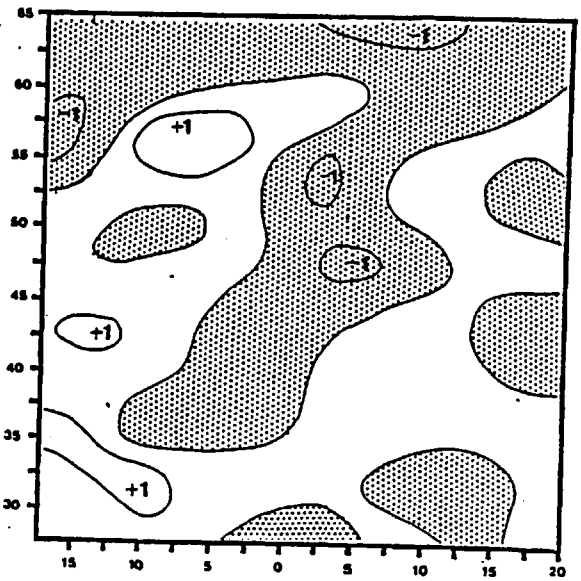
CI = 2 10^{-10} s^{-2}



$\nabla_H(\underset{\sim}{v}'\zeta')$

b) 500 mb

CI = 1 10^{-10} s^{-2}



c) 700 mb

CI = 1 10^{-10} s^{-2}

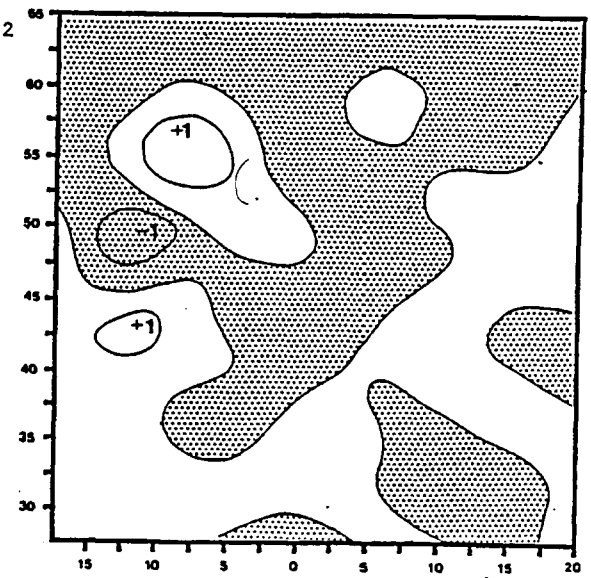


Fig.3.5: Horizontal divergence of eddy relative vorticity $\nabla_H(\overline{\underset{\sim}{v}'\zeta'})$ (10^{-10} s^{-2}). Thick black line: $\overline{\zeta}$ at 300 mb.

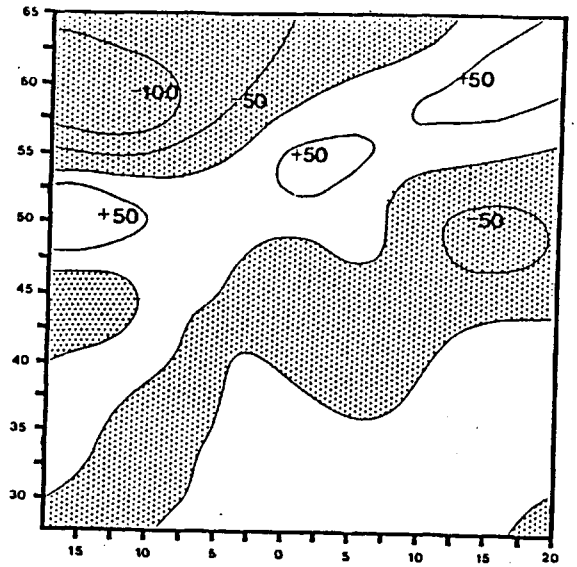


Fig.3.6 : Eddy momentum transfer $\overline{u'v'}$ (m^2s^{-2}) at 300 mb.

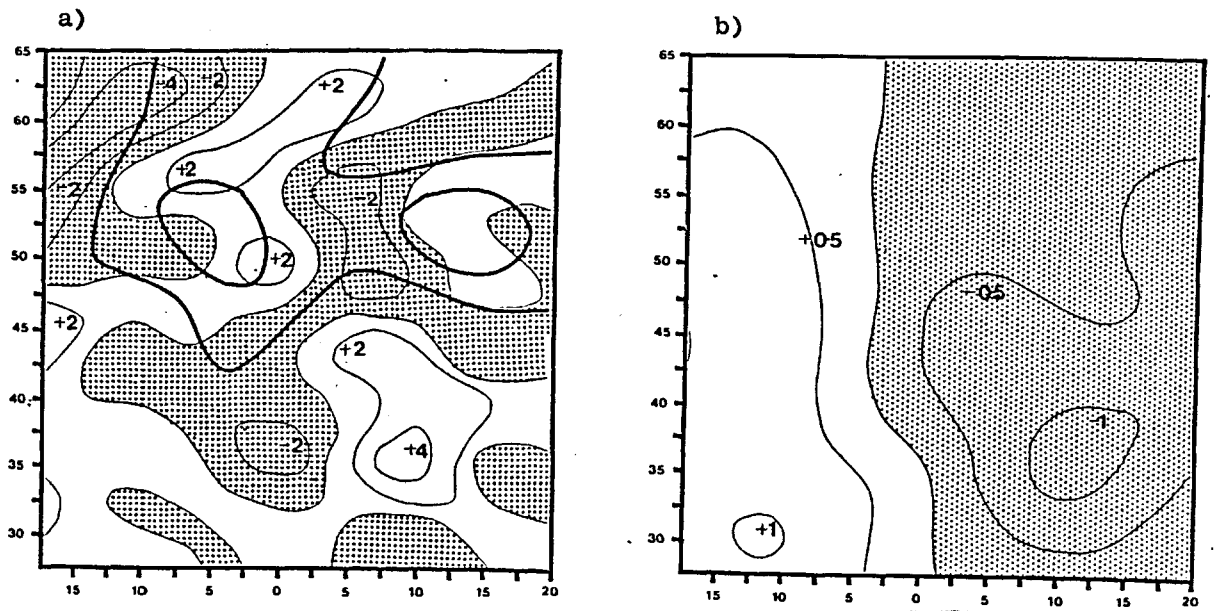


Fig.3.7 : a) Total vorticity forcing $\bar{v}\cdot\nabla\bar{\xi} + \nabla_H(\overline{v'\xi'}) + \beta\bar{v}$ at 300 mb. CI = 2 $10^{-10}s^{-2}$.

b) Horizontal advection of planetary vorticity $\beta\bar{v}$ CI = 0.5 $10^{-10}s^{-2}$.

Figs. 3.4 and 3.5 strongly suggest that the positive eddy forcing is generating negative vorticity downstream:

$$\bar{\underset{\sim}{V}} \cdot \nabla_H \bar{\xi} + \nabla_H \cdot \left(\overline{\underset{\sim}{V}' \xi'} \right) \approx 0$$

If a mean zonal flow $\bar{u}$ moves through a region of eddy forcing of intensity F, then in a distance L, the mean flow vorticity can be changed by an amount $\Delta\bar{\xi}$ given by

$$\Delta \bar{\xi} = \frac{FL}{\bar{u}}$$

So for values typical of the blocking region: $F \sim 2 \times 10^{-10}\ s^{-2}$ $L \sim 5 \times 10^2$ km, $\bar{u} \sim 20\ m\ s^{-1}$ and $\Delta\bar{\xi}$ is $\sim 0.5 \times 10^{-5}\ s^{-1}$ as observed.

In Chapter 2 we evaluated the Reynolds stresses $\overline{u'v'}$ and $\overline{u'^2 - v'^2}$ using station data but were unable to confirm (due to the inadequacy of the data set) the importance of eddy-transfer hypothesised by Green (1977) on the basis of the $\overline{u'v'}$ fields. For interest, the horizontal distribution of $\overline{u'v'}$ calculated from the gridded data set at 300 mb, (shown in Fig.3.6), is in close correspondence with the pattern evaluated using station data (Fig.2.5).

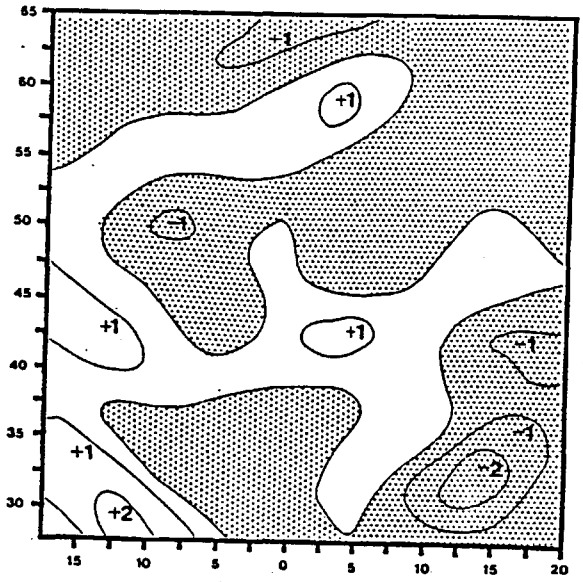
3.4.4 Total vorticity forcing

The total vorticity forcing by both mean and eddy: $\bar{\underset{\sim}{V}} \cdot \nabla_H \left(\bar{\xi} + f \right) + \nabla_H \cdot \left(\overline{\underset{\sim}{V}' \xi'} \right)$ at 300 mb is shown in Fig. 3.7(a). The mean flow advection of planetary vorticity $\beta\bar{v}$ (Fig.3.7(b)) is much smaller than the other two terms or their sum.

Equation (3.1) shows that the net-horizontal advection of vorticity is balanced by the vortex stretching term $f_0 \frac{\partial \bar{\omega}}{\partial p}$. Fig.3.7 shows that there is vortex compression to the west of the two anticyclonic maxima and stretching in the central and eastern regions. It is

a) 500 mb

CI = 1 10^{-10} s^{-2}



b) 700 mb

CI = 1 10^{-10} s^{-2}

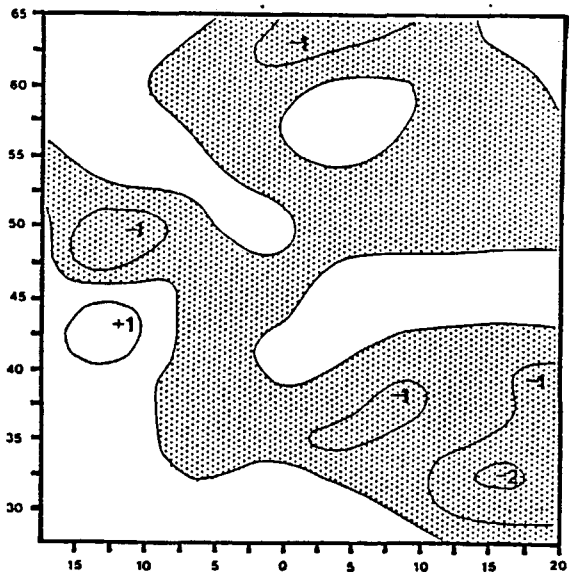


Fig.3.8 : Mean vortex stretching $f_0 \frac{\partial \bar{\omega}}{\partial p}$ $(10^{-10} s^{-2})$.

White region: vortex stretching: $\partial\bar{\omega}/\partial p > 0$

Dotted region: vortex compression: $\partial\bar{\omega}/\partial p < 0$

the spatial distribution of the vortex stretching here, just beneath the tropopause, which determines the vertical motion through the whole troposphere (see Section 3.5) for the stretching $\frac{\partial \bar{\omega}}{\partial p}$ is much smaller at 500 and 700 mb (Fig.3.8).

3.5 Vertical velocity

3.5.1 Introduction

The vertical velocity distribution is obtained by integrating the stretching term $\frac{\partial \bar{\omega}}{\partial p}$ vertically:

$$\bar{\omega}_p - \bar{\omega}_{p_0} = \int_{p_0}^{p} \frac{\partial \bar{\omega}}{\partial p} \, dp \qquad -(3.5)$$

where ω_p denotes the pressure velocity $\frac{Dp}{Dt}$ at pressure level p, and ω_{p_0} represents the corresponding (assumed known) quantity at level p_0. In order to start off the integration, the vertical motion field needs to be specified at some level. We have assumed that the vertical velocity at 200 mb is zero: here in the stratosphere it is supposed that vertical motion is inhibited by the large static stability (see Section 3.6.2 on "static stability", and Table I). Using Eqn.(3.5) and the stretching deduced from the vorticity budgets, the vertical velocity distribution can be obtained.

Fig.3.9 shows the distribution of $\bar{\omega}$ at various pressure levels (300, 500 and 700 mb). There is sinking motion over and to the east of the anticyclonic maxima and rising motion to the west. The magnitude of $\bar{\omega}$ increases going down through the upper troposphere where $\frac{\partial \bar{\omega}}{\partial p}$ is large. It is roughly constant in the lower troposphere where $\frac{\partial \bar{\omega}}{\partial p}$ is small. In the blocking region, the vertical velocity has a maximum value of 1 cms^{-1}, and is of the same order as is found by other investigators (Lau, 1979).

The vertical velocity can be determined by the kinematic method, the adiabatic method, the omega equation or the vorticity method, used here.

Since the analysis procedure tends to make the wind non-divergent, the kinematic method is inappropriate. The adiabatic method assumes no diabatic heating, which is unlikely on a time scale of a month: the diabatic heating is a particularly difficult quantity to evaluate. The omega equation method has the advantage of not needing to know the rate of change of vorticity but involves differentiating variables three times in the horizontal and once in the vertical.

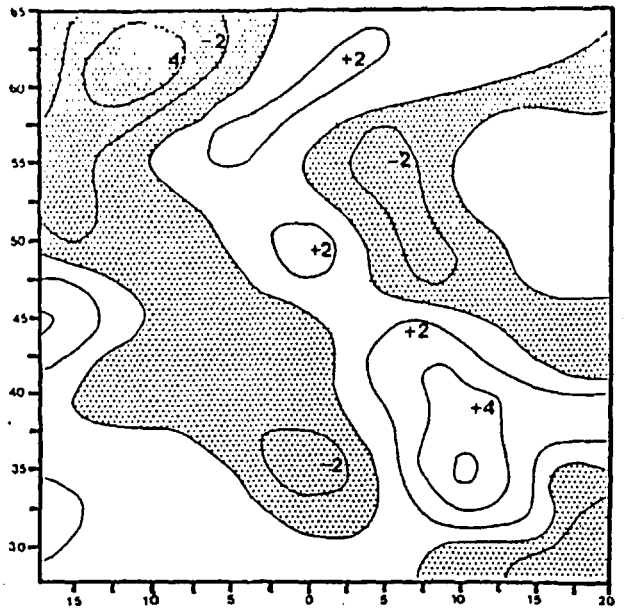
A more direct way of getting the ω field would be to use a forecast model field. A set of 6h forecast fields of vertical motion from NMC analyses have been computed for the period 1975-76. However, since such data are not presently available, here we use the vorticity method to compute vertical velocity. Lau (1979) compares this method with the forecast field ω's and finds qualitative agreement.

The choice of $\omega = 0$ at 200 mb is somewhat arbitrary but had the integration been started from the top of the surface boundary layer (using boundary layer theory) and continued upwards, the ω obtained would have been qualitatively and quantitatively similar.

Our vertical velocity and vorticity field have a small spatial scale; this is accentuated by the movement of the blocking centre during the averaging period. Small scale variability is often removed in diagnostic studies by Fourier analysing the fields and eliminating the highest wavenumbers. For example, Lau (1979) filters the relative vorticity field retaining only the first ten zonal harmonics. Had this procedure been adopted here, our fields would also be smoother.

a) 300 mb

CI=2 10^{-4} mbs^{-1}



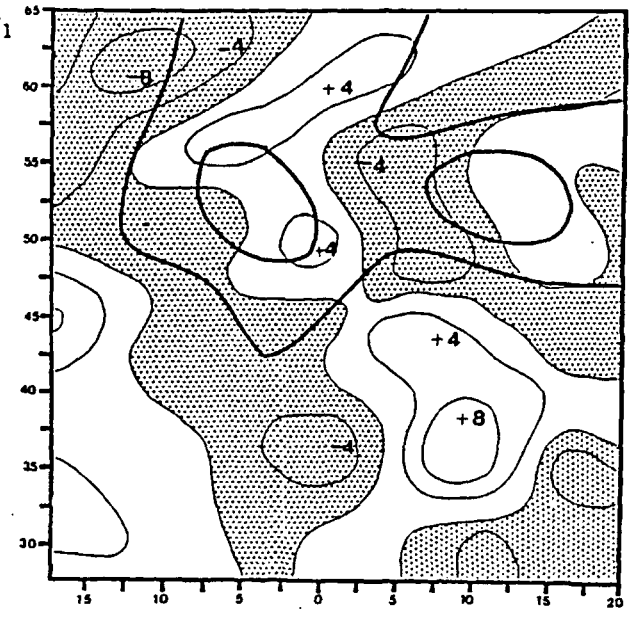
$\bar{\omega}$

b) 500 mb

CI=4 10^{-4} mbs^{-1}

10^{-4} mbs^{-1} =

0.6 cms^{-1}



c) 700 mb

CI=4 10^{-4} mbs^{-1}

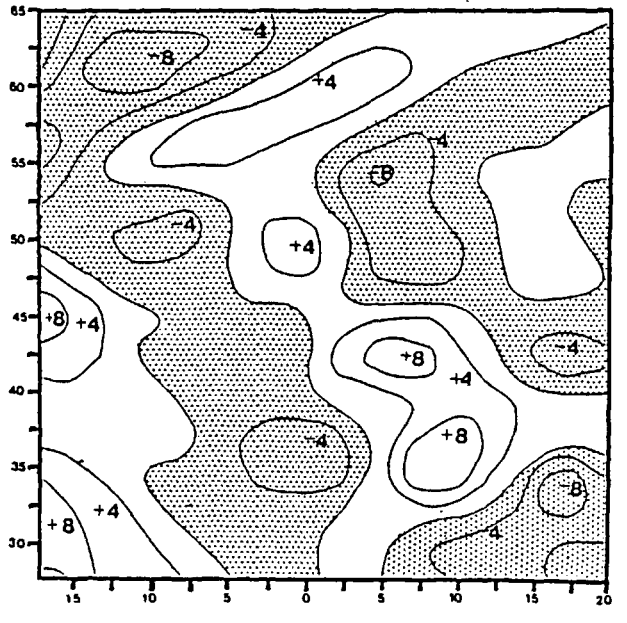


Fig.3.9 : Mean pressure velocity $\bar{\omega}$ (10^{-4} mbs^{-1}).
Dotted region: rising motion.
White region: sinking motion.
Thick black line: $\bar{\zeta}$ at 300 mb.

The sinking motion in the blocking region itself, evident at all the levels, is dynamically driven by the positive forcing near the tropopause: there is a close similarity between the pattern of the total vorticity forcing at 300 mb and that of $\overline{\omega}$ at 500 mb (compare Figs. 3.7a and 3.9b). Because the vorticity advection shows a bi-modal structure due to the shift in the block centre during the averaging period, so does the vertical velocity. In this forcing process the eddy-flux divergence is playing a crucial role, giving a major contribution to the distribution of the stretching term and hence driving the vertical motion.

3.5.2 Vertical velocity into the boundary layer

The distribution of vertical velocity at 700 and 850 mb is reasonably well correlated with the distribution of the relative vorticity at these levels (see Figs.3.9c, 3.3c). There is sinking motion in the anticyclonic regions and rising motion in the cyclonic regions.

According to the boundary layer theory, there is the following relationship between the vertical velocity at the top of the boundary layer , the relative vorticity, and the depth of the boundary layer (see, for example, Holton (1972)):

$$w = \zeta \cdot \frac{D}{2\pi} \qquad \text{—(3.6)}$$

where D is the depth scale of the boundary layer given by

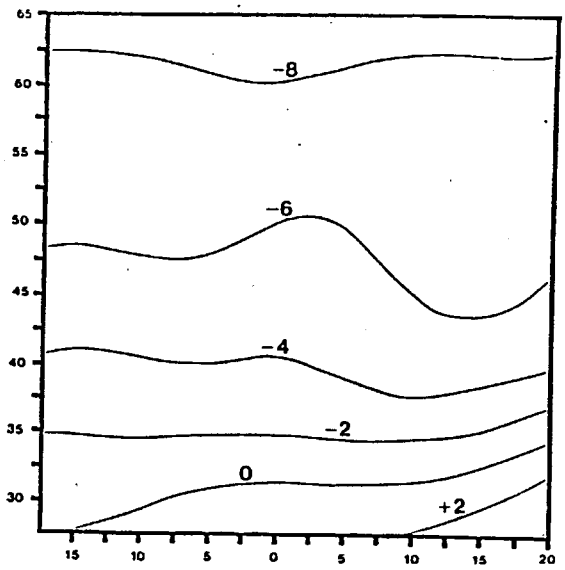
$$D = \pi/(f/2K)^{1/2}$$

and K is the vertical turbulent diffusion coefficient for momentum.

a) 300 mb

CI = $2^{o}K$

$\overline{T}_A$ = 237.8

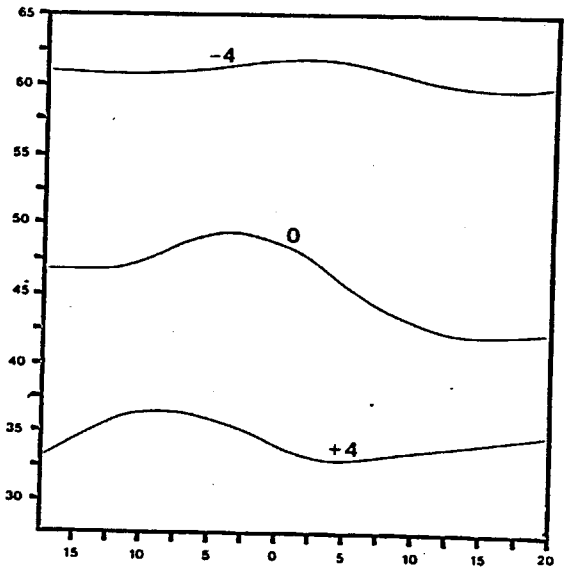


$\delta\overline{T} = \overline{T} - \overline{T}_A$

b) 500 mb

CI = $4^{o}K$

$\overline{T}_A$ = 259.8



c) 700 mb

CI = $4^{o}K$

$\overline{T}_A$ = 273.3

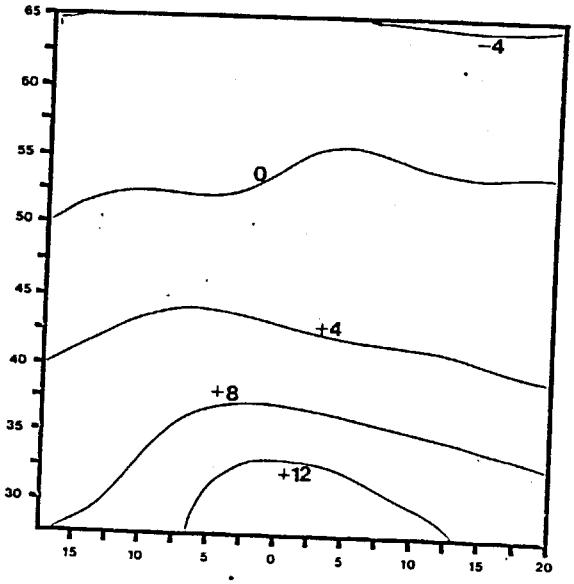


Fig.3.10 : Mean temperature $\delta\overline{T}$ (^{o}K), expressed as a deviation from hemispheric averaged values $\overline{T}_A$

From Fig.3.9(c) in the region of anticyclonic vorticity $\overline{\zeta} = -10^{-5}\ s^{-1}$, the sinking motion is 0.3 cm s^{-1}. Use of Eqn.3.6 gives a boundary layer thickness of $D \sim 1.8$ km.

This shows that quite a deep boundary layer is required to absorb the vertical velocity, extending up towards the 700 mb surface. Deep boundary layer convection was observed during the drought. The unusually dry conditions resulted in very deep, dry convection up to two or three kilometres, which was particularly enjoyed by glider pilots (K.J. Bignell, private communication).

3.6 Maintenance of the mean temperature

3.6.1 Mean temperature field

Daily charts show that the blocking ridge is warm compared with the accompanying trough over western Russia (see Chapter 1). Monthly mean temperature shows the same behaviour, although the ridge in the isotherms is not very pronounced (see Fig.3.10). The ridge is centred over the British Isles and only about one degree warmer than the surroundings. Its position does not change in the vertical and it becomes stronger in the upper troposphere.

The pronounced bi-modal structure in the twice more differentiated vorticity pattern is not seen in the temperature field. The relatively high temperatures of the block have been smoothed out during the west-east movement of the blocking centre.

3.6.2 Static stability

The static stability term enters the governing equations through Eqn.(3.2) and in pressure coordinates it may be written:

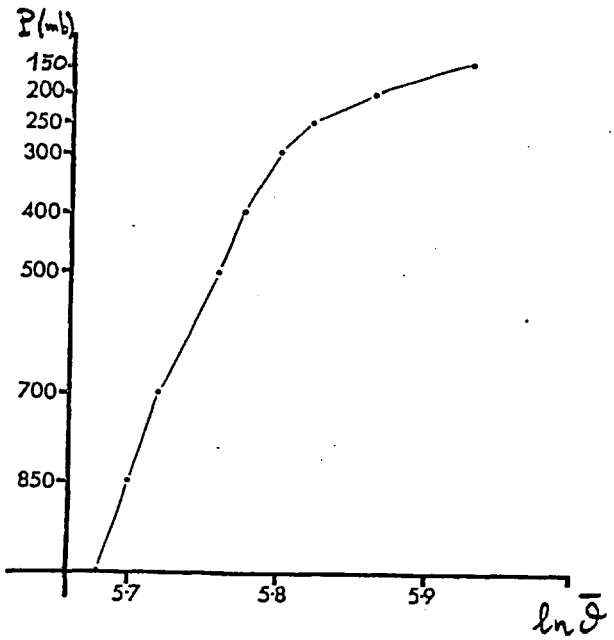


Fig.3.11 : Plot of $\ln \bar{\vartheta}$ as a function of pressure. $\bar{\vartheta}$ represents monthly mean values averaged over the 20 x 20 grid.

TABLE I.

mb	$\bar{T}$	$\frac{\partial(\ln \bar{\vartheta})}{\partial p}$ 10^{-2} mb^{-1}	S_p 10^{-2} K mb^{-1}
1000	294·8		
850	286·7	1·32	3·78
700	277·0	1·44	3·99
500	260·7	1·67	4·35
400	248·4	1·92	4·76
300	234·1	2·20	5·15
250	226·9	8·00	18·15
200	222·0	10·67	23·69
150	218·2		

$$S_p = \frac{R\bar{T}}{pc_p} - \frac{\partial \bar{T}}{\partial p} = -\frac{\bar{T}}{\bar{\vartheta}}\frac{\partial \bar{\vartheta}}{\partial p} = -\bar{T}\frac{\partial}{\partial p}\ln\bar{\vartheta} \qquad -(3.7)$$

where $\bar{\vartheta} = \bar{T}(p_0/p)^{R/c_p}$ is the potential temperature.

To evaluate the variation of the static stability in the vertical in the blocking region, monthly mean values of temperature, averaged over the 20 x 20 grid, have been used.

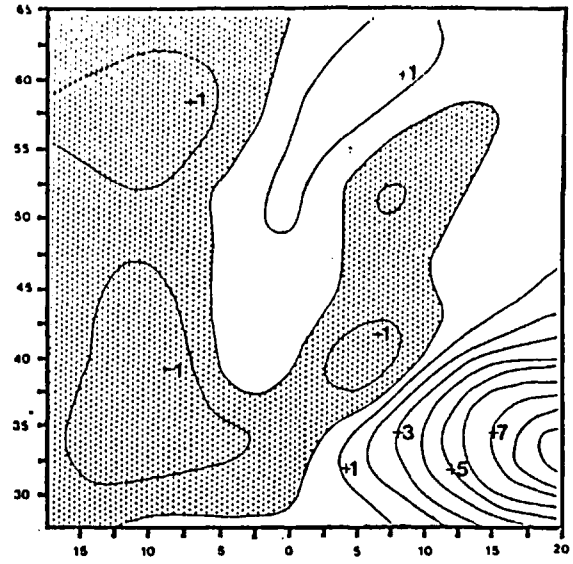
Fig.3.11 shows the plot of $\ln\bar{\vartheta}$ as a function of pressure. The abrupt increase in the slope of $\ln\bar{\vartheta}$ between 300 and 250 mb can be interpreted as representing the increase in static stability at the tropopause. It indicates that the tropopause is at about 275 mb. The derivative $\frac{\partial}{\partial p}(\ln\bar{\vartheta})$ was calculated using Fig.3.11 at each pressure level and hence the static stability S_p calculated from Eqn.(3.7). The results are shown in Table I.

3.6.3 Mean and eddy advection of heat

The mean flow advection of heat $\bar{\underset{\sim}{v}}\cdot\nabla_H\bar{T}$ and the eddy heat flux divergence $\nabla_H(\overline{\underset{\sim}{v}'T'})$ are shown in Figs. 3.12 and 3.13 respectively. Because the temperature field is an undifferentiated quantity, the patterns have a larger scale than the vorticity advection terms. The mean flow advection of heat changes sign across the temperature ridge, giving a divergence upstream and a convergence downstream of about $1^{\circ}K/day$.

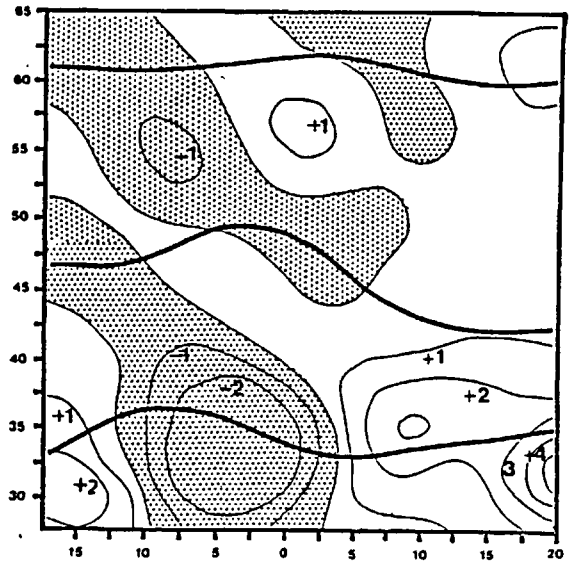
The $\nabla_H(\overline{\underset{\sim}{v}'T'})$ term is of comparable magnitude, becoming relatively more important in the lower troposphere. There is a heat flux divergence in the blocking region: the eddies are transferring heat out of the block from high to low temperature.

a) 300 mb



$\bar{v} \cdot \nabla_H \bar{T}$

b) 500 mb



c) 700 mb

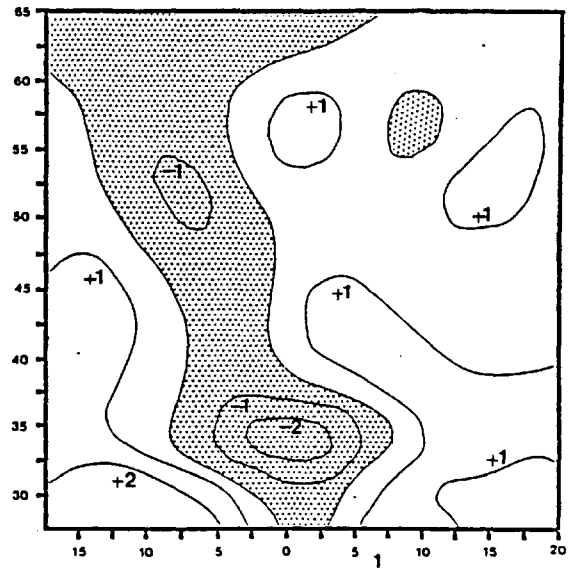
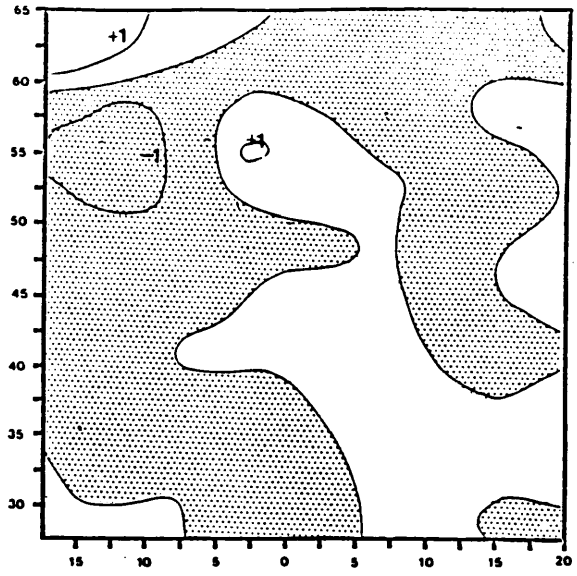


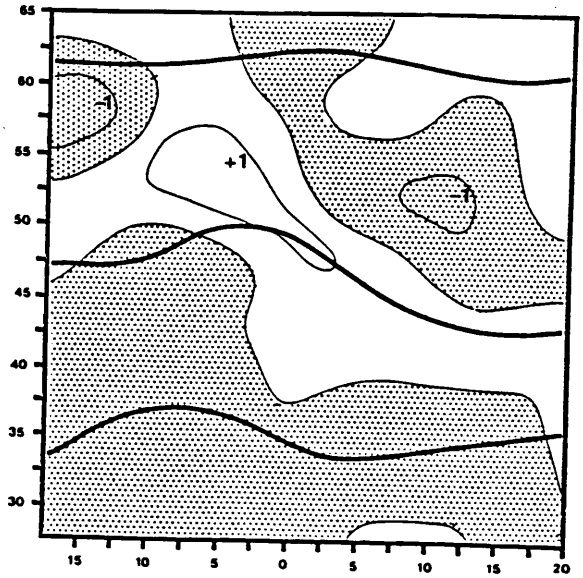
Fig.3.12 : Horizontal advection of heat by the mean flow $\bar{v} \cdot \nabla_H \bar{T}$ (^{o}K/day). Thick black line: $\bar{T}$ at 500 mb CI = 1^{o}K/day

a) 300 mb



$\nabla_H(\underset{\sim}{v}'T')$

b) 500 mb



c) 700 mb

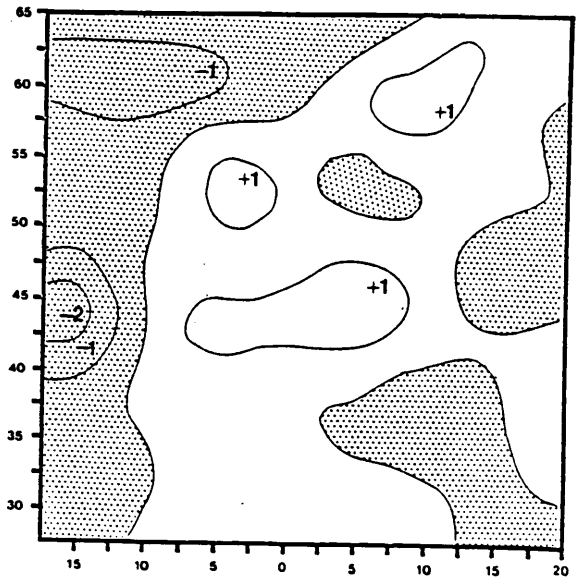
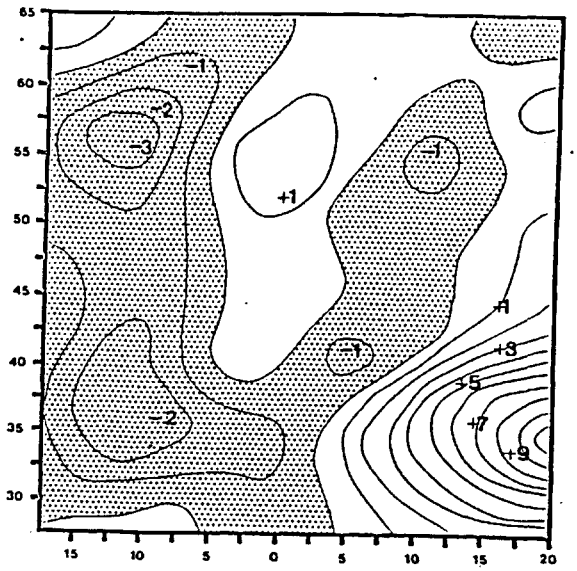


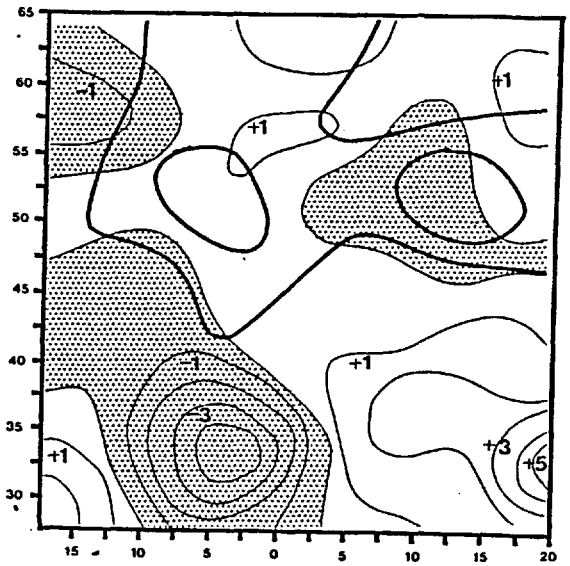
Fig.3.13 : Horizontal divergence of eddy-heat flux $\nabla_H(\overline{\underset{\sim}{v}'T'})$ (^oK/day)
Thick black line: $\overline{T}$ at 500 mb.
CI = 1^oK/day.

a) 300 mb



$\bar{\underset{\sim}{V}} \cdot \nabla_H \bar{T} + \nabla_H (\overline{\underset{\sim}{V}' T'})$

b) 500 mb



c) 500 mb

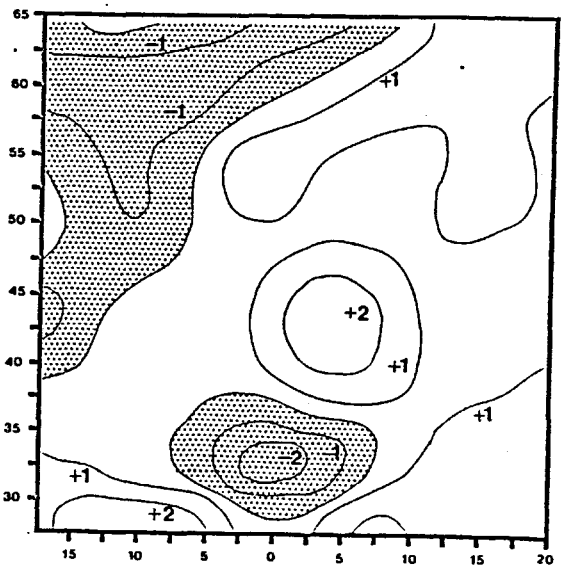


Fig.3.14 : $\bar{\underset{\sim}{V}} \cdot \nabla_H \bar{T} + \nabla_H (\overline{\underset{\sim}{V}' T'})$ (^{o}K/day).
Thick black line: $\bar{\zeta}$ at 500 mb.

Fig.3.14 shows that the combined effect of eddies and mean flow is to transport heat out of the temperature ridge at a rate of 1-2°K/day in the lower troposphere. The eddies make the major contribution.

3.6.4 Diabatic and adiabatic heating

The local diabatic heating is determined as a residual in the thermodynamic equation (Eqn.(3.2)) using the vertical velocity deduced from the vorticity budget (see Section 3.5) to evaluate the vertical advection term - the "adiabatic" heating.

The horizontal variation of $\bar{H}$ at 300, 500 and 700 mb is shown in Fig.3.15. Reasonable magnitudes of a few degrees/day are obtained in the blocking region. The large diabatic-warming to the southeast over the Mediterranean may be due to latent heat release due to convection. The spatial pattern (at 500 mb, for example) resembles that of the vertical velocity (compare with Fig.3.9). There is diabatic warming in the region of rising to the west, and diabatic cooling in the region of sinking motion over and to the east of the anticyclonic maxima. At the centre of the anticyclonic maxima, although there is diabatic cooling, it is offset by the adiabatic warming of the sinking air parcels, keeping the anticyclone warm:

$$\underset{(-)}{\bar{H}} + \underset{(++)}{S_p \bar{\omega}} > 0$$

The fact that the adiabatic warming more than compensates for the diabatic cooling (associated with the high temperatures) can be seen from the distribution of the total advection of heat (Fig.3.14). By Eqn.(3.2) this measures the sum of the diabatic and adiabatic heating. In the blocking region it is positive at all the levels.

When interpreting the maps of Fig.3.15, it must be remembered that $\bar{H}$ is calculated as a residual and so contains errors as well as real diabatic sources and sinks.

Fig.3.15 is not a realistic diabatic heating field. For example, it is difficult to reconcile the apparent diabatic warming of 2°K/day between the two anticyclonic maxima, presumably associated with latent heat release during convection, with the low rainfall observed during the drought.

A diabatic warming of H °/day implies a condensation rate

$$\frac{dm}{dt} = \frac{H c_p p_o}{L_c g}$$

where L_c is the latent heat of condensation $\simeq 2.5\ 10^6$ J kg^{-1}

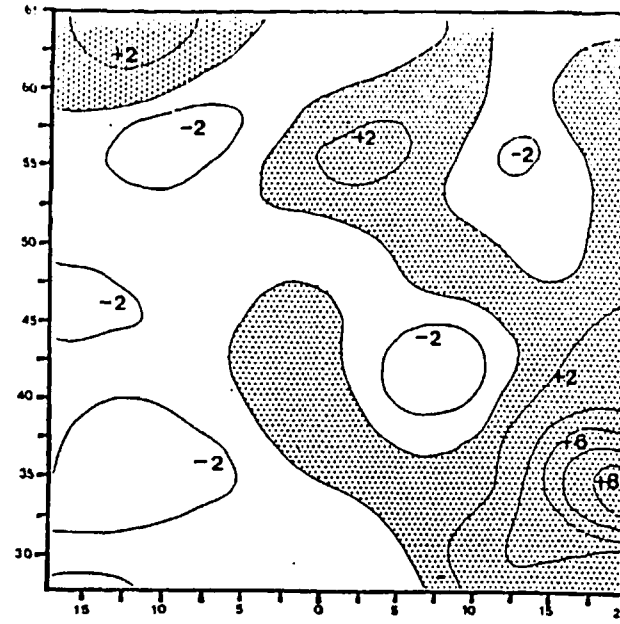
c_p is the specific heat at constant pressure $\simeq 10^3$ K K^{-1} kg^{-1}

if the latent heat released is distributed uniformly over the entire atmospheric column of mass $p_o/g \simeq 10^4$ kg m^{-2}.

An H of 2°/day would require a $dm/dt \simeq 8$ kg/day or a rainfall of 0.8 cm/day. This is an unrealistically high value for the drought. A possible conclusion is that the adiabatic heating is in error by about 2°/day.

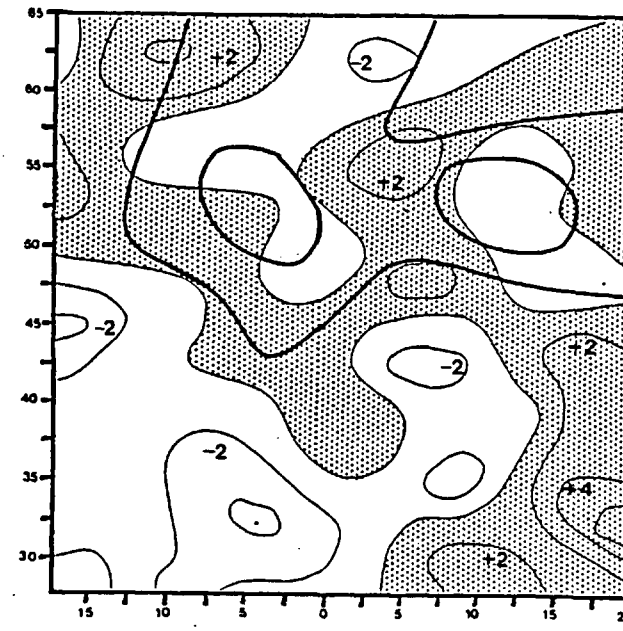
An average diabatic warming of 6°/day at 300 mb in the Eastern Mediterranean is again too large. In the tropics a peak of 10°/day at 300-400 mb can be observed during deep convection. Over the Eastern Mediterranean the rainfall (Fig.3.2) was up to eight times the average, and so the latent heat release is abnormally large, but this cannot account completely for such large diabatic heating rates, which are probably due to some systematic misrepresentation in the data.

a) 300 mb



$\bar{H}$

b) 500 mb



c) 700 mb

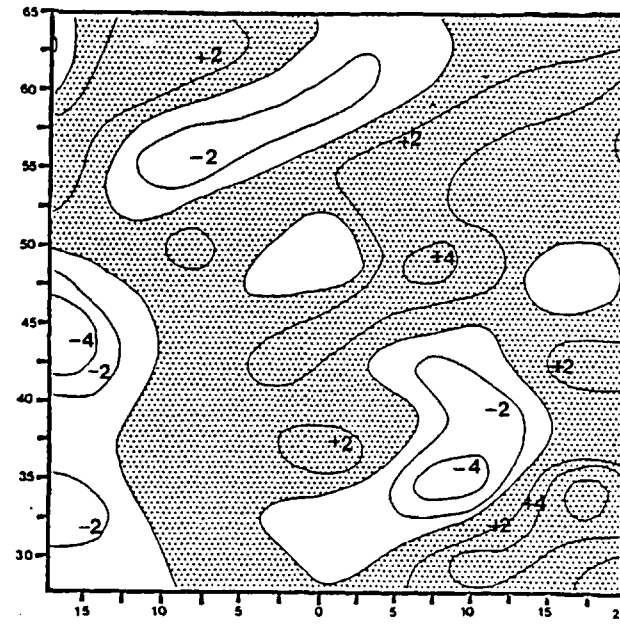


Fig.3.15 : Mean diabatic heating $\bar{H}$ (^{o}K/day), as residual in the thermodynamic equation.
Thick black line: $\bar{\zeta}$ at 300 mb.
White region: diabatic cooling. Dotted region: diabatic warming.

TABLE II.

	VORTICITY $10^{-10}\ s^{-2}$				THERMODYNAMIC °K/day			10^{-2} °K mb^{-1}	10^{-4} mb s^{-1}	°K/day
$P_{(mb)}$	$\bar{\zeta}\cdot\nabla_H\bar{\zeta}$	$+\nabla_H\cdot(\overline{\underset{\sim}{v}'\zeta'})$	$+\beta\bar{v}$	$=$total	$\bar{\underset{\sim}{v}}\cdot\nabla_H\bar{T}$	$+\nabla_H\cdot(\overline{\underset{\sim}{v}'T'})$	$=$total	S_p	$-\omega$	H
200	−·09	·95	·20	1·06	−·45	−1·07	−1·52	24·7	0	−1·52
250	−·12	1·11	·18	1·17	−·19	−1·05	−1·24	18·9	·11	−2·08
300	·07	·93	·14	1·14	−·18	·01	−·17	5·7	·33	−2·59
400	·00	·23	·11	·34	−·25	·98	·73	5·0	1·90	−·22
500	−·03	−·10	·10	−·03	−·10	·89	·79	4·3	2·00	−·19
700	−·08	−·09	·05	−·12	·65	·48	1·13	4·7	1·45	·44
850	·03	−·04	−·10	−·11	·78	·36	1·14	3·8	−·33	1·26

3.7 Discussion

3.7.1 Area-averages of vorticity and heat budgets

To summarise the processes involved in the maintenance of the anticyclone and to emphasise the importance of eddy-forcing, the governing equations (Eqns. (3.1) and (3.2)) have been averaged over the centre of the anticyclone (following the contour of $\overline{\zeta} = -0.05 \times 10^{-4}\ s^{-1}$ at 300 mb).

The averaging region is represented by the shaded area in Fig. 3.3(a). The same region is averaged over at each level in the vertical. Table II gives a summary of the values obtained after this averaging process. As we expect, $\left[\overline{\underset{\sim}{v}} \cdot \nabla_H \overline{\zeta}\right]_A$ is small. The eddy forcing $\left[\nabla_H \cdot \left(\overline{\underset{\sim}{v}' \zeta'}\right)\right]_A$, on the other hand, is large and positive near the tropopause. The area-averaged vorticity $\left[\overline{\zeta}\right]_A$ of $-0.08 \times 10^{-5}\ s^{-1}$ can be generated in 2 days by the eddy forcing. Although the mean flow advection was locally comparable to the eddy flux divergence of vorticity, in the area-average it is ten times smaller. The mean horizontal flow cannot itself maintain the anticyclone.

The sinking motion $\left[\overline{\omega}\right]_A$, driven by the upper tropospheric eddy forcing, reaches a value of 2×10^{-4} mb s^{-1} (~ 0.3 cm s^{-1}) at 500 mb.

Middle level tropospheric cooling $\left[H\right]_A$ is offset by adiabatic warming caused by the sinking. The net warming (adiabatic + diabatic) of order $1^{\circ}K$/day is balanced by a transfer of heat out of the region, principally by eddies.

In the lower troposphere, the area-average gives a diabatic warming and a small upward motion at 850 mb. This is caused by the geographically fixed averaging region. In the upper troposphere the

phase lines are vertical and so the fixed averaging area samples the centre of the block at each level. Lower down, the core of the anti-cyclone drifts away from the averaging area.

3.7.2 Summary

Vorticity and heat budgets have shown that the eddy-forcing is important in the maintenance of the anticyclone over Europe, during July '76. The eddy-vorticity forcing is large near the tropopause and forces downward motion. The resulting adiabatic warming offsets the diabatic cooling (associated with high temperature there) and so warm, dry air is brought down to the surface, generating the surface anticyclone which can be dissipated by frictional torque.

CHAPTER 4

THE BLOCK IN TERMS OF POTENTIAL VORTICITY

4.1 The potential vorticity conservation

4.1.1 Ertel and quasi-geostrophic potential vorticity

In this chapter we study the dynamics of the block in terms of potential vorticity. Potential vorticity was first defined by Ertel (1942), as

$$P = (1/\rho)\left(\text{curl}\ \underset{\sim}{V} + 2\underset{\sim}{\Omega}\right).\nabla\vartheta \qquad \text{—(4.1)}$$

where $\rho \equiv$ air density

$\underset{\sim}{v} \equiv (u, v, \omega)$

$\underset{\sim}{\Omega}$ = angular velocity of the Earth ($f = 2\Omega\sin\theta$)

θ = potential temperature

In adiabatic frictionless motion, P is conserved

$$\frac{D}{Dt}P = 0 \qquad \text{—(4.2)}$$

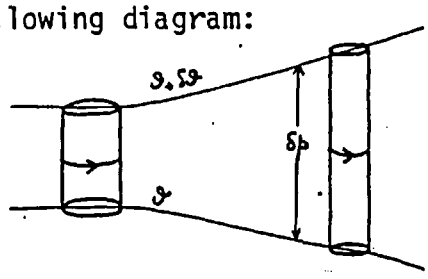
where $\frac{D}{Dt} = \frac{\partial}{\partial t} + \underset{\sim}{V}_H \cdot \nabla_H + \omega\frac{\partial}{\partial p}$

The full Ertel potential vorticity (4.1) can, if the Richardson number is large, be approximated by

$$P^* = (\zeta + f)\frac{\partial\vartheta}{\partial p} .$$

P^* can be interpreted as a measure of the ratio of the vertical component of absolute vorticity to the length of a vortex tube lying

between surfaces of constant potential temperature, as shown schematically in the following diagram:



Using approximations consistent with quasi-geostrophic motion ($1 >> \zeta/f_o = R_o >> R_i^{-1/2}$), P^* may itself be approximated by:

$$P^* = f_o \Theta_p \left[1 + (\zeta + \beta y)/f_o\right]\left[1 + \theta'_p/\Theta_p\right] \simeq P_o + P_1$$

where $\Theta(p)$ is a basic potential temperature, θ' the deviation from it,

$$P_o = f_o \Theta_p \quad \text{and} \quad P_1 = \Theta_p\left(\zeta + f + f_o\,\theta'_p/\Theta_p\right)$$

and P_o is only a function of pressure. The conservation of P^* can therefore be written as:

$$\frac{D_H}{Dt} P_1 + \omega \frac{\partial}{\partial p} P_o = 0 \qquad \text{—(4.3)}$$

Substituting for ω from the thermodynamic equation in the absence of diabatic heating

$$\frac{D_H}{Dt}\theta' + \Theta_p \omega = 0$$

Eqn.(4.3) becomes

$$\frac{D_H}{Dt}\left[\Theta_p\left(\zeta + \beta y + f_o\,\theta'/\Theta_p\right) - f_o \frac{D_H}{Dt}\left(\theta/\Theta_p\right)\frac{\partial}{\partial p}\Theta_p\right] =$$

$$= \frac{D_H}{Dt}\left[\Theta_p\left(\zeta + \beta y + f_o \frac{\partial}{\partial p}\left(\theta'/\Theta_p\right)\right)\right] =$$

$$= \Theta_p \frac{D_H}{Dt}[q] = 0 \qquad \text{—(4.4)}$$

where q is the quasi-geostrophic potential vorticity.
The vertical advection of P^* is accounted for in the conservation of q by moving the $1/\Theta_p$ inside the vertical derivative of the temperature term.

Therefore the conservation of Ertel can be variously approximated by

$$\frac{D}{Dt} P \simeq \frac{D}{Dt} P^* \simeq \Theta_p \frac{D_H}{Dt} q$$

Eqn.(4.2) was first written down by Ertel (1942) (following a previous work of Rossby (1940)). Eqn.(4.4) (e.g. Charney, 1962) states that q is conserved following the horizontal geostrophic motion.

The connection between P, P^* and q has been discussed by, for example, Charney and Stern (1962) and Green (1970).

The approximation to Ertel, P^*, has been used in diagnostic studies (e.g. Lau,1979), but because it is significantly advected by vertical motion as well as in the horizontal, interpretation of maps of P^*, fluxes of P^* and flux divergence,is made more difficult. In this study, therefore, we will discuss the dynamics of the block in terms of q instead of P^*, because q is conserved in horizontal motion. We also wish to understand the dynamical processes within the context of the quasi-geostrophic theory and so it is sensible to analyse the observations in the same framework. The conservation of q is particularly useful in prognostic studies of the large scale circulation (e.g. Philips, 1956); however in this diagnostic study it will not be necessary to make some of the approximations usually made in q ,

because we have access to real, rather than geostrophic winds.

4.2 Quasi-geostrophic potential vorticity budget

4.2.1 Introduction

The quasi-geostrophic potential vorticity has been evaluated using the following expression:

$$q = \zeta + f - f_0 \frac{\partial}{\partial p}\left(\delta T / S_p\right)$$

where $S_p = -\pi \frac{\partial}{\partial p} \ln \theta$ is the static stability

and ζ has been calculated using the real wind (u, v)

In middle latitudes, because the Rossby number is small, ζ is a good approximation of the geostrophic relative vorticity, ζ_g.

The choice of the best finite difference approximation of $\frac{\partial}{\partial p}\left(\delta T / S_p\right)$ presents some difficulties because the temperature data are only available at standard pressure levels, and vertical derivatives must be evaluated in regions where quantities are varying rapidly, such as near the tropopause.

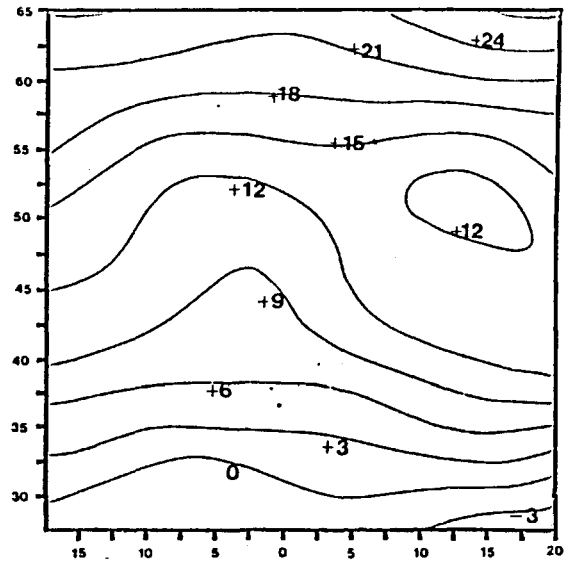
In the present calculations, the following finite difference expression is adopted:

$$\frac{\partial}{\partial p}\left(\delta T / S_p\right) \simeq \frac{\left(\pi_2 / S_{p_2} - \pi_1 / S_{p_1}\right)}{\Delta p}$$

where π_1 and π_2 are weighted averages of the temperatures at the upper, middle and lower pressure levels, and S_{p_1} and S_{p_2} are constant static stabilities in each layer.

a) 300 mb

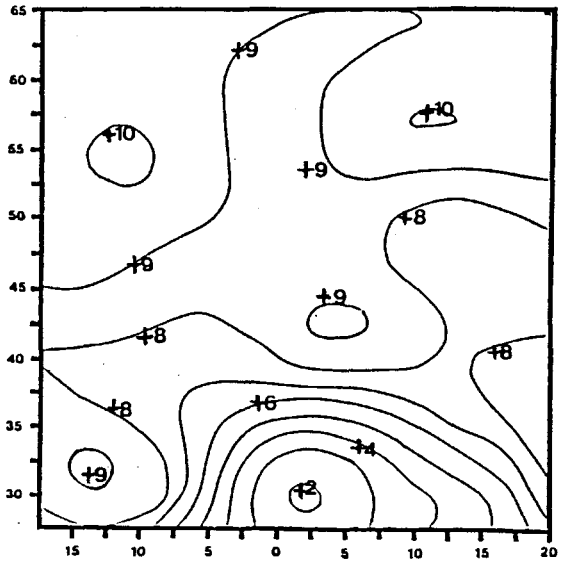
CI = 3 10^{-5} s^{-1}



$\bar{q}$

b) 500 mb

CI = 1 10^{-5} s^{-1}



c) 700 mb

CI = 2 10^{-5} s^{-1}

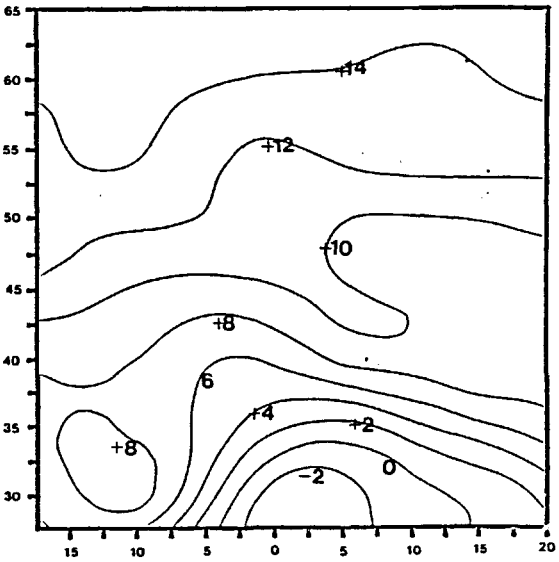
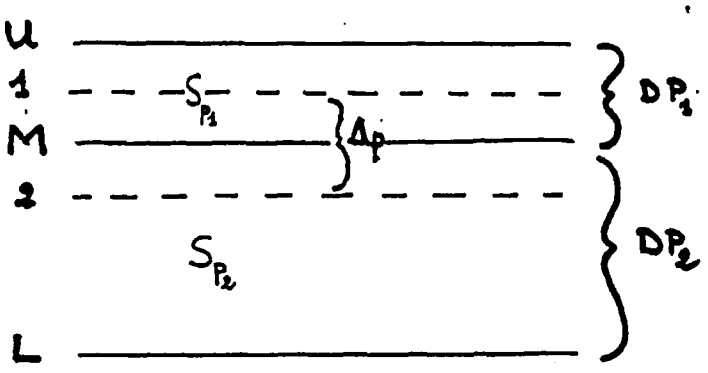


Fig.4.1 : Mean quasi-geostrophic potential vorticity

$\bar{q} = \zeta + f - f_0 \frac{\partial}{\partial p} \delta\bar{\pi}/s_p$ (10^{-5} s^{-1}).



$$T_1 = (T_U + T_M)/2$$

$$T_2 = \frac{(DP_2 - DP_2/2)}{DP_2} T_M + \frac{DP_2/2}{DP_2} T_L$$

The mean flow advection and the eddy flux divergence of quasi-geostrophic potential vorticity have been evaluated using the NMC data, according to the steady state time-averaged quasi-geostrophic potential vorticity equation:

$$\bar{\underset{\sim}{v}} \cdot \nabla_H \bar{q} + \nabla_H (\overline{\underset{\sim}{v}' q'}) = -f_0 \frac{\partial}{\partial p} (\bar{H}/S_p) \qquad \text{—(4.5)}$$

in the presence of diabatic heating, H .

4.2.2 The block and its mean potential vorticity

Fig.4.1 shows maps of monthly mean quasi-geostrophic potential vorticity $\bar{q}$ for July '76 at 300, 500 and 700 mb. The background planetary vorticity, f , following latitude circles, is distorted by the motion, $\bar{\zeta}$, and temperature field $-f_0 \frac{\partial}{\partial p}\left(\delta \bar{T}/S_p\right)$ In the blocking region the $\bar{q}$ contours are displaced northwards, showing that the block is a region of low potential, as well as low absolute vorticity. This is particularly evident in the middle and upper troposphere (300, 500 mb). The mean q at 300 mb shows a double minima due to the influence of the two anticyclonic centres. Both $(\bar{\zeta} + f)$ and $-f_0 \frac{\partial}{\partial p}(\delta T/S_p)$ (Fig.4.2) are small in the blocking region.

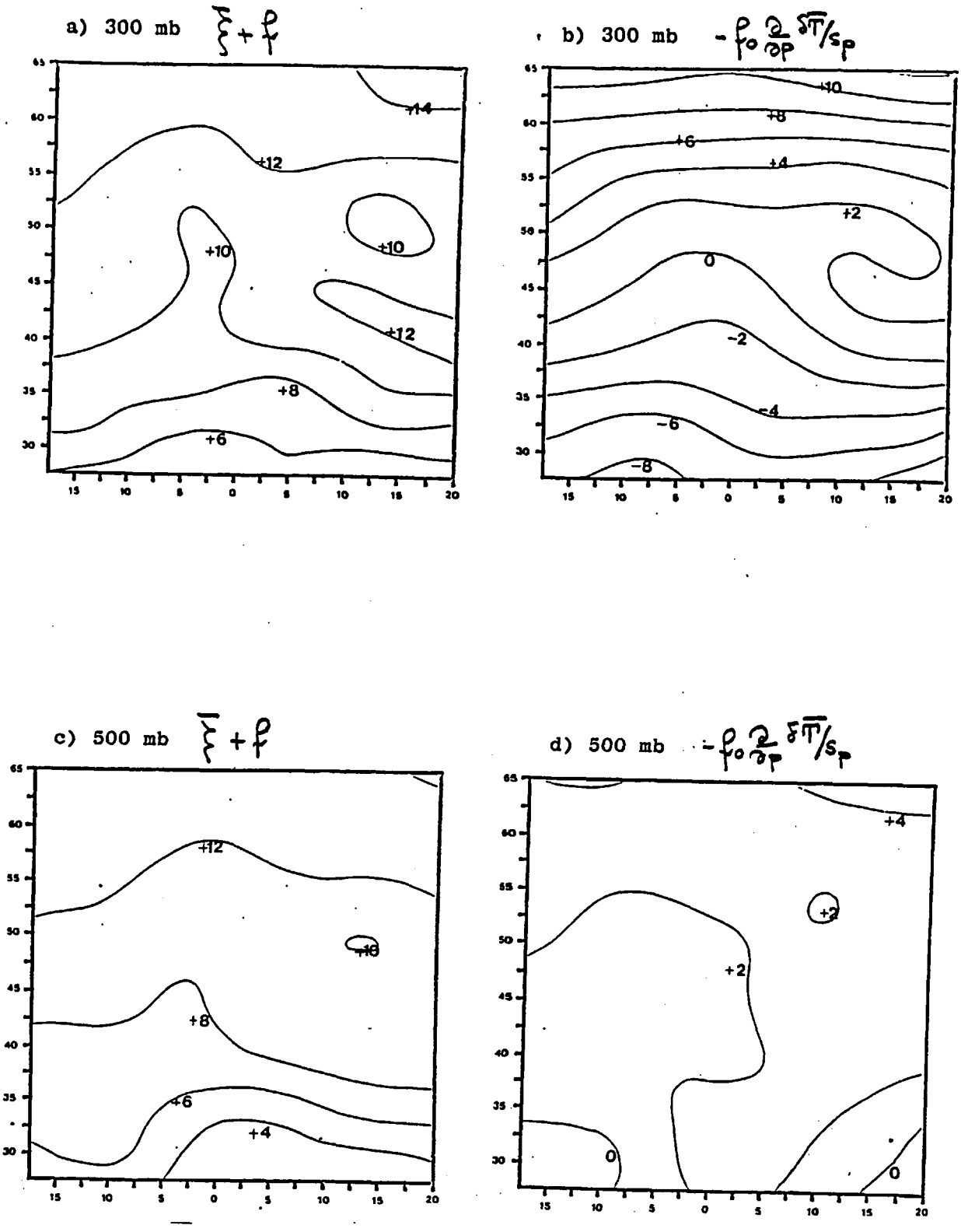
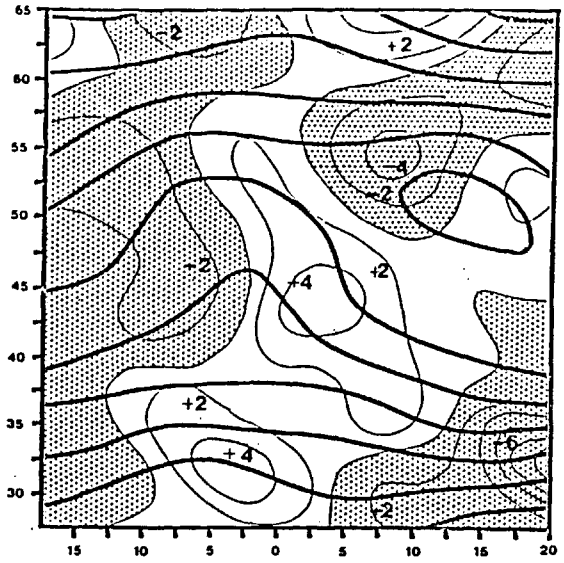


Fig.4.2 : Terms in the quasi-geostrophic potential vorticity: $\bar{\zeta} + f$ and $-f_0 \frac{\partial}{\partial p} \delta\bar{T}/s_p$ ($10^{-5} s^{-1}$).
CI = 2 $10^{-5} s^{-1}$.

a) 300 mb

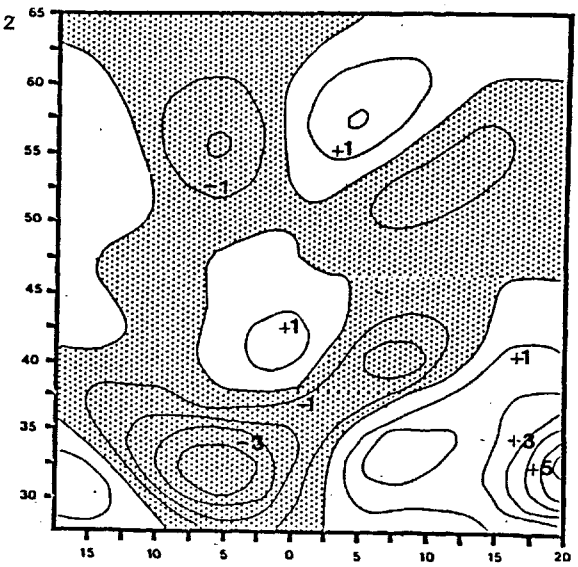
CI=2 10^{-10} s^{-2}



$\underset{\sim}{V} \cdot \nabla_H \bar{q}$

b) 500 mb

CI=1 10^{-10} s^{-2}



c) 700 mb

CI=1 $10^{-10}s^{-2}$

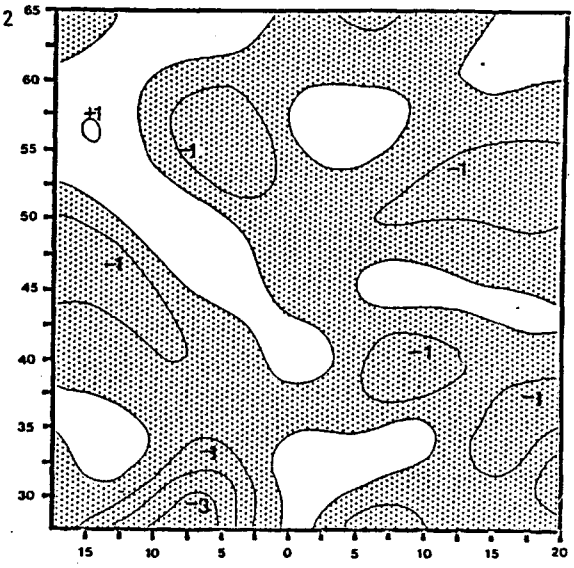


Fig.4.3 : Horizontal advection of potential vorticity by the mean flow $\underset{\sim}{\bar{V}} \cdot \nabla_H \bar{q}$ ($10^{-10}s^{-2}$).
Thick black line: $\bar{q}$ at 300 mb.

The fact that the block is a minimum not only in relative vorticity $\bar{\zeta}$ but also in potential vorticity $\bar{q}$, shows that the relative vorticity tendency is not compensated for by vortex stretching. One possible hypothesis is, for example, that in the region of large anticyclonic vorticity the mean vortex tubes were compressed to conserve potential vorticity. In reality they are stretched so that the block is more anomalous in $\bar{q}$ than it is in $(\bar{\zeta}+f)$ (compare $\bar{q}$, Fig.4.1, with Fig.4.2).

4.2.3 Mean flow advection of potential vorticity

The advection of $\bar{q}$ by the mean flow: $\bar{\underset{\sim}{v}} \cdot \nabla_H \bar{q}$ is shown at 300, 500 and 700 mb in Fig.4.3. It is large in the upper troposphere and reaches the maximum at 300 mb, where the mean flow is strongest. The $\bar{q}$ contours at 300 mb (the thick black line) have been superimposed. The convergence upstream of the minimum in $\bar{q}$ and divergence downstream is a result of mean zonal flow "blowing through" the $\bar{q}$ -pattern (see Chapter 3, for similar discussion of $\bar{\underset{\sim}{v}} \cdot \nabla_H \bar{\zeta}$). The mean advection tends to advect the mean q -pattern downstream. If the low q is to be maintained, this mean flow advection must be balanced: it could be balanced by either eddy transport or diabatic heating.

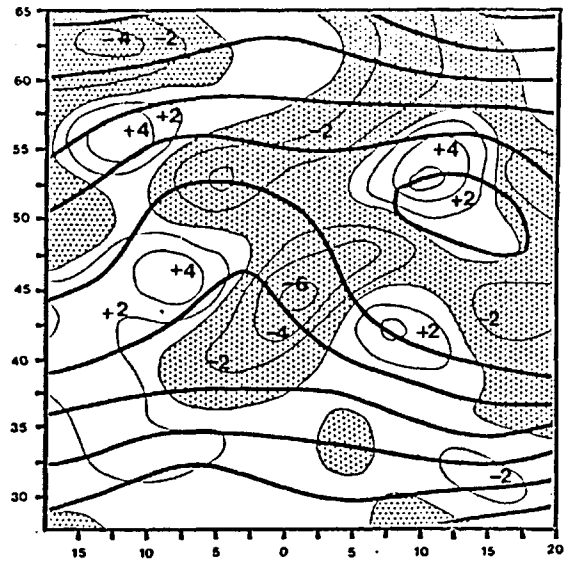
This analysis shows that $\bar{q}$ -pattern cannot be the result of steady-adiabatic orographic forcing (Charney and De Vore (1979)), which would be characterized by zero mean advection of $\bar{q}$.

4.2.4 Eddy- q flux divergence

The divergence of the eddy flux of q at 300, 500 and 700 mb is shown in Fig.4.4. It is fully comparable in magnitude with the mean

a) 300 mb

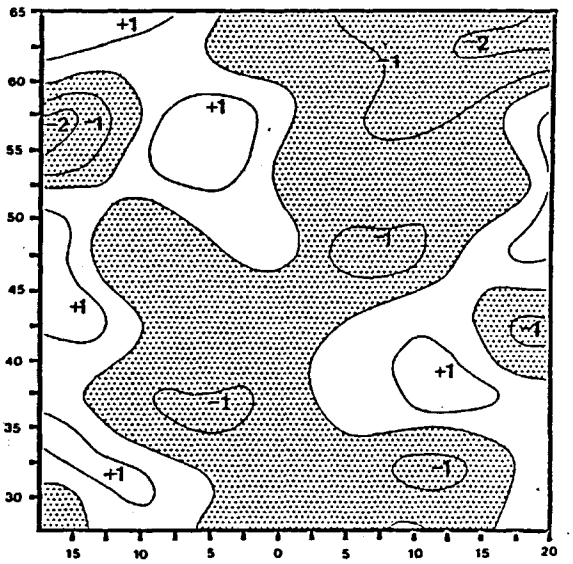
CI=2 10^{-10} s^{-2}



$\nabla_H \cdot (\overline{\underset{\sim}{v}' q'})$

b) 500 mb

CI=1 10^{-10} s^{-2}



c) 700 mb

CI=1 10^{-10} s^{-2}

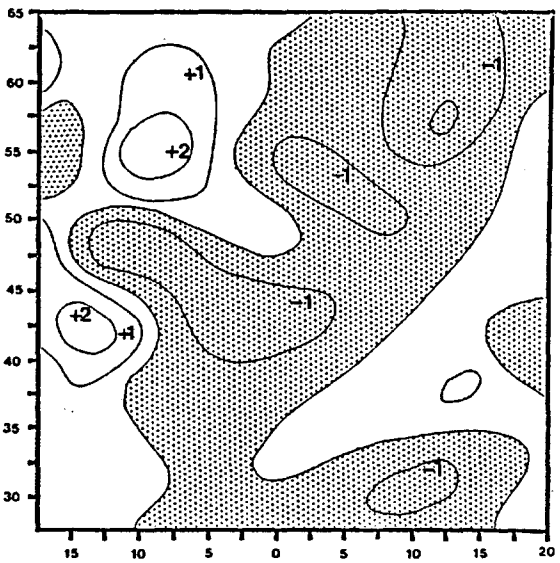


Fig.4.4 : Horizontal divergence of eddy potential vorticity flux $\nabla_H \cdot (\overline{\underset{\sim}{v}' q'})$ (10^{-10} s^{-2}). Thick black line: $\overline{q}$ at 300 mb.

flow advection. It is particularly large at the 300 mb level. Comparing Fig.4.4a with Fig.4.3a, we see that it is the eddy q -flux divergence which tends to balance the mean flow advection:

$$\bar{\underset{\sim}{v}} \cdot \nabla_H \bar{q} + \nabla_H \cdot (\overline{\underset{\sim}{v}' q'}) \simeq 0$$

Therefore it is eddy forcing $\nabla_H \cdot (\overline{\underset{\sim}{v}' q'}) > 0$ upstream that is generating low $\bar{q}$ downstream.

We can visualize the eddy- q flux divergence as being made up of two parts:

$$\nabla_H \cdot (\overline{\underset{\sim}{v}' q'}) = \nabla_H \cdot (\overline{\underset{\sim}{v}' \zeta'}) - f_0 \nabla_H \cdot \left(\overline{\underset{\sim}{v}' \frac{\partial}{\partial p} (\delta\pi'/s_p)} \right)$$

The first term is the advection of relative vorticity by the eddies in the horizontal (the term discussed in Chapter 3). The second is a vortex stretching term due to eddies. Fig.4.5 shows the eddy-vortex stretching term

$$\frac{\partial \bar{\omega}_E}{\partial p} = \nabla_H \cdot \left(\overline{\underset{\sim}{v}' \frac{\partial}{\partial p} (\delta\pi'/s_p)} \right)$$

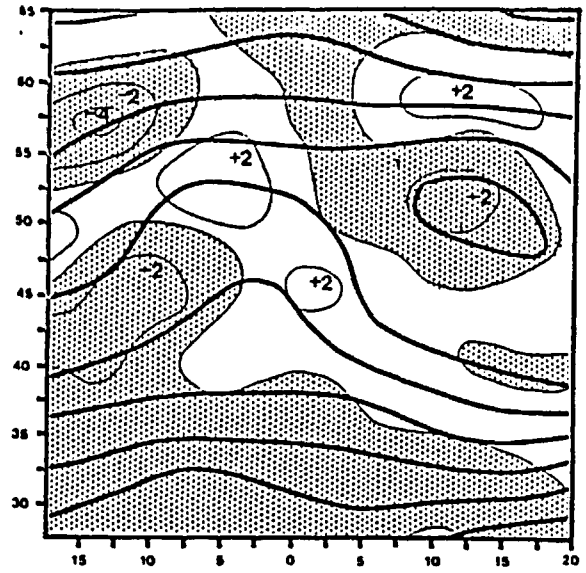
with the $\bar{q}$ at 300 mb again superimposed. Comparison with Fig.3.5 shows that it is comparable in magnitude to the eddy-relative vorticity flux divergence.

The two components of the eddy q flux divergence combine so that it is enhanced: where there is vorticity flux divergence, $\nabla_H \cdot (\overline{\underset{\sim}{v}' \zeta'}) > 0$, there tends to be vortex compression, $\frac{\partial \bar{\omega}_E}{\partial p} < 0$, and *vice versa*.

The $\frac{\partial \bar{\omega}_E}{\partial p}$ term makes a large contribution to the total vortex stretching $\frac{\partial \bar{\omega}}{\partial p}$ (compare Fig.4.5a with Fig.3.7a, Chapter 3). It is positive on and to the east of the blocking

a) 300 mb

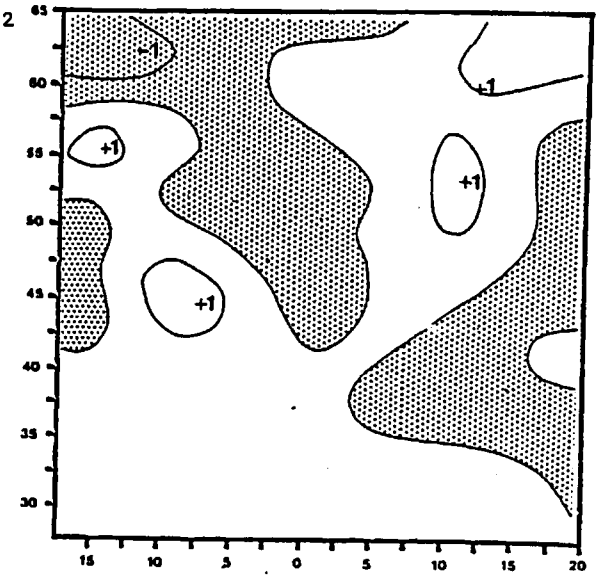
CI = 2 10^{-10} s^{-2}



$f_0 \frac{\partial \overline{\omega}_E}{\partial p}$

b) 500 mb

CI = 1 10^{-10} s^{-2}



c) 700 mb

CI = 1 10^{-10} s^{-2}

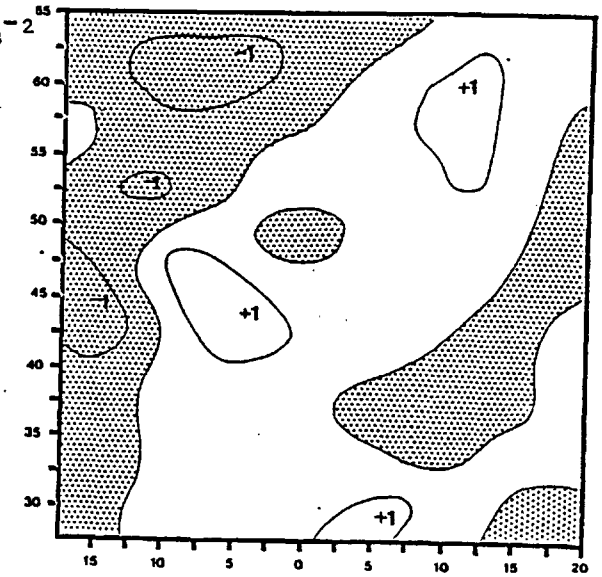
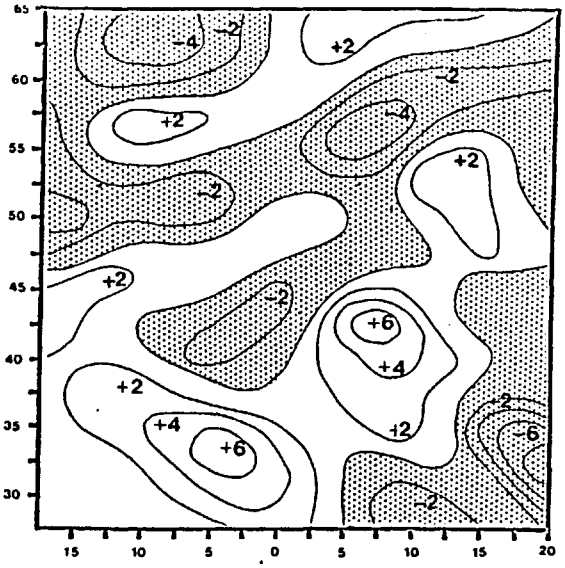


Fig.4.5 : Eddy-vortex stretching: $f_0 \frac{\partial \overline{\omega}_E}{\partial p} = f_0 \nabla_H \left(\overline{\frac{\nu}{-\partial p} \frac{\partial T'}{S_p}} \right) (10^{-10} s^{-2})$

Thick black line: $\overline{q}$ at 300 mb.
White region: vortex stretching
Dotted region: vortex compression.

a) 300 mb

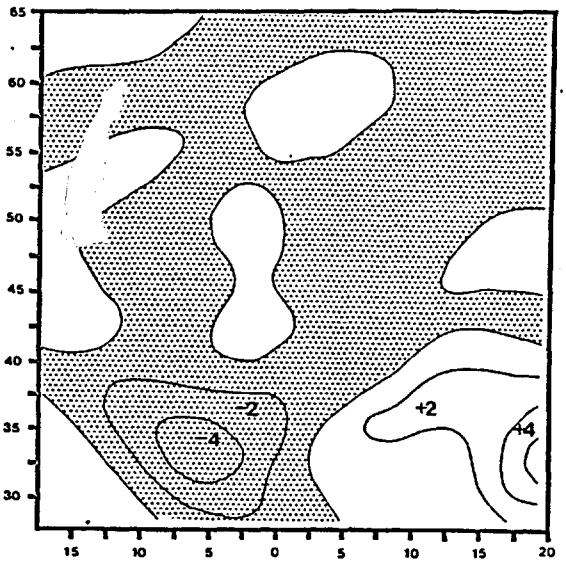
CI = 2 10^{-10} s^{-2}



$\bar{\underset{\sim}{v}} \cdot \nabla_H \bar{q} + \nabla_H (\overline{\underset{\sim}{v}' q'})$

b) 500 mb

CI = 2 10^{-10} s^{-2}



c) 700 mb

CI = 1 10^{-10} s^{-2}

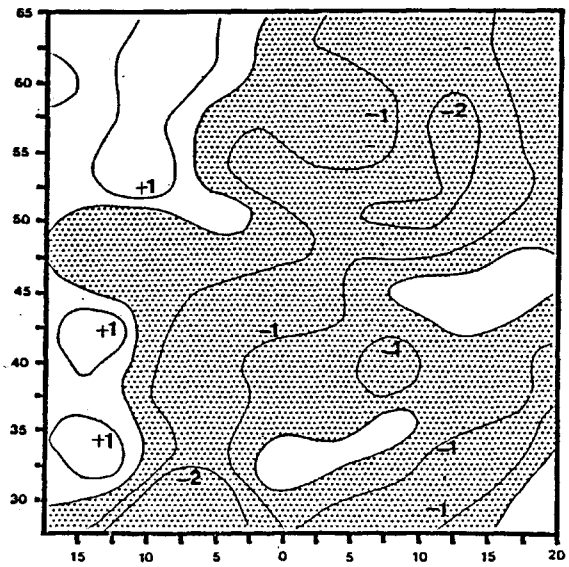


Fig.4.6 : Residual in the potential vorticity equation:

$$\bar{\underset{\sim}{v}} \cdot \nabla_H \bar{q} + \nabla_H (\overline{\underset{\sim}{v}' q'}) \simeq -f_0 \frac{\partial}{\partial p} \bar{H}/s_p \qquad (10^{-10}\ s^{-2}).$$

centre forcing sinking motion.

4.2.5 Residual in the potential vorticity equation

In adiabatic, frictionless motion, the steady state quasi-geostrophic potential vorticity equation (4.5) shows that the mean advection of $\bar{q}$ must be exactly balanced by an eddy-flux divergence:

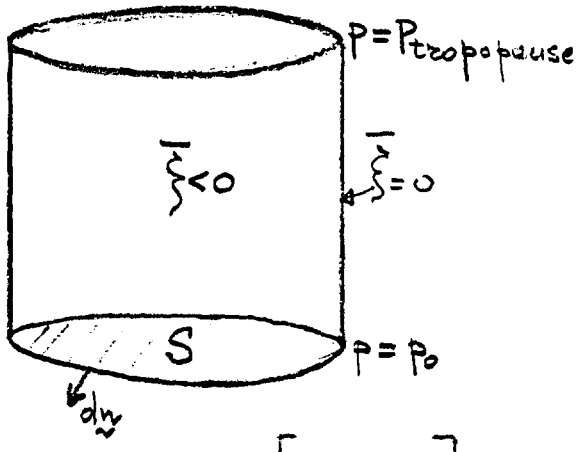
$$\bar{\underset{\sim}{v}} \cdot \nabla_H \bar{q} + \nabla_H \cdot (\overline{\underset{\sim}{v}' q'}) = 0 \qquad -(4.6)$$

Fig.4.6 shows the residual in the potential vorticity equation at 300, 500 and 700 mb. It includes diabatic and friction terms as well as errors. The $\partial/\partial p$ of the $\bar{H}/s_p$ calculated in section 3.6.4 must balance this residual. In the blocking region (north of 40°) the eddy terms are important and tend to cancel the mean flow advection of q : here the residual is smaller than either term. South of 40° where the eddy term is less important and the mean flow advection large, the residual is large and could be due to strong diabatic warming effects.

Discussion (on Chapters 3 and 4)

It has been found that the block is a region of anomalously high temperature, low relative vorticity and low potential vorticity. Synoptic scale systems transfer warm, low relative and potential vorticity air into the block.

The importance of eddy-transfer can easily be seen if we consider an integral vorticity balance. Integrating Eqn.(2.6) over the anticyclonic region bordered by a line of zero relative vorticty, and from the top of the boundary layer (where $\bar{\omega} = \bar{\omega}_{EK}$), to the tropopause (where $\bar{\omega} = 0$)



it reduces to:

$$\int_{P=P_o}^{P=P_{trop}} \overline{\underset{\sim}{v}'\zeta'} \cdot d\underset{\sim}{A}\, dp = -\varepsilon \left[\int_S \bar{\zeta}\, ds \right]$$ at the top of the boundary layer

where $\int_{\bar{\zeta}=0}$ is the integral over the $\bar{\zeta} = 0$ surface

$\int_S$ is the integral at the surface $p = p_o$ bordered by $\bar{\zeta} = 0$

ε is a constant of proportionality between $\bar{\omega}_{EK}$ and the vorticity at the top of the boundary layer.

The only term that can maintain the anticyclone against its dissipation at the ground is the transfer of anticyclonic vorticity into the region by eddies. The mean flow advection and vortex stretching terms can only redistribute vorticity within the region: they cannot generate vorticity.

This case study has shown that the eddy-flux divergence terms are important in the monthly mean budgets. There is a tendency for the mean flow advection to be balanced by the eddy-terms in the relative vorticity and potential vorticity budgets. Perhaps this is not surprising if we keep in mind that the monthly mean flow pattern is nothing more than an average of synoptic charts. These charts show considerable variability from day to day with the instantaneous split jet changing position and the high pressure system decaying to be replaced by new ones. (See Chapter 1 for synoptic description.) The monthly mean shows a ridge over the British Isles because, more often than not, highs were growing and decaying there. Questions such as "does the eddy-forcing cause the jet to split" become less important if one accepts that transients are an integral part of blocking, and that splitting the flow into mean and eddy parts may be a rather arbitrary distinction in the case of blocking. A better understanding of the phenomenon will require an understanding of how the eddies become organized.

Such a view seems to be in contrast with the mathematical analyses of, for example, Charney and De Vore (1979) and McWilliams (1981), who find mean flow solutions resembling blocks without explicitly considering the effects of transient phenomena. Our data analysis may not be incompatible with these quasi-steady mean flow solutions. It has been suggested that smaller scale motions can change the number and position of the multiple equilibrium states (Kallen, 1982), and influence the transition from one state to another (Malguzzi and Speranza, 1981). Further study needs to be carried out to find closer links between these ideas.

Tibaldi and Ji (1982) carried out a numerical study of blocking using the ECMWF spectral model. They showed that the horizontal resolution affects the ability of the model to maintain a block: at low resolution, incapable of resolving the synoptic scale, a block cannot be maintained, whereas at high resolution the model is in good agreement with the observed blocking. This supports our hypothesis that synoptic scale systems are important in the maintenance of blocking.

There are other long wave features, more permanent than blocking, which are usually thought of as stationary phenomena but in which transients may be important. For example, conventionally we would think that the Siberian anticyclone is thermally driven: an analysis carried out by Holopainen (1981) indicates that eddy transfer is also important there. Holopainen has further shown that transient disturbances tend to maintain other stationary features typical of the wintertime circulation, such as the North Pacific low and the North Atlantic low. Eddy-transfer into these systems can balance the whole dissipation of vorticity at the ground. The equivalent barotropic anomalies observed by Edmon (1980) in the wintertime circulation, are unlikely to be a response to anomalous thermal forcing but could be forced by anomalous transient eddy vorticity transport.

Shutts (1982) has performed experiments, with a model incorporating parametrizations of synoptic scale eddies, to investigate how anomalous the vorticity forcing must be to generate phenomena such as blocking. The experiments carried out produce warm highs and cold lows with a vorticity forcing of $2\ 10^{-10}\ s^{-2}$, comparable to the eddy vorticity flux divergence found in our data (see Fig.3.5). To investigate further the nature of the interaction between eddies and blocking flows, Shutts has been studying the way in which the distortion of waves by a split mean flow alters their transfer properties. In a barotropic model waves are forced upstream of a split mean flow.

They propagate up to the split, where they are sheared out as they are constrained to travel to the north and to the south. The change in shape of the eddies, caused by the mean flow changing from predominantly zonal to meridional, alters the correlations between velocity components and results in a divergence of the eddy-relative vorticity flux upstream of the split, in the correct sense to maintain the split.

CHAPTER 5

EDDY-FLUX

5.1 Introduction

In this chapter we discuss the distribution of the storm tracks, eddy-kinetic energy, and the eddy-fluxes of heat and potential vorticity.

The storm tracks and the eddy-kinetic energy confirm that the synoptic eddies are blocked by the anticyclone and steered preferentially to the north of it.

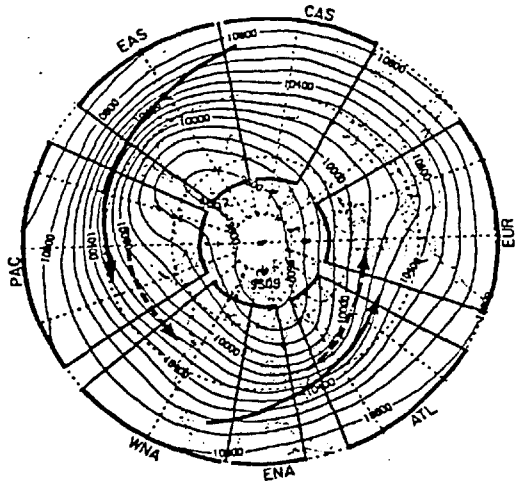
The eddy-heat and potential vorticity fluxes have a large rotational component which vector-rotates around the storm tracks.

Using the eddy-variance equation, it is shown that a rotational flux can be identified that balances the mean flow advection of the eddy-variance. The remaining flux takes part in the conversion processes and is directed more down gradient than the total flux.

a) $\overline{h}$ at 250 mb

CI = 100 m

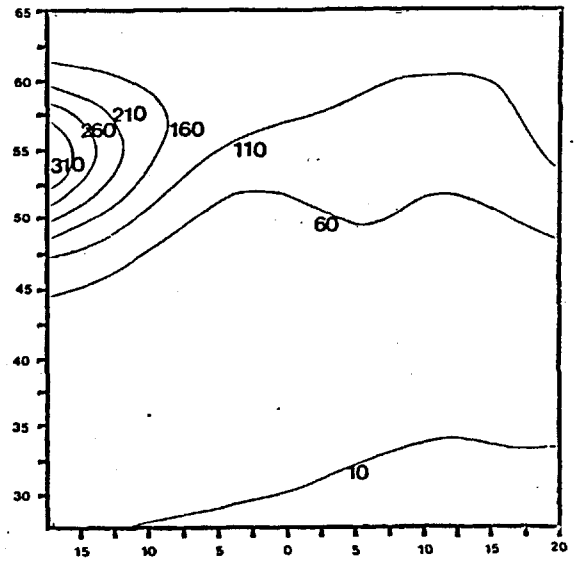
(from Lau, 1978)



b) $\overline{h'^2}$

$(10^2 m^2)$

at 400 mb



c) $K' = \overline{u'^2 + v'^2}$

$(m^2 s^{-2})$

at 400 mb

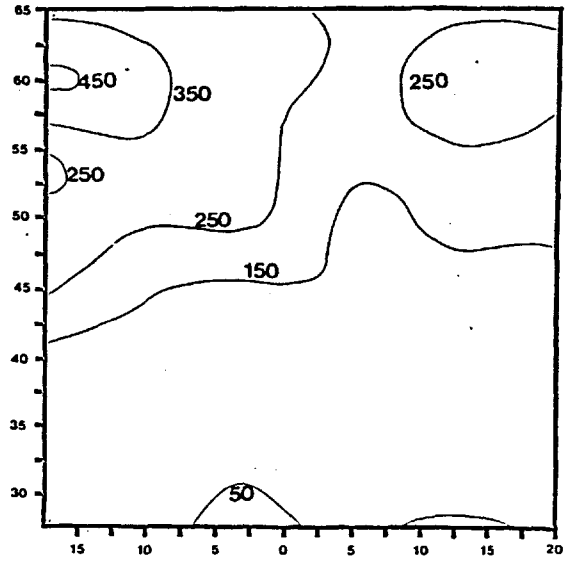


Fig.5.1 : a) Wintertime mean geopotential height at 250 mb. Black thick arrows: jet streams. Dashed arrows; storm tracks.

b) Temporal variance of 400 mb geopotential height for July '76.

c) Eddy kinetic energy K' at 400mb for July '76.

5.2 Eddy activity: storm tracks $\overline{h'^2}$ and eddy kinetic energy K'

Due to zonal asymmetries in orographic and diabatic forcing, the growth and decay of eddies becomes organized so that eddies grow preferentially at one longitude (east coasts of the continents) and move downstream where they decay at another longitude (west coasts of the continents), producing the observed storm tracks over the Oceans.

Major cyclonic activity is associated with pronounced height variability. Therefore the temporal variance of geopotential height $\overline{h'^2}$ gives an indication of the path followed by the storms. Fig.5.1(a) from Lau (1978), shows the two major storm tracks over the Atlantic and the Pacific.

The distribution of $\overline{h'^2}$ at 400 mb in the blocking region, is shown in Fig.5.1(b). There is a maximum to the west of Europe in the region of decaying eddies at the end of the Atlantic storm track.

The eddy-kinetic energy $K'\left(=\overline{u'^2+v'^2}\right)$ at 300 mb (Fig.5.1(c)) is large over the northern part of the region with two maxima, one on the west and the other to the northeast.

The distribution of $\overline{h'^2}$ and K' is consistent with synoptic observations that the free passage of depressions was interrupted by the block: depressions were concentrated to the west of the block with a few being steered around mainly in the northwards branch of the split jet. The difference in the spatial distribution of $\overline{h'^2}$ and K' is a sign of the change in scale of the baroclinic waves across the block. Supposing our eddies to be wavelike, then

$$h' \propto e^{i\underset{\sim}{K}(\underset{\sim}{x}-ct)}$$

$$\underset{\sim}{v}' \simeq i\,\underset{\sim}{K}\,h'$$

where $\underset{\sim}{K}$ is the wave vector

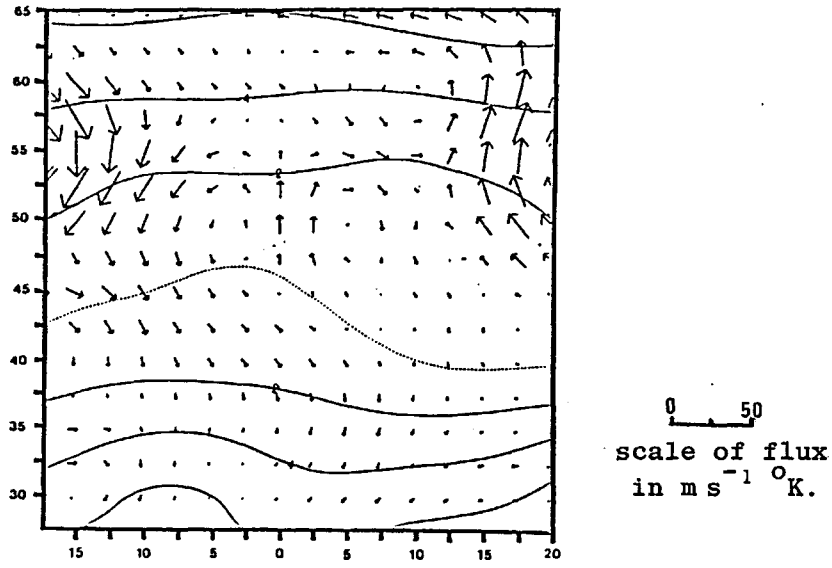


Fig.5.2 : a) Eddy-heat flux $\overline{v'T'}$ at 400 mb, superimposed to 400 mb $\overline{T}$ (CI = 2°K/day).

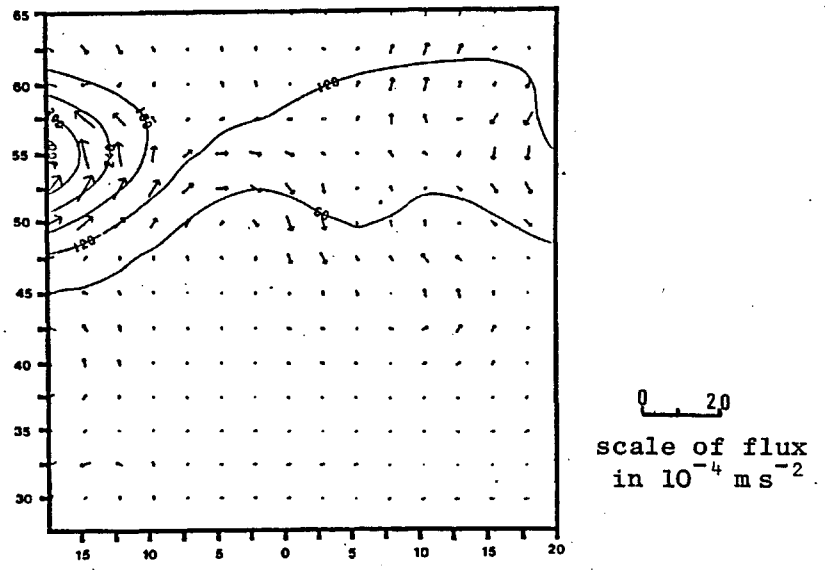


Fig.5.2 : b) Eddy-relative vorticity flux at 400 mb, superimposed to 400 mb $\overline{\zeta'v'}$ (CI = 60 dam^2).

and so

$$\left|\overline{\underset{\sim}{V}'^2}\right| = \left|\underset{\sim}{K}^2\right| \overline{h'^2}$$

Upstream of the block both $\left|\overline{\underset{\sim}{V}'^2}\right|$ and $\overline{h'^2}$ tend to be large but downstream $\overline{h'^2}$ tends to be small with $\left|\overline{\underset{\sim}{V}'^2}\right|$ large. So $\left|\underset{\sim}{K}^2\right|$ must increase across the block: the wavelength of the baroclinic waves changes as the split of the jet occurs. Upstream, where the flow is still broad and zonal, longer baroclinic waves are dominant. Downstream the flow becomes more meridional and the waves shorter, probably due to a reduction in their meridional scale. This change in scale can be seen in synoptic charts.

5.3 Eddy flux

It was the eddy-flux divergence at the end of the Atlantic storm track that made an important contribution in the block maintenance. In this section we show maps of the eddy-fluxes themselves.

5.3.1 Eddy-heat flux

The eddy-heat flux at 400 mb is plotted against $\overline{T}$ in Fig.5.2(a). Upstream of the block there are large upgradient fluxes and downstream large downgradient fluxes. The heat fluxes tend to rotate around the storm tracks. Compare Fig.5.2(a) with Fig.5.1(b).

Lau (1978) first recognized that eddy fluxes often rotate around the storm tracks. Lau and Wallace (1979) attributed this to the geostrophic nature of the weather systems.

If the flow is geostrophic then:

$$T' \propto -\frac{\partial h'}{\partial p} \propto h'$$ where the constant of

proportionality between T' and ρ' is positive if it is assumed that ρ' increases with height.

Because

$$\underset{\sim}{v}' \propto \underset{\sim}{k} \wedge \nabla \rho'$$

then

$$\overline{\underset{\sim}{v}'T'} \propto \underset{\sim}{k} \wedge \nabla \overline{\rho'^2} \qquad \text{—(5.1)}$$

So a component of the eddy-heat flux is expected to rotate anticyclonically around the storm tracks. It is this flux that gives the large upgradient flux to the west of the block.

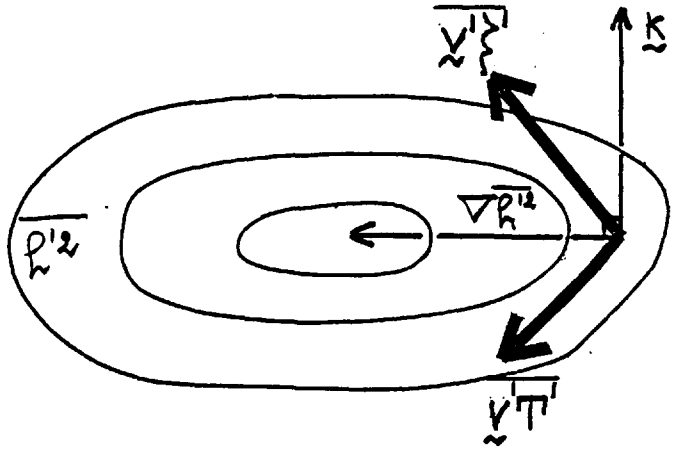
In a similar way, for the relative vorticity flux:

$$\zeta' \propto -\rho'$$

and

$$\overline{\underset{\sim}{v}'\zeta'} \propto -\underset{\sim}{k} \wedge \nabla \overline{\rho'^2} \qquad \text{—(5.2)}$$

Fig.5.2(b) shows the relative vorticity flux at 400 mb rotating cyclonically (in the opposite sense to the heat flux) around the storm track. The following schematic diagram shows the sense of rotation of the fluxes:



The fluxes in Fig.5.2 have a prominent component which rotates around the $\overline{p'^2}$ contours. If the constants of proportionality in Eqns.(5.1) and (5.2) are independent of horizontal position, then this flux is non-divergent and so cannot force the mean flow. It is important to be aware of this when interpreting maps of eddy fluxes. For example, in the blocking region, although the eddy-fluxes are large on either side of the block, these fluxes are predominantly non-divergent and so unimportant in the mean flow dynamics. The heat flux divergence is of the same magnitude all over the region (see Fig.3.13).

It is important to split the eddy fluxes into their rotational and divergent parts.

Lau and Wallace (1979) separated out the rotational flux exactly: they mathematically split their vector field into rotational and irrotational parts by solving Poisson equations for the flux stream-function Ψ , and the flux potential function χ , with boundary conditions Ψ = 0 and χ = 0, applied at 20°N, where eddy activity is small.

Instead, Marshall and Shutts (1981) have used the eddy-potential energy equation to suggest that a rotational flux may balance the flow advection of eddy-potential energy, with only the remaining flux taking part in energy transformations. This approach associates the rotational part of the flux with the spatial growth and decay of eddies. In the following section the blocking data will be used to investigate this hypothesis.

5.3.2 Eddy potential energy equation

In the baroclinically unstable westerlies, average eddy-heat fluxes have a component down the mean temperature gradient in order to release potential energy to the eddies. Although a baroclinic eddy must transfer heat downgradient to grow, the transfer in its mature or decaying phase is less certain but equally important. Maps of eddy fluxes show that in the mature phase the sense of the eddy heat flux is not constrained by the energetics.

It is the eddy-potential energy equation which relates the eddy-flux of heat across the horizontal temperature gradient to the advection and conversion of eddy-potential energy. It may be derived as follows.

Multiplying Eqn.(2.8) by Π gives the potential energy equation: (e.g. Pearce, 1978)

$$\frac{\partial}{\partial t}\Pi^2/2 + \underset{\sim}{V}\cdot\nabla_H \Pi^2/2 - S_p \omega \Pi = H\Pi \qquad \text{—(5.3)}$$

Multiplying Eqn.(2.10) by $\overline{\Pi}$ gives the potential energy equation for the mean flow:

$$\frac{\partial}{\partial t}\overline{\Pi}^2/2 + \underset{\sim}{\overline{V}}\cdot\nabla_H \overline{\Pi}^2/2 + \overline{\Pi}\cdot\nabla_H\left(\overline{\underset{\sim}{V}'\Pi'}\right) - S_p\,\overline{\omega}\,\overline{\Pi} = \overline{H}\,\overline{\Pi} \qquad \text{—(5.4)}$$

Averaging Eqn.(5.3) and subtracting from it Eqn.(5.4) gives the eddy potential energy equation:

$$\frac{\partial}{\partial t}\overline{\Pi'^2}/2 = \underbrace{-\overline{\Pi}\cdot\nabla\left(\overline{\underset{\sim}{V}'\Pi'}\right)}_{\text{conversion of mean flow potential energy}} + \underbrace{\nabla_H\cdot\left(\frac{\overline{\underset{\sim}{V}\Pi'^2}}{2} + \overline{\underset{\sim}{V}'\Pi'}\,\overline{\Pi}\right)}_{\text{advection term}} - \underbrace{\overline{\omega'\Pi'}S_p}_{\text{conversion to eddy kinetic energy}} = \underbrace{\overline{H'\Pi'}}_{\text{diabatic sources and sinks}} \qquad \text{—(5.5)}$$

Eqn. (5.5) is more usually written in the form:

$$\frac{\partial}{\partial t}\overline{\pi'^2/2} + \nabla_H\cdot\left(\overline{\underset{\sim}{v}\pi'^2/2}\right) + \overline{\underset{\sim}{v}'\pi'}\cdot\nabla\overline{\pi} - S_p\overline{\omega'\pi'} = \overline{H'\pi'} \qquad \text{—(5.6)}$$

where an advection and conversion term have been combined into a heat flux across the gradient using:

$$\overline{\underset{\sim}{v}'\pi'}\cdot\nabla_H\overline{\pi} = \underbrace{\nabla_H\cdot\left(\overline{\underset{\sim}{v}'\pi'}\,\overline{\pi}\right)}_{\text{advection term}} - \underbrace{\overline{\pi}\cdot\nabla_H\left(\overline{\underset{\sim}{v}'\pi'}\right)}_{\text{conversion term}}$$

This derivation of the eddy potential energy equation emphasizes that the flux across the gradient represents both conversion and advection of potential energy.

Eqn.(5.6) enables us to understand why, for example, at the end of our Atlantic storm track upgradient heat fluxes are observed, e.g. Fig.5.2(a). Eddy potential energy generated upstream is advected by the mean flow to the end of the storm track forcing the heat flux to point upgradient:

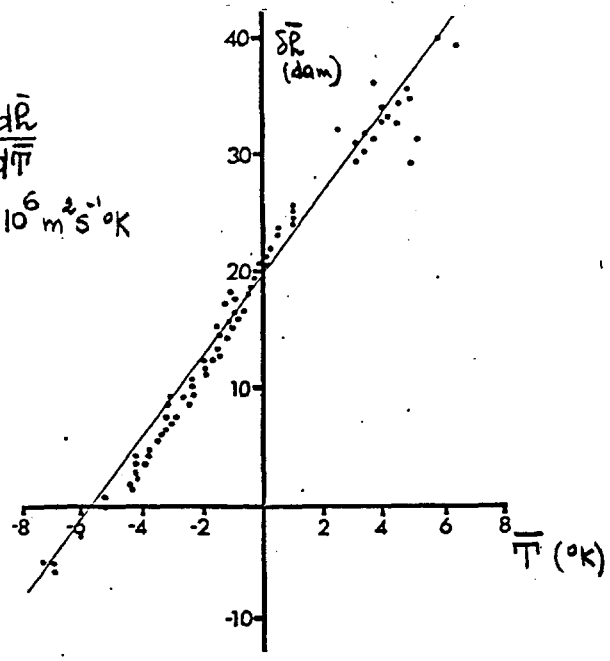
$$\underset{(-)}{\overline{\underset{\sim}{v}}\cdot\nabla_H\overline{\pi'^2/2}} + \underset{(+)}{\overline{\underset{\sim}{v}'\pi'}\cdot\nabla_H\overline{\pi}} \simeq 0$$

At the beginning of storm tracks the flux is downgradient to offset $\overline{\pi'^2}$ conversion to eddy kinetic energy and balance the advection of the eddy potential energy out of the region:

$$\underbrace{\overline{\underset{\sim}{v}}\cdot\nabla_H\overline{\pi'^2/2}}_{(+)} - \underbrace{S_p\overline{\omega'\pi'}}_{(-)} + \underbrace{\overline{\underset{\sim}{v}'\pi'}\cdot\nabla_H\overline{\pi}}_{(--)} \simeq 0$$

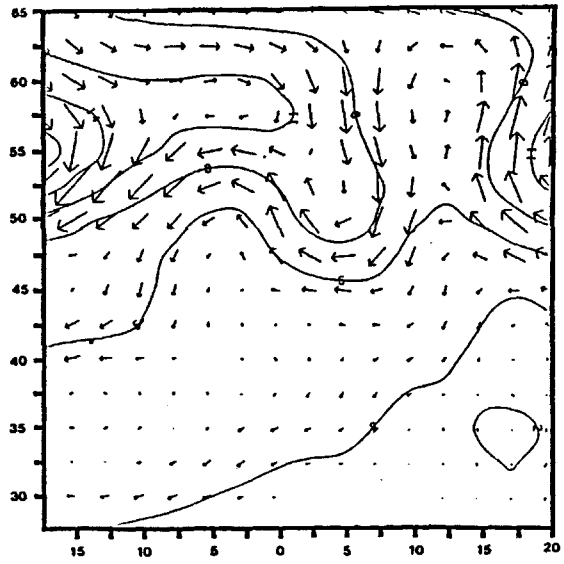
a) 400 mb

$$\frac{d\bar{\Psi}}{d\bar{\pi}} = \frac{g}{f}\frac{d\bar{R}}{d\bar{\pi}} \simeq 3.2\ 10^6\ m^2 s^{-1} {}^oK$$



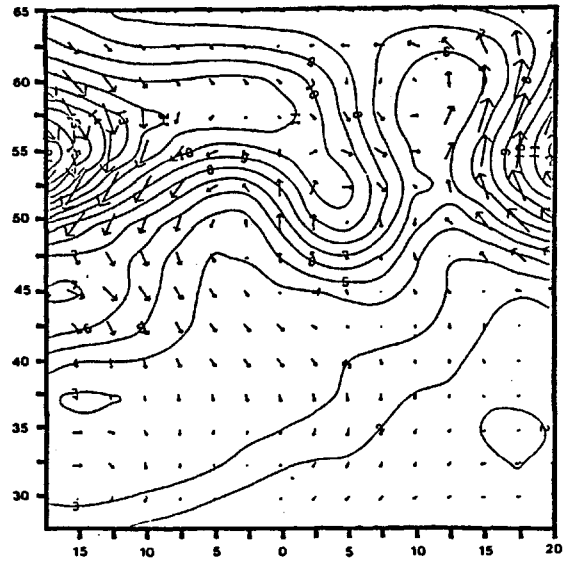
b) 400 mb

$(\overline{v'\pi'})_R$



c) 400 mb

$(\overline{v'\pi'})$



b), c)

0 50

scale of flux in $m\,s^{-1}\ {}^oK$.

Fig.5.3 : a) Plot of $\bar{\pi}$ as a function of $\delta\bar{R}$ to evaluate $d\bar{\Psi}/d\bar{\pi}$

b) $(\overline{v'\pi'})_R = 1/2 \frac{d\bar{\Psi}}{d\bar{\pi}} \lesssim \wedge \nabla_H \overline{\pi'^2}$ superimposed to $\overline{\pi'^2}$
(CI = $3\ {}^oK^2$)

c) $(\overline{v'\pi'})$ superimposed to $\overline{\pi'^2}$
(CI = $1\ {}^oK^2$)

Marshall and Shutts (1981) have shown that if the deviation of mean flow from mean temperature contours is small (so that $\bar{\psi} = \bar{\psi}(\bar{\pi})$), then a flow which circulates around $\overline{\pi'^2}$ can be identified, the component of which across the gradient balances the flow advection of $\overline{\pi'^2}$

$$\left(\overline{\underset{\sim}{v}'\pi'}\right)_R \cdot \nabla_H \bar{\pi} + \underset{\sim}{\bar{v}} \cdot \nabla_H \frac{\overline{\pi'^2}}{2} = 0 \qquad \text{—(5.7)}$$

where[1] $\left(\overline{\underset{\sim}{v}'\pi'}\right)_R = \frac{1}{2} \frac{d\bar{\psi}}{d\bar{\pi}} \underset{\sim}{k} \wedge \nabla \overline{\pi'^2}$

Further, if $\frac{d\bar{\psi}}{d\bar{\pi}}$ is a constant, $\left(\overline{\underset{\sim}{v}'\pi'}\right)_R$ is a rotational, non-divergent flux.

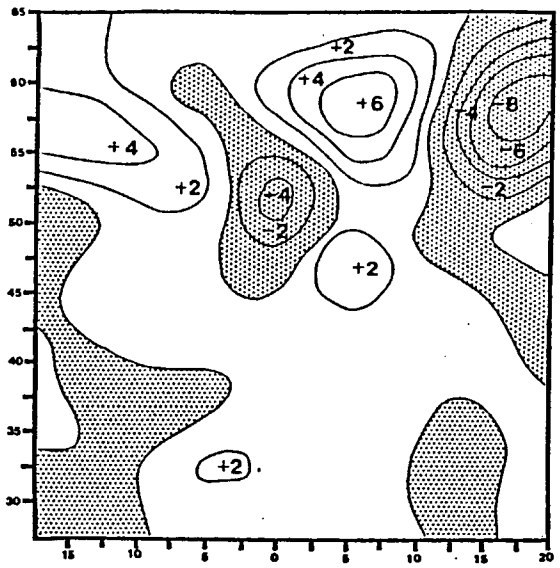
5.3.3 Rotational heat flux balancing advection of eddy potential energy

In this section an attempt is made to compute a rotational heat flux which balances the mean flow advection of eddy potential energy. The extent to which this is successful depends on how closely there is a linear relationship between the mean height and the mean temperature.

Fig.5.3(a) shows the plot of $\bar{\psi}$ against $\bar{\pi}$ at 400 mb over the blocking region. Because there is a nearly linear relationship, the flow advection of $\overline{\pi'^2}$ can be balanced by the rotational flux Eqn.(5.7). Fig.5.3(b) shows $\left(\overline{\underset{\sim}{v}'\pi'}\right)_R$ (with the constant calculated from the slope of Fig.5.3(a)) plotted against the $\overline{\pi'^2}$ contours. Comparison with the total flux plotted against $\overline{\pi'^2}$, Fig.5.3(c), shows that the major features are due to this rotational flux. Fig. 5.3(c) also shows that the eddy-heat flux more closely follows the

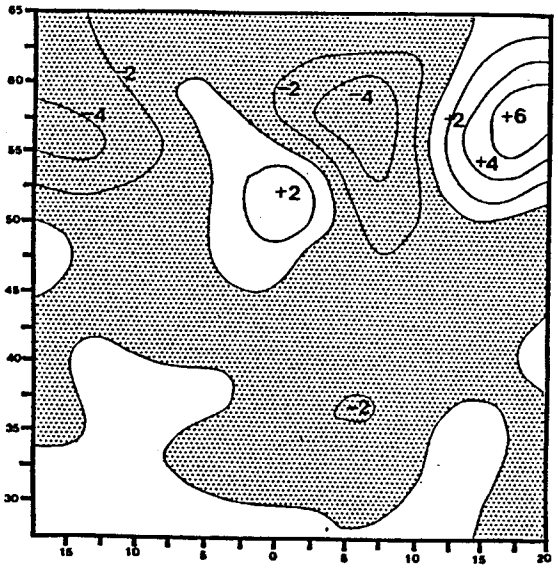
1. The subscript R is meant to remind the reader that the flux vector rotates around $\overline{\pi'^2}$ contours. The flux is only non-divergent if $d\bar{\psi}/d\bar{\pi}$ is not a function of horizontal position.

a)



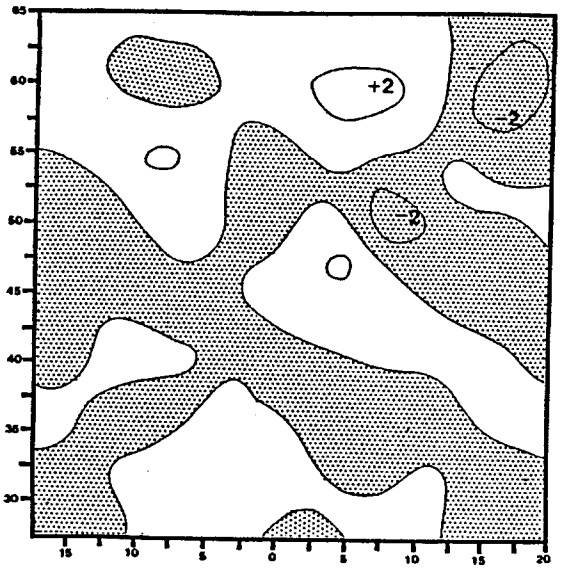
$(\overline{\underset{\sim}{v}'T'})_R \cdot \nabla\overline{T}$

b)



$\overline{\underset{\sim}{v}} \cdot \nabla_H \overline{T}^2/2$

c)



Σ

Fig.5.4 : at 400 mb. a) $(\overline{\underset{\sim}{v}'T'})_R \cdot \nabla\overline{T}$, b) $\overline{\underset{\sim}{v}} \cdot \nabla_H \overline{T}^2/2$

c) $\Sigma = \overline{\underset{\sim}{v}} \cdot \nabla_H \overline{T}^2/2 + (\overline{\underset{\sim}{v}'T'})_R \cdot \nabla_H \overline{T}$ — CI = 2 10^{-5} $^oK^2s^{-1}$

$\overline{\pi'^2}$ contours than it does the storm tracks, Fig.5.1(b).

In order to determine the extent to which Eqn.(5.7) is satisfied, $\bar{\underset{\sim}{v}} \cdot \nabla_H \overline{\pi'^2}/2$, $\left(\overline{\underset{\sim}{v}'\pi'}\right)_R \cdot \nabla_H \bar{\pi}$ and their sum (Σ) have been plotted, Fig.5.4. The sum (Σ) is much smaller than either of the two terms, showing that we have succeeded in isolating a rotational component of the heat flux which is balancing the mean flow advection. This flux is non-divergent and so cannot alter mean temperature gradients.

The remaining flux: $\overline{\underset{\sim}{v}'\pi'} - \left(\overline{v'\pi'}\right)_R$, Fig.5.5(a), is much less rotational and much more downgradient than $\overline{\underset{\sim}{v}'\pi'}$, Fig.5.2(a). The term $\left(\overline{\underset{\sim}{v}'\pi'} - \left(\overline{v'\pi'}\right)_R\right) \cdot \nabla_H \bar{\pi}$ is shown in Fig.5.5(b). Because it is significantly larger than the sum (Σ), Fig.5.4(c), it must be balanced by sources or sinks of eddy potential energy:

$$\left(\overline{\underset{\sim}{v}'\pi'} - \left(\overline{v'\pi'}\right)_R\right) \cdot \nabla_H \bar{\pi} \simeq \overline{H'\pi'} + \overline{\omega'\pi'} S_p$$

From Fig.5.5(b), the left-hand side is large and negative on, and to the north of, the split jet, implying that there is a sink of eddy potential energy there:

$$\overline{H'\pi'} + \overline{\omega'\pi'} S_p < 0$$

Two likely processes are:

baroclinic instability $\quad \overline{\omega'\pi'} S_p < 0$

or

radiative damping of eddies to space $\quad \overline{H'\pi'} < 0$

Supposing that there is a linear thermal damping $H' = -\lambda \pi'$, our data shows that a λ^{-1} of 10 days would be needed to balance the

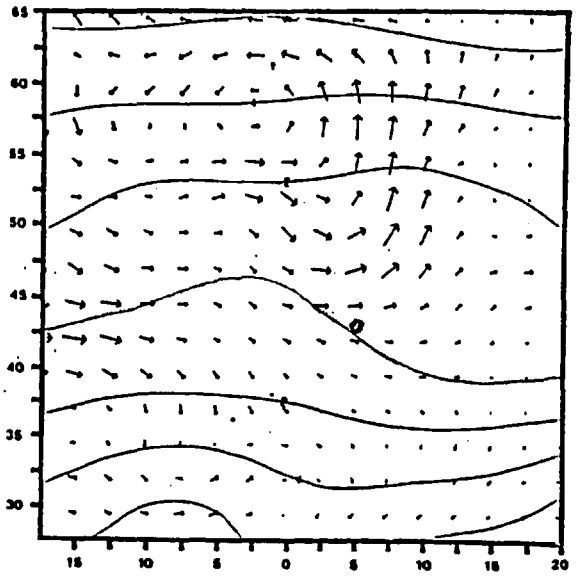


Fig.5.5 : a) $\overline{\underset{\sim}{v}'T'} - \left(\overline{\underset{\sim}{v}'T'}\right)_R$ at 400 mb, superimposed to 400 mb mean temperature $\overline{T}$ (CI = 2^{o}K/day).

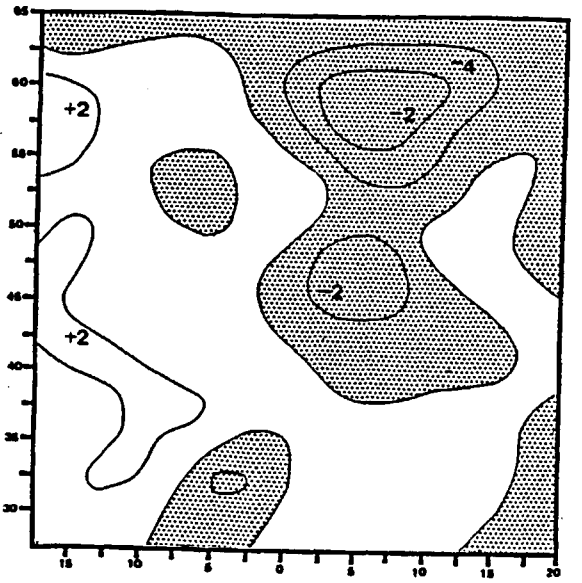


Fig.5.5 : b) $\left(\overline{\underset{\sim}{v}'T'} - \left(\overline{\underset{\sim}{v}'T'}\right)_R\right) \cdot \nabla_H \overline{T}$ at 400 mb. (CI = 2 10^{-5} ^{o}K^{2} s^{-1}).

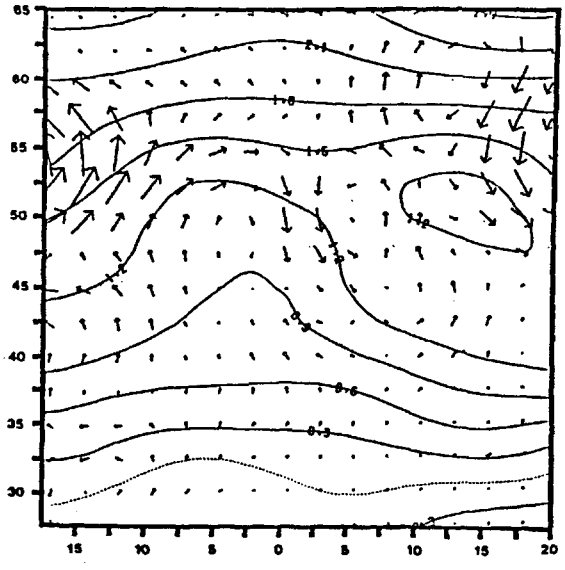
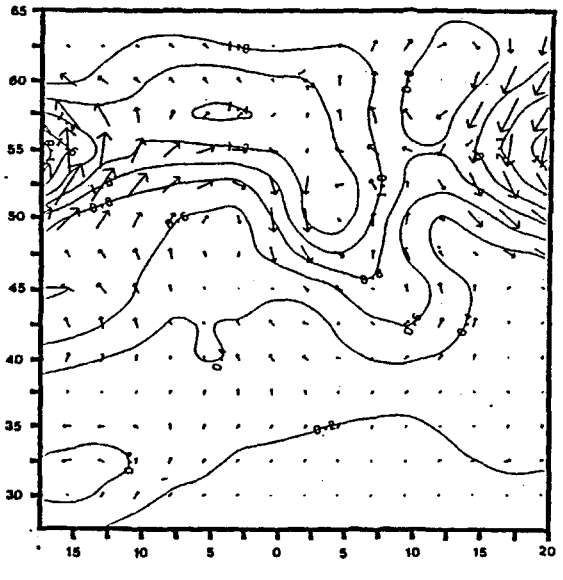


Fig.5.6 : a) $\overline{\underset{\sim}{v}'q'}$ at 300 mb, superimposed to 300 mb $\bar{q}$
(CI = 0.3 10^{-4} s^{-1}).



0 20

scale of flux
in $10^{-4} ms^{-2}$

Fig.5.6 : b) $\overline{\underset{\sim}{v}'q'}$ at 300 mb, superimposed to 300 mb $\overline{q'^2}$
(CI = 0.2 10^{-8} s^{-2}).

$\left(\overline{\underset{\sim}{v}'\pi'} - \left(\overline{\underset{\sim}{v}'\pi'}\right)_R\right) \cdot \nabla_H \bar{\pi}$ term. Since a λ of this magnitude would give an eddy cooling rate of less than 1° a day, it follows that the $\overline{H'\pi'}$ term must be important in the eddy potential energy equation. Probably baroclinic instability and radiative processes are both important.

5.3.4 Eddy potential vorticity flux

The eddy potential vorticity flux plotted against $\bar{q}$ and $\overline{q'^2}$ at 300 mb is shown in Fig.5.6. A rotational flux rotating around the $\overline{q'^2}$ contours is evident, leading to regions of q -flux both up and down the mean potential vorticity contours.

Again it is useful to look at the appropriate eddy-variance equation - the eddy enstrophy equation. In the steady state it can be written

$$\underbrace{\bar{\underset{\sim}{v}} \cdot \nabla_H \overline{q'^2}/2}_{\text{advection of eddy enstrophy}} + \underbrace{\overline{\underset{\sim}{v}'q'} \cdot \nabla_H \bar{q}}_{\text{flux across the gradient}} - \underbrace{\overline{S_q' q'}}_{\text{dissipation of eddy enstrophy}} = 0 \qquad \text{—(5.8)}$$

where S_q is the source/sink term in the potential vorticity equation (Eqn.4.5).

It can be seen that the rotational flux in Fig.5.6 rotates in the sense to balance the advection of $\overline{q'^2}$. The region of up-gradient flux west of the block is primarily due to advection of $\overline{q'^2}$ in by the mean flow, while the down-gradient flux east of the block is principally due to advection of $\overline{q'^2}$ out of that region by the mean flow.

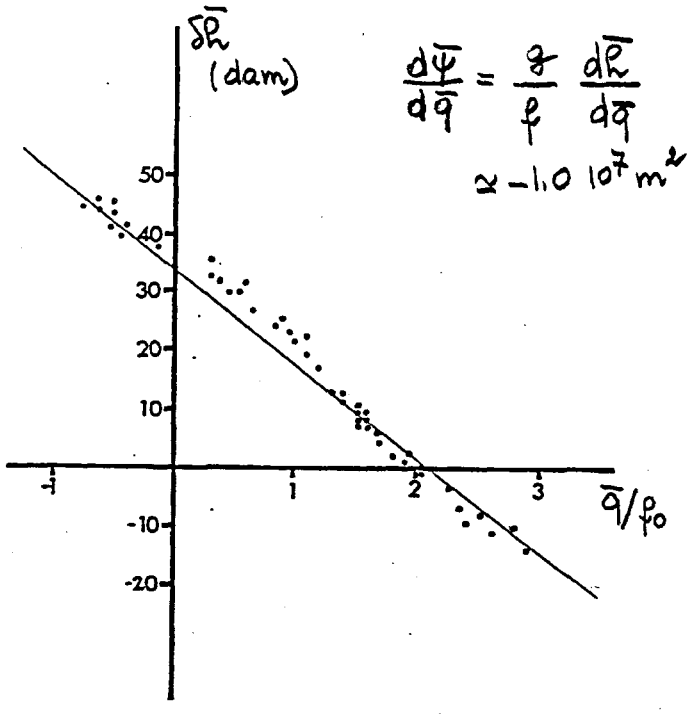
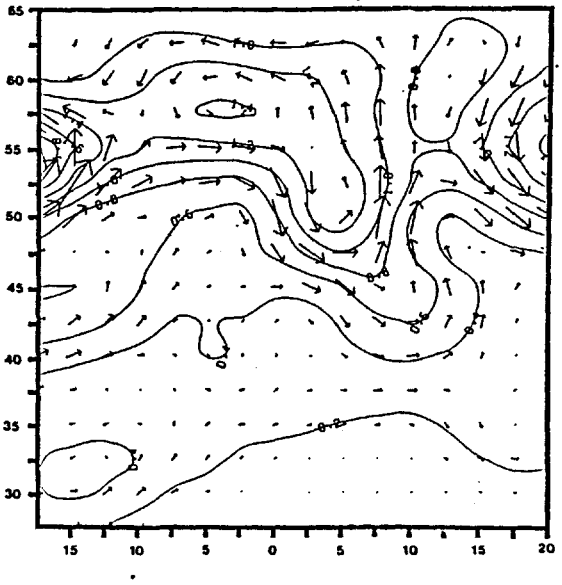


Fig.5.7 : a) Plot of $\bar{q}$ as a function of $\delta\bar{z}$ to evaluate $d\bar{\psi}/d\bar{q}$ at 300 mb.



0 20

scale of flux in $10^{-4} ms^{-2}$

Fig.5.7 : b) $(\underset{\sim}{v}'q')_R = \frac{1}{2}\frac{d\bar{\psi}}{d\bar{q}}\,\underset{\sim}{k} \wedge \nabla_H \overline{q'^2}$ superimposed to 300 mb $\overline{q'^2}$ (CI = 0.2 $10^{-8} s^{-2}$).

If the mean streamfunction $\bar{\Psi}$ is a linear function of the mean potential vorticity $\bar{q}$, so that $d\bar{\Psi}/d\bar{q}$ is a constant, then the non-divergent flux

$$(\overline{\underset{\sim}{v}'q'})_R = \frac{1}{2}\frac{d\bar{\Psi}}{d\bar{q}}\,\underset{\sim}{k}\wedge\nabla\overline{q'^2}$$

across the gradient can balance the mean flow advection of $\overline{q'^2}$

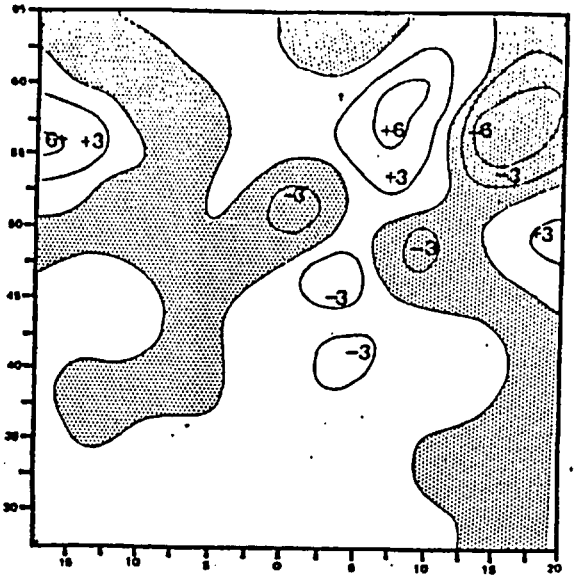
$$(\overline{\underset{\sim}{v}'q'})_R\cdot\nabla_H\bar{q} + \underset{\sim}{\bar{v}}\cdot\nabla_H\overline{q'^2}/2 = 0 \qquad \text{—(5.9)}$$

The $\bar{\Psi}$ plotted against $\bar{q}$, Fig.5.7(a), is approximately linear. Fig.5.7(b) shows the rotational flux $(\overline{\underset{\sim}{v}'q'})_R$ with the multiplying constant calculated from the slope of the graph. There is a striking similarity between Fig.5.6(b) and Fig.5.7(b), showing that the q-flux at 300 mb is almost all rotational flux.

The terms in Eq.(5.9) and their sum are shown in Fig.5.8. The rotational flux does balance the mean flow advection in most of the region. The balance is not good where $\bar{q}$ contours are closed (see Fig.5.6(a)) because the single valued functional relationship between $\bar{\Psi}$ and $\bar{q}$ is broken.

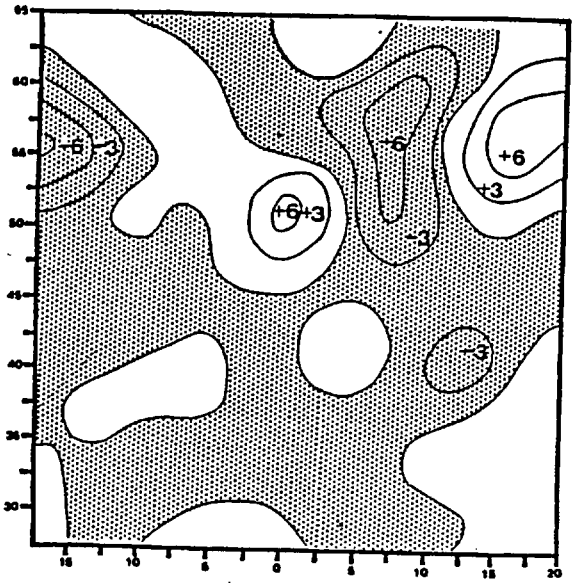
The remaining flux $\left(\overline{\underset{\sim}{v}'q'} - (\overline{\underset{\sim}{v}'q'})_R\right)$, Fig.5.9(a), is small and points both up and downgradient. Its divergence forces the mean flow. The magnitude of $\left(\overline{\underset{\sim}{v}'q'} - (\overline{\underset{\sim}{v}'q'})_R\right)\cdot\nabla_H\bar{q}$ (Fig.5.9(b)) is not significantly larger than the sum (*Fig. 5.8c*). This suggests that the enstrophy dissipation in Eqn.(5.8) is not dominant in the blocking region. Regions of large positive $\left(\overline{\underset{\sim}{v}'q'} - (\overline{\underset{\sim}{v}'q'})_R\right)\cdot\nabla_H\bar{q}$ would indicate that the eddy field is enhancing mean potential vorticity gradients. Although upstream

a)



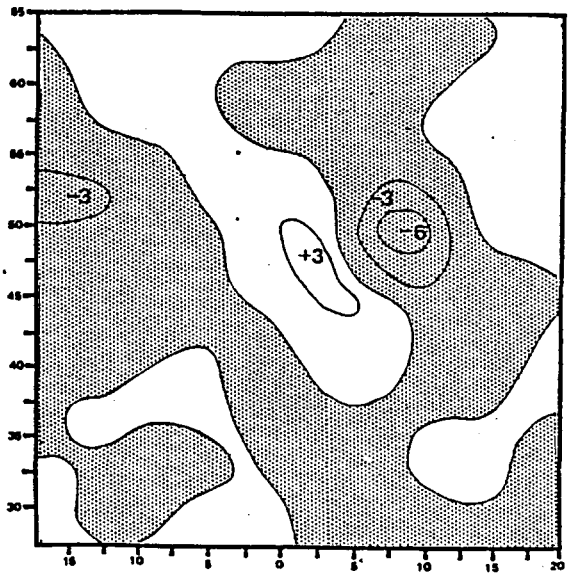
$(\overline{\underset{\sim}{v}'q'})_R \cdot \nabla_H \bar{q}$

b)



$\bar{\underset{\sim}{v}} \cdot \nabla_H \overline{q'^2}/2$

c)



Σ

Fig.5.8 : at 300 mb. a) $(\overline{\underset{\sim}{v}'q'})_R \cdot \nabla_H \bar{q}$ b) $\bar{\underset{\sim}{v}} \cdot \nabla_H \overline{q'^2}/2$

c) $\Sigma = \bar{\underset{\sim}{v}} \cdot \nabla_H \overline{q'^2}/2 + (\overline{\underset{\sim}{v}'q'})_R \cdot \nabla_H \bar{q}$

(CI = 3 10^{-15} s^{-3}).

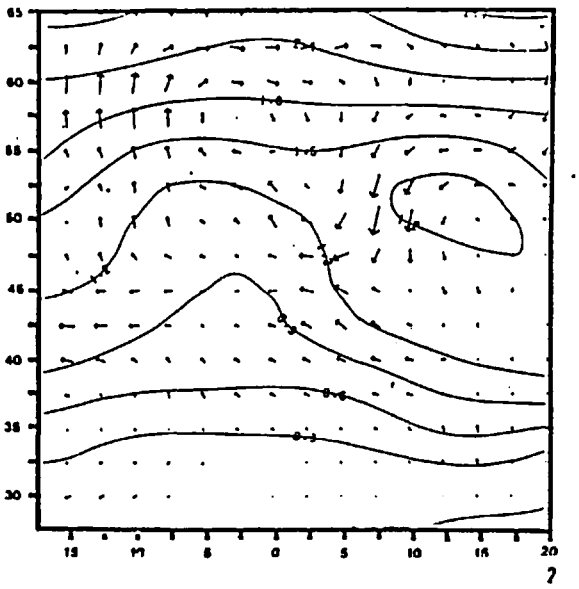


Fig.5.9 : a) $\overline{\underset{\sim}{v}'q'} - (\overline{\underset{\sim}{v}'q'})_R$ at 300 mb, superimposed to 300 mb $\bar{q}$ (CI = 0.3 10^{-4} s^{-1}).

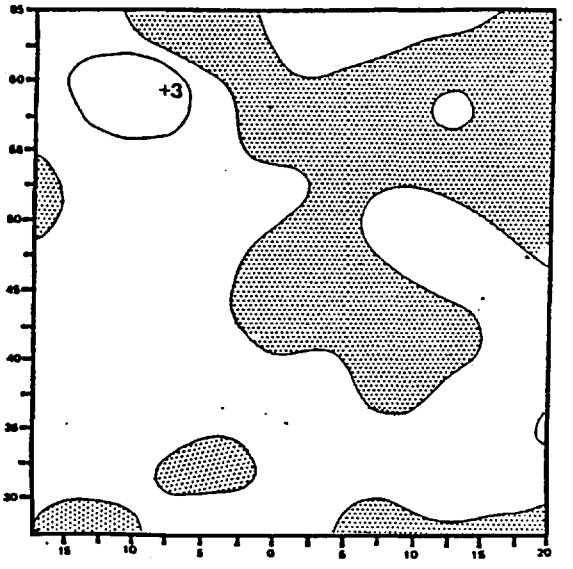


Fig.5.9 : b) $\overline{\underset{\sim}{v}'q'} - (\overline{\underset{\sim}{v}'q'})_R \cdot \nabla_H \bar{q}$ at 300 mb.
(CI = 3 10^{-15} s^{-3}).

of the block $\left(\overline{\underset{\sim}{v}'q'} - (\overline{\underset{\sim}{v}'q'})_R\right) \cdot \nabla_H \bar{q}$ is positive, because it is of small magnitude, such a conclusion can only be tentatively drawn.

5.4 Summary

It is the eddy-flux divergence discussed in Chapters 3 and 4 that contribute to the mean flow vorticity and thermodynamic budgets. Much care must be taken in making deductions about eddy mean flow interaction from the eddy fluxes themselves. The eddy fluxes are of interest because often they, rather than the flux divergence, are the subject of parameterization schemes (e.g. Green (1970)). Such simple parameterization schemes of synoptic scale systems are not adequate representation of the time-mean local flux. Eddy fluxes often present large rotational fluxes with components up, down and along mean gradients.

The major difficulty in the parameterization problem is that too little is known about the transfer properties of the mid-latitude weather systems. So far parameterization schemes have been based principally on the intuition gained from instability analyses of zonal flows, which give information only about the growing phase. It is not surprising, therefore, that they are inadequate to describe the transfer properties of a field of growing and decaying eddies. Further study of real and model eddy transfers is needed.

In this Chapter, calculations have been presented which support the idea (Marshall and Shutts, 1981) that a rotational component can be identified, which closely balances the flow advection term in the eddy variance equation. The flux is associated with the spatial

growth and decay of eddies. The remainder takes part in the energy conversions. It would be interesting to extend our study to see how the "Marshall and Shutts" flux compares with the complete rotational flux computed in the manner of Wallace and Lau (1979). This could most easily be done by repeating the calculations over the whole hemisphere rather than confining ourselves to the blocking region.

CONCLUSIONS AND SUGGESTIONS FOR FUTURE WORK

The analysis of the Drought of 1976 has enabled a consistent dynamical picture of the block to be drawn. Vorticity, heat and potential vorticity budgets have shown that eddy-forcing is crucial in the maintenance of the blocking anticyclone. The eddy-vorticity forcing is large near the tropopause and forces downward motion. The resulting adiabatic warming offsets the diabatic cooling (associated with the high temperature there) and so warm, dry air is brought down to the surface, generating the surface anti-cyclone, which can be dissipated by frictional torque.

Further diagnostic studies need to be carried out to see if similar dynamical processes are occurring in other blocking cases.

The dynamical insights gained from these diagnoses must then be tested in our models. For example, simplified but realistic forcing functions could be used in low resolution climate models in order to simulate blocking.

We need to determine the extent to which the eddy-transfer taking place in the block is anomalous. Further study of the transfer properties of the middle latitude synoptic scale, using real and model data, is essential here.

Our study of block maintenance should be extended to include the dynamics of block initiation and decay: of particular interest is the possible role of transients in the transition from blocked to unblocked flow.

It will be necessary to diagnose blocking cases in the high resolution G.C.M.'s to see if the dynamical processes identified in our case study are also occurring in the models. It may be found that the difficulty the G.C.M.'s have in producing blocks

is a result of their inability to resolve the eddy-transfer processes which we believe are crucial to the block maintenance.

Finally, other ways of treating the data need to be considered. For example, one approach would be to investigate the block in terms of particle trajectories rather than the means at a point. This Lagrangian description could bear a closer relation to the synopticians view of blocking and give more insight into the transport of the warm low potential vorticity air into the block by the moving air masses.

REFERENCES

Atlas of Drought in Britain 1975-76 Institute of British Geographers, London.

Austin, J.F. 1980 The blocking of mid-latitude westerly wind by planetary waves. Quart.J.R.Met.Soc., 106, 327-350.

Berggren, R., B. Bolin and C.G. Rossby 1949 An aerological study of zonal motion, its perturbation and breakdown. Tellus, 1, 14-37.

Blackmon, M.L., J.M. Wallace and N-C Lau and S.L. Mullen 1977 An observational study of the Northern Hemisphere Wintertime circulation. J.Atmos.Sci., 34, 1040-1053.

Brezowsky, H. H. Flohn and P. Hess 1951 Some remarks on the climatology of blocking action. Tellus, 3, 191-194.

Charney, J.G. and M. Stern 1962 On the stability of internal baroclinic jets in a rotating atmosphere. J.Atmos.Sci., 19, 159-162.

Charney, J.G. and De Vore, J.G. 1979 Multiple flow equilibria in the atmosphere and blocking. J.Atmos.Sic., 36, 1205-1216.

Charney, J.G., J. Shukla and K.C. Mo, 1981 Comparison of a barotropic blocking theory with observations. J.Atmos.Sci., 38, 762-779.

Edmon, H.J. 1980 A study of the general circulation over the Northern Hemisphere during the Winters of 1976-1977 and 1977-1978. Mon.Wea.Rev., 108, 1538-1553.

Egger, J. 1978 Dynamics of blocking highs. J.Atmos.Sci., 35, 1788-1801.

Elliot, R.D. and T.B. Smith 1949 A study of the effects of large blocking highs on the general circulation in the Northern Hemisphere Westerlies. J.Meteor. 6, 67-85.

Ertel, H. 1949 Ein neuer hydrodynamischer Wirbelsete. Meteorol.Zeit. 59 (1942), 277-281.

Everson, P.J. and D.R. Davies 1977 On the use of a simple two-level model in General Circulation studies. Quart.J.R.Met.Soc., 96, 404-412.

Green, J.S.A. 1970 Transfer properties of the large scale eddies and the general circulation of the atmosphere. Quart.J.R.Met.Soc., 96, 157-185.

Green, J.S.A. 1977 The weather during July 1976: Some dynamical consideration of the drought. Weather, 32, 120-128.

Hartmann, D.L. and S.J. Ghan 1980 A statistical study of the Dynamics of of Blocking. Mon.Wea.Rev., 108, 1144-1159.

Holopainen, E.O. 1978 On the dynamic forcing of the long term mean flow by the large-scale Reynolds stresses in the atmosphere. J.Atmos.Sci., 35, 1596-1604.

Holopainen, E.O. and A.H. Oort 1981 On the role of large-scale transient eddies in the maintenance of the Vorticity and Enstrophy of the time-mean atmospheric flow. J.Atmos.Sci., 38, 270-280.

Holton, J.R. 1979 An introduction to dynamic meteorology. Academic Press, New York.

Illari, L., P. Malguzzi and A. Speranza 1981 On the breakdown of the westerlies Geoph.Astroph. F.Mech. 17, 27-49.

Källén, E. 1982 Bifurcation properties of quasi-geostrophic, barotropic models and their relation to atmospheric blocking. (To appear in Tellus.)

Kikuki, Y. 1969 Numerical simulation of the blocking process. J.Meteor.Soc.Japan, 47, 29-54.

Kikuki, Y. 1971 Influence of mountains and land-sea distribution on blocking action. J.Meteor.Soc.Japan, 49, 564-572.

Lau, N-C. 1979 a) The structure and energetics of transient disturbances in the Northern Hemisphere Wintertime circulation. J.Atmos.Sci., 36, 982-995.

Lau, N-C. 1979 b) The observed structure of tropospheric stationary waves and the local balances of vorticity and heat. J.Atmos.Sci., 36, 996-1016

Lau, N-C. and J.M. Wallace 1979 On the distribution of horizontal transports by transient eddies in the Northern Hemisphere Wintertime circulation. J.Atmos.Sci., 36, 1844-1861.

Lau, N-C. and A.H. Oort	1981	A comparative study of observed Northern Hemisphere Circulation Statistics based on GFDL and NMC analysis. Part I: The time-mean fields. Mon.Wea.Rev. 109. 1380-1403.
Malguzzi, P. and A. Speranza	1981	Local multiple equilibria and regional atmospheric blocking. J.Atmos.Sci., 38, 1939-1948.
Marshall, J.C. and G. Shutts	1981	A note on rotational and divergent fluxes. J.Phys.Oceanography, 11, 1677-1680.
McWilliams, J.	1980	An application of equivalent modons to atmospheric blocking. Dyn.Atm. and Oceans. 5, 43-66.
Miles, M.K.	1977	Atmospheric circulation during the severe drought of 1975/76. Met.Mag. 106, 154-162.
Montalto, M., M. Conte and M. Urbani	1973	Comparison and Summary of the Characteristics of long and short lived Blocking systems in the Euro-Atlantic Area. Rome, Min.Aero.
Murray, R.	1977	The 1975/76 Drought over the United Kingdom - Hydrometeorological aspects. Met.Mag. 106, 129-145.
Namias, J.	1947	Characteristics of the general circulation over the Northern Hemisphere during the abnormal winter of 1946-1947. Mon.Wea.Rev., 75, 145-152.
Namias, J.	1950	The index cycle and its role in the general circulation. J.Meteor. 7, 130-139.
Namias, J.	1959	Recent seasonal interaction between North Pacific waters and the overlying atmospheric circulation. J.Geophys.Res., 64, 631-645.
Namias, J.	1964	Seasonal persistence and recurrence of European blocking during 1958-1960. Tellus, 16, 397-407.
Namias, J.	1978	Multiple causes of the North American abnormal winter 1976-77. Mon.Wea.Rev., 106, 279-295.

Oort, A.H. and E.M. Rasmussen 1971 Atmospheric circulation Statistics. NOAA Professional Paper, 5.

Ratcliffe, R.S.A. 1977 A synoptic climatologist's viewpoint of the 1975/76 drought. Met.Mag., 106, 145-154.

Ratcliffe, R.A.S. 1978 Meteorological aspects of 1975-1976 drought. Proc.R.Soc.Lond. A.363, 3-20.

Rex, D.F. 1950 Blocking action in the middle troposphere and its effect upon regional climate.
Part I: An aerological study of blocking action. Tellus, 2, 196-211.
Part II: The climatology of blocking action. Tellus, 2, 275-301.

Rex, D.F. 1951 The effect of Atlantic blocking action upon European climate. Tellus, 3, 199-212.

Rosen, R.D. and D.A. Salstein 1980 Comparison between circulation statistics computed from conventional data and NMC Hough analysis. Mon.Wea.Rev., 108, 1087-1278.

Rossby, C.G. 1940 Planetary flow patterns in the atmosphere. Suppl. Quart.J.R.Met.Soc., 66, 68-87.

Sanders, R.A. 1953 Blocking highs over the Eastern North Atlantic and Western Europe. Mon.Wea.Rev., 81, 67-73.

Savijarvi, H.I. 1977 The interaction of the monthly mean flow and large scale transient eddies in two different circulation types. Part II: Vorticity and temperature balance. Geophysica, 14, 207-229.

Shaw, M.S. 1977 Exceptional heat waves of 23 June to 8 July, 1976. Met.Mag., 106, 329-346.

Shutts, G.J. 1982 Monthly-mean climatology and the parametrization of travelling weather systems. Advances in Geophysics (accepted).

Pearce, R.P. 1978 On the concept of available potential energy. Quart.J.R.Met.Soc., 104, 737-755.

Sumner, E.J. 1959 Blocking anticyclones in the Atlantic - European sector of the Northern Hemisphere. Met.Mag., 88, 300-311.

Tibaldi, S. and L.R. Ji. 1982 On the effect of model resolution on numerical simulation of blocking. Internal Report, E.C.M.W.F. Reading.

Tung, K.K. and R.S. Lindzen 1979 A theory of stationary long waves. Part I: A simple theory of blocking. Mon.Wea.Rev., 107, 714-734.

White, W.B. and N.E. Clarke 1975 On the development of blocking ridge activity over the Central North Pacific. J.Atm.Sci., 32, 489-502.

Yeh, T.C. 1949 On energy dispersion in the atmosphere. J.Meteor., 6, 1-16.

ACKNOWLEDGEMENTS

I would like to thank Dr. J.S.A. Green for his inspiring supervision and all members of the Atmospheric Physics Group, especially Dr. J.C. Marshall and Dr. G.J. Shutts.

Thanks also go to Dr. S. Tibaldi and E.C.M.W.F. for providing the NMC data, and to Mrs. J. Ludlam for careful typing of the manuscript.

The work was supported by an E.E.C. scholarship.